Study of Cell-Cell Communication Using 3D Living Cell Microarrays

by

Winston Timp

B.S. Electrical Engineering(2001), Biochemistry(2002),
Chemistry(2002), Physics(2002)
University of Illinois at Urbana-Champaign

M.S. Electrical Engineering (2005)
Massachusetts Institute of Technology

Submitted to the Department of Electrical Engineering and Computer
Science
in partial fulfillment of the requirements for the degree of

Doctor of Philosophy in Electrical Engineering and Computer Science

at the

MASSACHUSETTS INSTITUTE OF TECHNOLOGY

September 2007

Author . . . .
Department of Electrical Engineering and Computer Science
July 25, 2007

Certified by. . . . .
Paul Matsudaira
Professor of Biology and Biological Engineering
Thesis Supervisor

Accepted by . . . .
Arthur C. Smith
Chairman, Department Committee on Graduate Students

Study of Cell-Cell Communication Using 3D Living Cell Microarrays

by

Winston Timp

Abstract

Cellular behavior is not dictated solely from within; it is also guided by a myriad of external cues. If cells are removed from their natural environment, apart from the microenvironment and social context they are accustomed to, it is difficult to study their behavior in any meaningful way. To that end, I describe a method for using optical trapping for positioning cells with submicron accuracy in three dimensions, then encapsulating them in hydrogel, in order to mimic the *in vivo* microenvironment. This process has been carefully optimized for cell viability, checking both prokaryotic and eukaryotic cells for membrane integrity and metabolic activity.

To demonstrate the utility of this system, I have looked at a model "quorum sensing" system in *Vibrio Fischeri*, which operates by the emission and detection of a small chemical signal, an acyl-homoserine lactone. Through synthetic biology, I have engineered plasmids which express "sending" and "receiving" genes. Bacteria containing these plasmids were formed into complex 3D patterns, designed to assay signaling response. The gene expression of the bacteria was tracked over time using fluorescent proteins as reporters. A model for this system was composed using a finite element method to simulate signal transport through the hydrogel, and simple mass-action kinetic equations to simulate the resulting protein expression over time.

Thesis Supervisor: Paul Matsudaira
Title: Professor of Biology and Biological Engineering

Acknowledgments

The ability to indulge myself by spending the past 7 years doing experiments was both a gift . . . and a curse. I have been given essentially unrestricted use of cutting-edge equipment and facilities, as well as the opportunity to interact with scientists and fellow grad students representing the top of their fields. For this incredible opportunity, I'd like to thank my adviser, Paul Matsudiara.

I'd also like to thank the members of my committee, Pat Doyle, Jay Han and Joel Voldman, who have provided useful and accurate criticism when I desperately needed it. Points they have made have strengthened me as a researcher, as well as this work.

I'd also like to thank my collaborators in the Timp lab at the University of Illinois at Urbana. Science in the family business, and this project originally arose over discussions at family dinners – where we couldn't escape the table for fear of being press-ganged into dishes duty. My father, Greg Timp provided advice and support for the project, while my sister helped with some of the biological aspects, and my brother the optical aspects. Of course, my mother, Helen Timp, acted as the administrative assistant for the lab - ordering us the parts we needed, and all in all being the best AA that it is possible to have, as she also provided baked goods at opportune times. And of course, I have to thank the Uzbek postdoc that has worked tirelessly on this project overall project, Utkur Mirsaidov.

My fellow grad students in Boston also helped, providing advice as well as support. The triumvirate of myself, Barney Tam and Mekhail Anwar have been together for the past 6 years, each of us going through similar trials and tribulations. Mekhail in particular has provided useful advice on this project, as he has an opinion on everything, which most of the time happens to be, unfortunately, correct. Other more recent grad students, like Michael Murrell and Mariya Barch, have proved worthy additions and successors to the triumvirate, as we separate to different cities and

I'd also like to thank the undergrads, technicians, and postdocs who have worked with me over the years. In particular, undergrads Rowena Mittal and Ben Zeskind, both of whom are now in, or through, grad school, provided me substantial aid at vital

points in my project. Yelena Freyzon lent her incredible knowledge of microbiology to me for my work in plasmid construction and design. Finally, Dr. Muhammad Zaman, with his friendly, yet incisive criticism helped to guide me to the heart of many issues.

Last, but certainly not least, I'd like to thank my girlfriend, Elizabeth. Though she complains little, I know that my PhD has been almost as hard on her as it has on me, and I appreciate her constant support. I can honestly say that there is no way I could have done this without her.

Contents

List of Figures

Chapter 1

Introduction

"No man is an island, entire of itself; every man is a piece of the continent, a part of the main."[57] Though John Donne was describing the impossibility of human isolation, his comment is equally applicable to the study of cellular biology. A cell does not exist in a vacuum, rather it interacts heavily with its environment. An elaborate network of communication guides the behavior of a cell, allowing coordination of behavior to benefit the organism as a whole. Signaling networks control growth, differentiation, chemical production, immune response and wound healing, forming an integral part of multicellular life.

What kinds of interactions do cells have with their environment? First, one must consider the type of environment cells typically are exposed to *in vivo*. Are cells usually on a planar glass substrate, supported by a serum-rich, carefully balanced media? No, rather they are embedded in a stroma composed of different extracellular matrix (ECM) proteins and sugars, with nutrients diffusing throughout. The makeup of the ECM has an effect, both mechanically and chemically, on cellular function. If cells are placed in an effective ECM analog, they demonstrate different signal cascades, different responses depending on the distribution of cues in their local environment.[85, 47, 83]

The extracellular matrix is not the whole story, however. Neighboring cells also have a strong influence on a cell's behavior. Cells exist within a specific social context, both influencing and being influenced by other nearby cells. In a natural environment,

all cells are not necessarily a phenotypically identical population, rather they may hold different differentiated states. In fact, certain cell types, such as hepatocytes, cannot maintain their viability and function without a second cell type.[25]

Cells may even be of vastly different species, as in immune response or certain symbiotic relationships(*Rhizobium* and legumes; *V. Fischeri* and *E. Scolopes*).[56, 145] In fact, a typical adult human is composed of 10^{14} cells, of which only *10%* are actually human cells![149] The vast majority are parasitic or symbiotic cells which have colonized the organism.

Finally, it is important to measure aspects of cell-cell signaling on a small scale, dealing with few or small numbers of cells. One might consider than an easy way to determine the behavior of cellular interactions would be to simply through the cells in question into a test tube or culture dish in equal ratios, then determine their behavior. This idea is flawed for several reasons. First, the cells will saturate the growth media with signal, and at the same time not build up the concentrations in the right spatial/temporal pattern. In order to detect subtleties of cell behavior, it is desirable to look at isolated populations of cells

Traditional methods of assaying gene expression/cell behavior have worked on bulk populations. Specifically, time-resolved methods like fluorescent or luminescent plate detectors gives information about dynamic behavior of populations. Flow cytometry gives information about single cells, but prevents monitoring the same cell over time.

1.1 Cell Substratum

The majority of *in vitro* cell biology experiments have cells either suspended in solution or adherent to a glass substrate. Which one depends on the cell type, and the type of assay being attempted. There are several problems with having cells in this type of environment.

1.1.1 Soluble Signals

Cells in solution or cells on a glass substrate both are exposed to soluble signals through advective transport. The transport of soluble signals in such a system is determined by:

$$\frac{\partial C}{\partial t} + \mathbf{v} \cdot \nabla C = D\nabla^2 C \qquad (1.1)$$

where C is the concentration of the signal, t the time, $\mathbf{v}$ the velocity of the solution flow, and D the diffusion coefficient. In any macroscale ($>$1mm) unsealed container, there is substantial flow due to temperature gradients (Rayleigh-Bénard convection)[52], evaporation[141], surface tension (Bénard-Marangoni convection)[37], or even physical motion of the sample/sample holder. In contrast, in most extracellular substratum, diffusive transport is the dominant mechanism, reducing the governing equation to:

$$\frac{\partial C}{\partial t} = D\nabla^2 C \qquad (1.2)$$

This causes many changes in both the temporal and spatial distribution of soluble signals in standard culture conditions, as compared to *in vivo*.[173] Perhaps more importantly, it allows for local variation in signal concentration, allowing for gradients to be formed.

Changes in the soluble signals can have other important affects on cell behavior. Advective transport moves large molecules as fast as small, meaning that the cells do not see the expected difference on large peptide signals compared to smaller hormones. The rate of signal clearance also affect autocrine signaling, the ability of cells to signal themselves. Since signal is washed away rapidly, the cells don't locally build up the signal they themselves are producing.

The dominant transport mechanism, specifically the clearance rate, is a factor in systems such as bacterial "quorum sensing". In this system, bacteria are able to coordinate their efforts and determine their environmental conditions by releasing and sensing autoinducer molecules. Bacterial cells detect the buildup of this chemical in their surroundings, and modify their phenotype accordingly.[15] This buildup can be due to a large population of cells in the area, as would be expected from the term

quorum. However, a buildup of chemical may also occur due to a lack of flow. Constrained signal transport due to an extracellular matrix or gel like microenvironment will allow for a faster buildup than a environment with flow.[139, 61]

In order to better control the soluble signal concentration, cell biologists and bioengineers have recently begun experimenting with new culture systems and platforms. One type of platform is microfluidics. The length scale of microfluidics damps out undriven flow, keeping diffusion the dominant mechanism of mass transport. Another method is by encapsulating the cells in an extracellular matrix analog, either naturally derived such as collagen I or Matrigel™, or a polymer-based hydrogel such as poly (ethylene glycol) diacrylate.

1.1.2   Bound Signals

Soluble signals are affected indirectly, by the nature of the confined porous hydrogel that most ECM is composed of. The ECM itself also presents signals to the cells, as part of its composition. When sitting on a flat glass substrate, the cells are able to feel various adhesion and serum proteins that have adsorbed to the glass surface. Since they see no such proteins above them, they demonstrate a top-bottom polarization. In the case of ECM, the cells are exposed to ligands all around them, preventing polarization, and actually changing the gene expression of the cells.

To better simulate the *in vivo* microenvironment, cells may be placed in an extracellular matrix analog, as previously mentioned. For example, Flaim et al. have formed cellular microarrays on a combinatorial mix of different ECM proteins, determining the difference in behavior for different ECM formulations.[65] They demonstrate a dramatic difference in both embryonic stem cell differentiation and albumin production, depending on the bound signals presented to the hydrogel.

Moreover, the communication between ECM and cells is not a one-way street. Cells respond to ECM signals, but then secrete or destroy ECM, reshaping their environment in order to signal other cells or to move within their environment. Careful engineering of the hydrogel chemistry, by adding in proteolytically sensitive peptides, allows for study of this behavior.[135]

Cells on Glass   **Cells in Collagen**
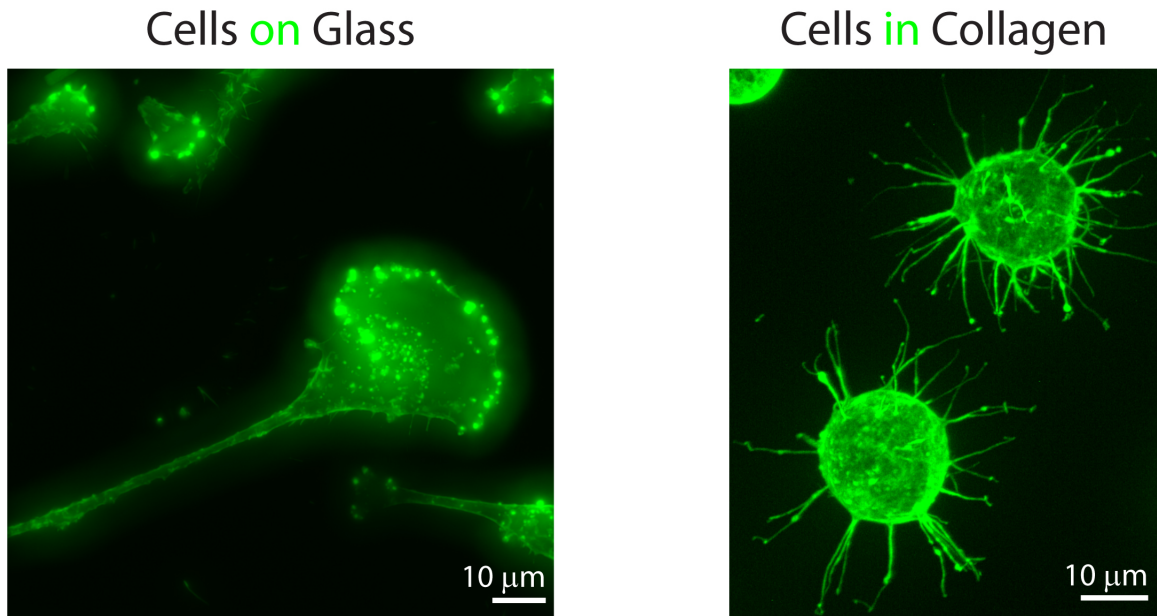
Figure 1-1: Comparison of cells on a flat glass surface to cells embedded in a ECM analog: (left) IC-21 cells stained with fitc-phalloidin on a glass surface (right) IC-21 cells stained with fitc-phalloidin in a collagen I matrix(1 mg/mL)

Tumor cells also modify the extracellular matrix to aid in their own development. If extracellular matrix which has been "trained" by tumor cells is used to harbor non-tumorogenic cells, the ECM modules the neoplastic potential of the cells. Barcellos-Hoff et al. have shown that in irradiated animals, a cleared mammary fat pad displays tumorigenic properties toward a susceptible cell line(COMMA-D).[13]

Certain types of cells require this communication in order to live and/or remain properly differentiated. Chrondrocytes loose some of their differentiated functions when placed in a monolayer 2D culture. However, if subsequently returned to a 3D culture, Benya et al. found that the differentiated phenotype could be restored.[20]

1.1.3 Substrate Stiffness

Cells are also able to detect the stiffness of the surface, exhibiting a relatively well characterized phenomenon known as *durotaxis*. A glass substratum has a stiffness of approximately E $\approx$ 76 GPa, whereas in a normal extracellular matrix, the stiffness is E $\approx$ 200 Pa, a difference of 8 orders of magnitude. Cells in different gel stiffness have

displayed different degrees of protein expression.[30]

The stiffness of the matrix also has a strong effect on cell behavior, as shown by Zaman et al. An assay for tumor cell motility in different concentrations of Matrigel^{TM}doped with fibronectin demonstrates a marked preference for softer substrates if matrix ligand is held constant.[174] Cells are able to move faster in less dense, softer 3D matrices.

1.1.4   Nonadherant Cells

Another problem which crops up in using 2D substrates is the difficulty of using nonadherant cells. Nonadherant cells are difficult to immobilize, and using a 3D matrix to hold them in place for study may help significantly.[94]

1.2   Heterotypic

Though cell biology has been able to obtain a vast amount of information from studying homotypic cultures, this is an incomplete view. This reductionist view of cellular biology allows for simpler experiments, with more control over the settings, but neglects important actors in which may guide cell behavior.

One example of this is in the case of cancer. It has been argued that looking at only cancer cells, with their accumulation of epigenetic and genetic factors, is not a reasonable approach to a deeper understanding of cancer mechanisms.[78] Indeed, if one considers the histopathology of a typical human carcinoma, the non-cancerous cells, or stromal cells, comprise up to 90% of the cells in the tumor mass.[164] Macrophages, fibroblasts, and other cell types all contribute to supporting tumor growth, as their signaling networks are hijacked by the cancer cells, and forced to do their bidding.[27, 134, 123, 171]

Perhaps most importantly in the case of cancer is the process known as angiogenesis. Once a tumor reaches a certain size, its growth becomes highly limited. Since a tumor has no vasculature, the transport of nutrients and waste, specifically O_2 is purely by diffusion, and once the tumor size reaches a characteristic size, about

18

200 μm, diffusion can no longer sustain it. The tumor then recruits endothelial cells in order to form capillaries, allowing the tumor to expand. This process is known as angiogenesis, and is a prime drug target for cancer therapy. If angiogenesis can be halted, the tumor size is limited, halting the growth of small tumors and even shrinking larger ones.[165]

Another example of a system where heterotypic systems are necessary is in studying hepatocyte function. Hepatocytes, or liver cells, actually require a second, support cell type in order to maintain their differentiated status.[24, 26] As liver function has a direct effect on several diseases and regulatory systems, and has a primary role in the drug clearance, the ability to have a working cell assay is vital. This is difficult without the use of heterotypic culture.

Even in 3D matrices, cell-cell interactions have proved important. A study by Underhill et al. demonstrated that, though hepatocytes were initially viable encapsulated in a poly(ethylene glycol) diacrylate (PEGDA) hydrogel, their viability was depressed over time. If cultured in patterned aggregates of 3T3 fibroblasts and hepatocytes, the viability was dramatically increased, demonstrating long-term albumin production(a common measure of hepatocyte function).[73]

1.3 Positioning

Not only is it important to place cells in 3D, and to have different types of cells, but the cells have to be organized into controlled patterns. In order to determine the effect of the cells on each other, to control their microenvironment, the position of the different cells relative to each other must be controlled. The shape and strength of the gradient will be defined, to a large degree, by this positioning.

In vivo, there are several different length scales over which cell behavior is affected. Sub-cellular structures (1-10 μm) affect the cellular environment, cell scale structures (10-100 μm) affect cell-cell interactions and supracellular structures (100-1000 μm) affect the overall tissue organization of the cells - their ability to work as one.[26]

There are several ways to pattern cells in two-dimensions, through use of various

surface chemistries to selectively modify a surface. For example, following Berg et al.[21] we have been able to chemically modify a surface to generate cell-exclusive and cell-adherent areas. If this surface is then seeded with cells, a pattern of cells then emerges. Chemically patterned surfaces of this kind may be formed easily through soft lithography[88, 46, 36, 175] or photolithography[23, 89, 104], among other methods.[144]
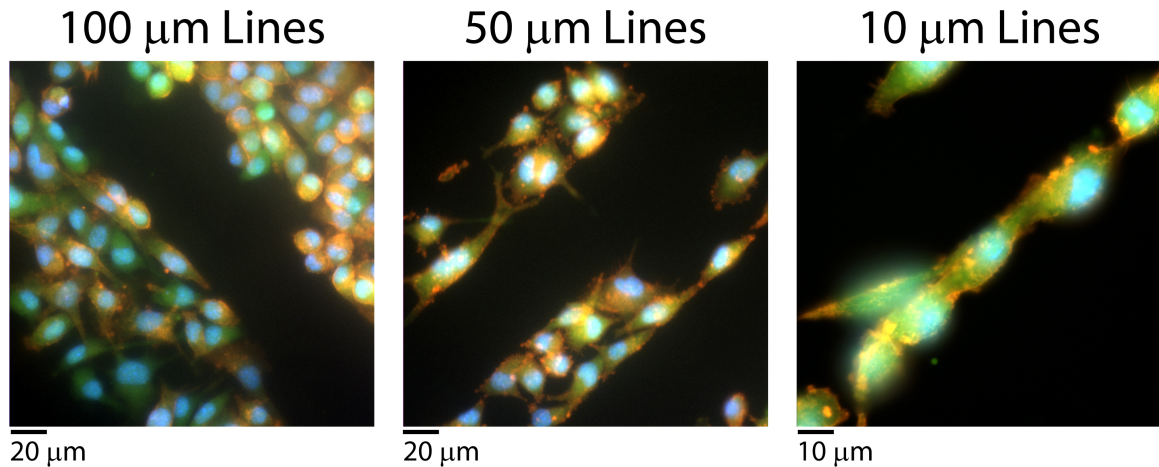
Figure 1-2: IC-21 cells patterned using polyelectrolyte multilayers; stained with Hoechst 33342 (blue; nuclear stain) CMFDA (green; volume stain) and Texas Red phalloidin (red; actin stain)

It is possible to have even finer control, using microfluidics to deposit cells only in certain areas. The advantage of microfluidics, with its low Reynolds number flow, or Stokes flow, is that the flow neglects effects of inertia, allowing for precise control of flows. Mixing is essentially absent, allowing flows to position cells precisely with respect to one another, even heterotypically.[66]

However, if we wish to pattern cells in a hydrogel, in three-dimensions, a different technique is needed. One popular method for cellular patterning in hydrogel is to use photopolymerizable hydrogel. Cells are placed in the pre-polymer mixture, then polymerized in a certain pattern using a mask. Using a system of polymerizing and washing, a pattern of different cell types can be built up. This technology's resolution is limited to a scale on the order of 10 μm, or the size of a small gel spot. What's more, there is no way to guarantee that a cell will be present in the gel spot, let alone

where in the gel spot a cell or multiple cells will be in relation to each other.[104, 93]

When combining this technology with other finer resolution patterning techniques, such as dielectrophoresis or optical trapping, cells may be patterned within the pre-polymer mixture, then the hydrogel may be polymerized around them, encapsulating the cells and holding them in place.[2, 1]

In fact, positioning cells in clusters together has been able to modulate their gene expression. Albrecht et al. has shown that by clustering chrondocytes close together in a hydrogel matrix, their production of extracellular matrix components is modulated.[3] The larger the cluster of cells, the less matrix material they synthesize, demonstrating the modulation of gene expression by cell-cell interactions.

1.4   Cell Populations vs. Single Cells

Cell measurements usually involve large populations of cells, which obscures more subtle variations of small groups of cells which may control overall behavior. Stochastic variations, variability which occurs locally, these effects are all neglected on this scale.

In general, biology tends take to take a relatively simplistic view of this complicated system. Cell biologists observe a single type of cells, a homotypic culture, in large numbers, and try to determine the behavior of cells from this bulk population in a 2D environment. Though these measurements have provided an *enormous* amount of information thus far, new techniques have recently become available which allow for more sophisticated measurements.

Flow cytometry or high-resolution microscopy may be used in order to gather single-cell data.[55] Though flow cytometry allows for massive throughput and single cell analysis, it does not allow spatial analysis of protein location within the cell, nor does it allow time-resolved behavior of individual cells. Microscopy on the other hand has a far lower throughput, even with the aid of automation, but allows the collection of time-resolved data. Localization of the fluorescent reporters within the gel is also possible using microscopy.

In order to detect production of soluble products, fluorogenic substrates are often used to detect production rates. However, it is extremely difficult to assay the behavior from cell to cell, rather, a overall production rate for the cell population can be obtained. This is a flaw with any measure of soluble signal production. Cai et al. have solved this by using a microfluidic to confine individual cells to small fluidic chambers, and measuring the soluble signal production per chamber.[32] The burst like gene expression results they observe would be completely masked in a larger population. Microfluidics allow for isolation of individual cells, and monitoring their behavior over time.

1.5 Summary

Overall, it is desirable to create a system which allows for precise positioning of cells in a 3D hydrogel substratum which is biocompatible. The microarrays should have the potential to be heterotypic, to allow investigation of some of the more complex cellular interconnects which form in physiological conditions. Finally, the cell microarrays should be chemically and mechanically isolated from each other, in order to assure that any stochastic or small group effect is detected, not lost in a bulk measurement.

Chapter 2

Photopolymerizable Hydrogel

2.1 Introduction

Most cell assays are, for simplicity's sake, performed on a glass surface. This glass surface is sometimes chemically treated treated, and often kept under carefully monitored environmental and fluid flow conditions. But in the end, it is a 2D stiff (E≈ 76 GPa[42]) surface with advective transport the dominating mechanism($Pe \gg 1$).

Compare this to the *in vivo* microenvironment of a cell. Cells are usually encapsulated within a squishy (E≈ 200 Pa[128]) three dimensional hydrogel. This hydrogel prevents flow($Pe \to 0$), making diffusion the dominant mode of transport, as well as presenting various bound ligands to the cell for contact signaling. This can markedly change cell behavior, altering the phenotype drastically, even changing the morphology(see 2-1)of the cell.[48, 20]

There has even been evidence that the stiffness of the hydrogel has an effect on the cell's ability to locomote[174]. So, in order to study cell behavior in a reasonable, *in vivo*-like environment, we want to be able to place cells in a hydrogel.

Several different hydrogel options are available which can provide the key features of diffusive-only transport, appropriate Young's modulus, and 3D environment.[107] First are the natural hydrogels, such as Matrigel$^{\text{TM}}$, a basal lamina analog purified from a mouse tumor. This gel is a liquid at 4°C and polymerizes within 1 hour at 37°C.[17] This gel has been used extensively for experiments involving 3D culture,
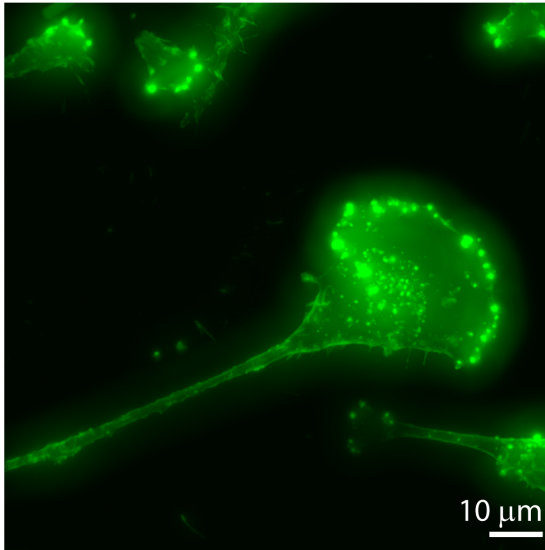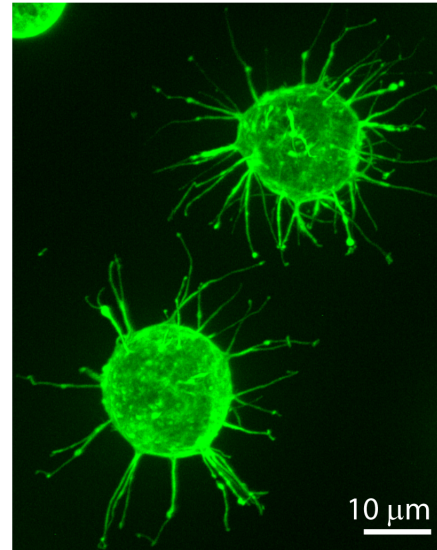
Figure 2-1: IC-21 cells stained with fitc-phalloidin: cells on the left are on a glass surface, cells on the right are in a collagen I matrix(1 mg/mL)

but as it contains many different natural growth factors, it is difficult to quantify cell-signaling behavior within.[101, 155, 172, 147]

Another option is to use a protein based hydrogel. Collagen I, the primary constituent of extracellular matrix, is another attractive material for use as a hydrogel.[122] The basic structure of collagen is a trihelical strand, which self-associates to form a more stable collagen fiber, which may be controlled by adjusting the pH and temperature. Collagen fibers and scaffolds may be adjusted with various chemical crosslinkers, or the addition of other proteins to change the mechanical properties or density of bound ligands[59].

A third option is to use a polymer-based hydrogel. Several different polymer chemistries which can produce biocompatible hydrogels have been explored in the literature.[94, 93, 135, 119, 4] A primary advantage of these methods is the ability to polymerize through means *other* than thermal polymerization. Thermal polymerization is relatively slow, and does not allow for precise control of the shape/size of the hydrogel. In contrast, photopolymerization, such as the kind allowed through free radical induced polymerization of acrylate based polymers, allows for precise control

of the shape and size of the hydrogel, while polymerizing quickly, in under 1 minute.

These gels may even be functionalized with peptides[93, 138] or whole proteins[4] to add bound ligands or other properties to the gel. With the appropriate, protease-sensitive peptides introduced into the hydrogel, the gel can be made degradable, allowing cells to cut through the matrix, to move through it or release bound signals from it.

However, it is vital to characterize these hydrogels, determining if the polymerization process itself negatively affects cell viability, or even function. The rates of nutrient and signal diffusion must be characterized, in order to be able to predict and control the behavior of cells in the gel.

To that end, we have attempted to determine the optimum conditions for polymerization of hydrogel for use in bacterial assays. We also describe a method for determining the diffusion coefficient inside the hydrogel, allowing for prediction of the various concentrations of chemical within the gel over time.

2.2 Methods

2.2.1 Cell Culture

For prokaryotic cell experiments, Escherichia Coli cells of the DH5α strain were used. Chemically competent cells of this strain were purchased(Invitrogen # 18258-012) and transformed with the GFP-M1 plasmid(see 2-2), henceforth called M1 cells. These cells were cultured on LB-agar plates using 100 μg/mL ampicillin as a selection marker, and grown up in M9-Glycerol media. M9-Glycerol is composed of : 0.2% (v/v) glycerol, 42 mM Na$_2$HPO$_4$, 22 mM KH$_2$PO$_4$, 19 mM NH$_4$Cl, 9 mM NaCl, 1 mM MgSO$_4$, 100 μM CaCl$_2$, 200 μM thiamine hydrochloride, and 0.2% (w/v) casamino acids. 100 μg/mL ampicillin is added to M9 media for use as a selection marker.

For eukaryotic cell experiments, Swiss 3T3 mouse fibroblasts were used. These cells were grown in DMEM media supplemented with 10% fetal bovine serum(FBS) and 50 IU pennicilin/50 μg/mL streptomycin. Cells were cultured at 37°C at 5%
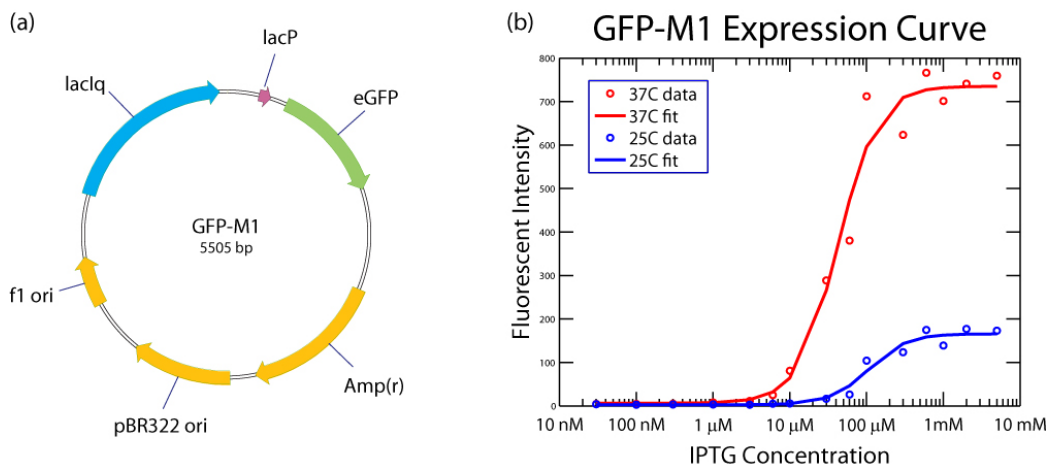
Figure 2-2: (a) The receiver plasmid, GFP-M1. It combines the lac operon with green fluorescent protein (GFP). Induction by IPTG initiates GFP production. The resulting fluorescence is used to indicate an active cell metabolism. (b) Fluorescent signal from M1 cells for various concentrations of IPTG at 25°C and 37°C. Curves were constructed from average fluorescence from individual bacteria measured using flow cytometry. The IPTG threshold estimated from a fit to the data is 24 μM.

CO_2, detaching with trypsin(0.05%) and splitting 1:5 every 3 days, preventing cells from reaching confluency.

2.2.2   Polymer Solutions

In these experiments, two different weight monomers were used, different repeat numbers of poly (ethylene glycol) diacrylate (PEGDA). A low molecular weight, either 400 Da MW PEGDA (Polysciences) or 575 Da MW(Sigma), and a high molecular weight, 3400 Da MW PEGDA (Nektar Theraputics now Laysan Bio).

High molecular weight PEGDA was dissolved in either 1X PBS(for mammalian cell work) or M9(for bacterial work). It was dissolved at a concentration of 10-20%(w/v). Lower molecular weight PEGDA was mixed with 1X PBS or M9, at a concentration of 10-20%(v/v).

Two different photoinitiators were tested: 2,2-dimethoxy-2-phenyl-aceophenone (Sigma)(Trade name Irgacur 651) and 2-hydroxy-2-methyl-propiophenone (Sigma) (Trade name Darocur 1173). Irgacure 651 was used dissolved in 1-vinyl-pyrrolidinone,

and Darocur 11179 was added directly to the pre-polymer solution.

2.2.3   Surface Treatment

Treating glass surfaces to enhance hydrogel adhesion was done with simple silane chemistry. The surface is treated with 3-(trimethoxysilyl) propyl methacrylate, composed as a 2%(v/v) solution in 95% ethanol, brought to pH 5 with glacial acetic acid (using 0.5%). After 5 min of treatment, it is then washed with 18 $M\Omega$ deionized water. The surface must be used soon after the treatment, as the surface degrades within approximately 4 hours of treatment in our hands.

2.2.4   Pattern Polymerization

A masked flood UV exposure was used to create a large scale pattern of hydrogel. A transparency mask was produced using a high-resolution printer[54]. This mask was then taped to the bottom of a Mattek dish. 100 μL of 10% 575 MW PEGDA/0.2% D1179 mixture was added to the dish. The mixture was then polymerized with a 30s exposure of light from a large UV lamp(UVP Model# B-100 AP/R). Finally, the mask was then removed and the pre-polymer solution rinsed off.

Spot exposure was accomplished with UV light coming from below. From below, polymerization is initiated by focusing light originating from a metal halide lamp(Exfo X-Cite 120), filtered with a 360/50 nm filter, through a Zeiss 200M microscope. Using a 100X objective, the spot size is approximately 100 μm in diameter.

2.2.5   Diffusion

To generate spots for the diffusion measurement, a pre-polymer solution of poly (ethylene glycol) diacrylate in M9 media was prepared at 5% (w/v) concentration, with 0.2% (v/v) 2-hydroxy-2-methyl-propiophenone photoinitiator. For alignment purposes, 1 μm fluorescent beads were added to a final concentration of $10^8 \frac{beads}{mL}$. The solution was then vortexed for 15s.

Using 100 μL of this solution, PEGDA spots were polymerized for 3s with 360nm UV light in an ibidi Slide VI. The channel was then washed with 300 μL of M9 media, and the resulting gel spot placed on a laser scanning confocal microscope. The gel spot was located using the fluorescent beads embedded within it. Once the gel spot was found, a 3D stack was taken for reference.

The microscope was then set to line scanning mode, scanning through the center of the hydrogel spot. Line scanning mode was used due to its high time resolution, with a scan being taken every 3 milliseconds or so. While taking line-scanning data, a 50 μM concentration fluorescein solution, was flowed into the channel. The fluorescence profile was recorded until the hydrogel spot reached equilibrium with its surroundings. A final 3D stack was then taken to ensure the spot remained intact.

2.2.6   Bacterial Viability Testing

To generate spots for bacterial viability testing, we used M1 cells. The cells were cultured overnight in 5 mL of M9 media at 37°C with agitation on an orbital shaker. The next morning, the cells were diluted 1:10, then allowed to grow at 25°C until they reached an OD_{633} of approximately 0.3, or mid-log phase. 1 mL of these cells was centrifuged 3 times for 5 min at 800g. Between each spin cycle the supernatant was aspirated, and the bacterial pellet resuspended in 1 mL of M9 media. Finally, after the final spin down, the pellet was resuspended in a pre-polymer solution of PEGDA and photoinitiator in M9.

The solution was placed in a Mattek dish, and placed on a Zeiss 200M inverted microscope. UV light from a metal halide lamp(Exfo X-Cite 120) filtered with a 360/50 nm filter, stopped down to various powers, was used for approximately 1s to polymerize the gel spots. The gel spots were then washed 2x with clean M9 media.

Fluorescent protein production was used to determine cell viability after hydrogel polymerization. First, 10 mM IPTG was added to the Mattek dish, in order to induce gene expression of GFP from the M1 cells. This provides a measure of cell metabolism from the cells, indicating viability.

2.2.7 Eukaryotic Viability Testing

To generate spots for eukaryotic viability testing, we used Swiss 3T3 mouse fibroblasts. Cells from a 25 cm^2 flask were detached with 1 mL of 0.05% trypsin for $\leq$5 minutes at 37°C, then brought up to 5 mL with DMEM media. The cell solution was centrifuged at 600g for 5 minutes. The supernatant was aspirated, and the cells were resuspended at 1×10^6 cells/mL concentration. This cell solution was then added to a pre-polymer solution for a final concentration of 5% (w/v) of 3400 MW PEGDA and 0.2% (v/v) Darocur 1179. The cells were polymerized for 10s using a 10X Zeiss Plan-Neofluor objective.

2.3 Results

2.3.1 Polymerization

Poly (ethylene glycol) diacrylate (PEGDA) is a linear polyether terminated with acrylate groups, having the general structure:
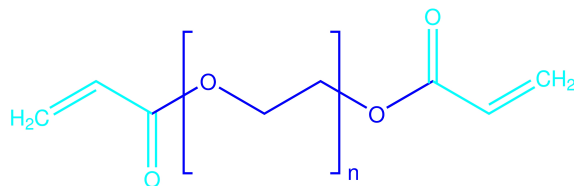
Figure 2-3: Chemical structure of poly (ethylene glycol) diacrylate, with acrylate group colored cyan, and the PEG polymer colored blue.

In order to create PEGDA from poly (ethylene glycol), a PEG solution can be derivatized by a simple overnight reaction with triethylamine and acryloyl chloride under argon.[45]

To generate the activation energy required for polymerization, various different chemical mechanisms may be used. In the case of photopolymerization, a photoinitiator absorbs light at its characteristic wavelength, generating a free radical. This method is used extensively in industrial and medical applications, due to the precise
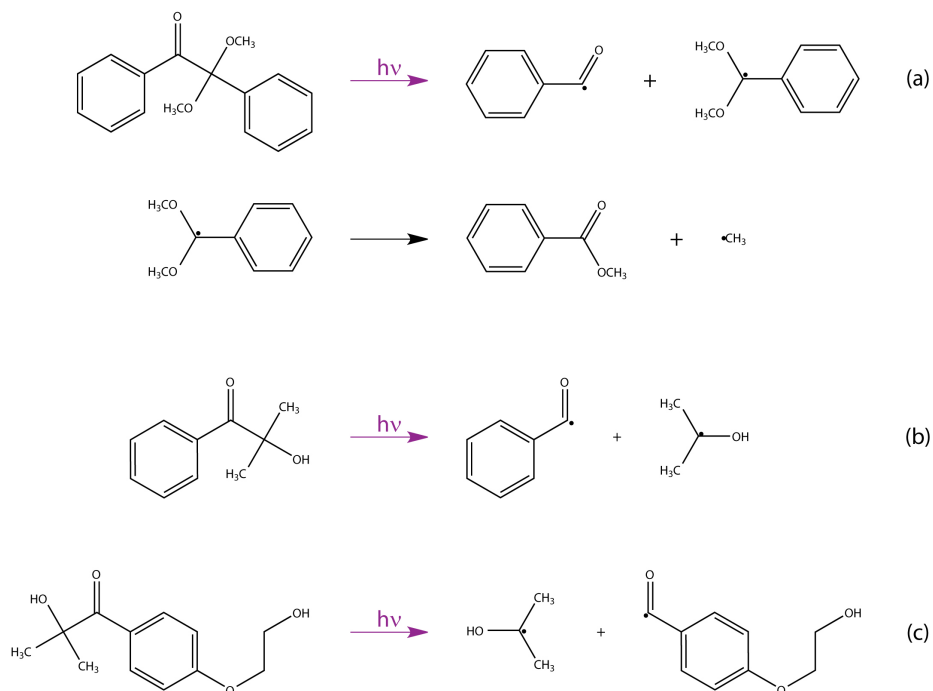
Figure 2-4: Photoinitiator free radical generation: a) Gauger 651 cleavage by UV light - there is a post cleavage reduction of one of the free radicals to a methyl radical; b) Darocur 1159 cleavage by UV light; c) Darocur 2959 cleavage by UV light.

spatial control over the area of polymerization, as well as the rapid polymerization rate.[119]

Photoinitiators we used in this experiment generate free radicals through photocleavage, breaking apart. Different photoinitiators produce different free radicals, as shown in 2-4, which will have different reactivity and diffusion constants.

The photoinitiator free radical attacks the carbon-carbon double bond of a PEGDA acrylate group, breaking the bond and giving the acrylate a free radical. This free radical then reacts with another PEGDA molecule, causing that acrylate group to gain a free radical of its own, forming a chain reaction, shown in 2-5.[112]

This polymerization chain reaction can be terminated in one of two ways. First is through reaction of a PEGDA radical with another PEGDA radical. This can happen through either combination, where two PEGDA radicals join together, or disproportionation, where the PEGDA molecules transfer a hydrogen, loosing their free radicals in favor of one molecule having a double bond, and the other a single

30
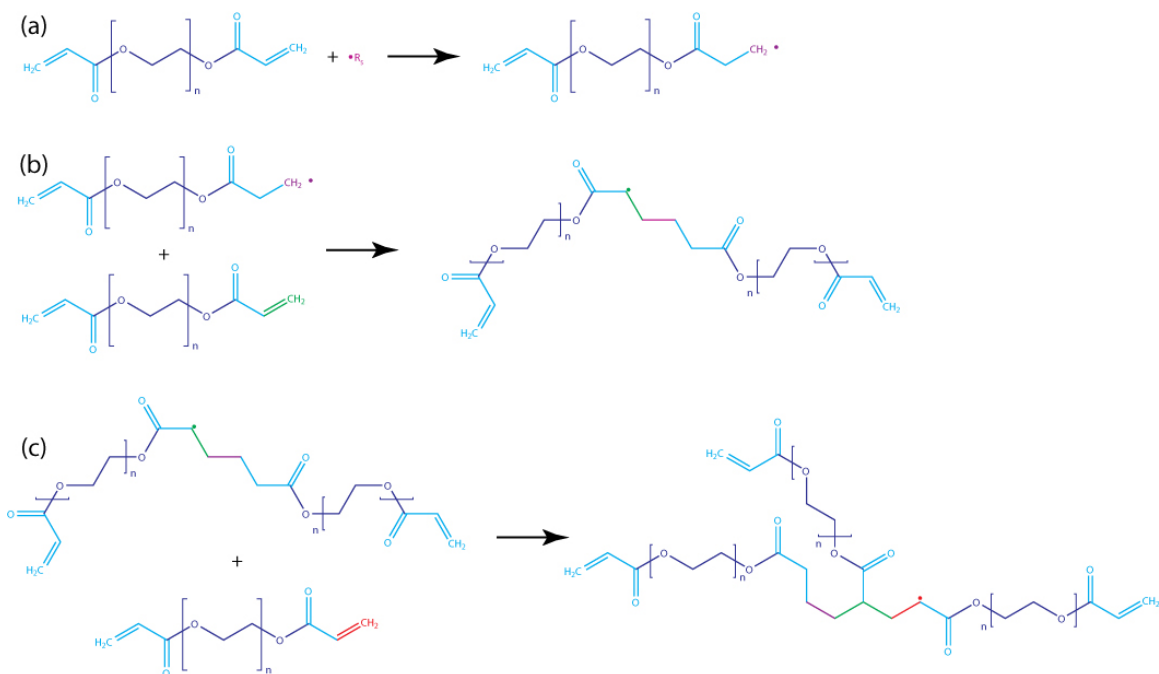
Figure 2-5: Mechanism of PEGDA polymerization. (a) The photoinitiator free radical(purple) reacts with the double bond of one of the acrylate groups on the PEGDA molecule, breaking the bond and forming a free radical. (b) This radical PEGDA molecule reacts with another PEGDA molecule(green), breaking its double bond and creating another free radical on the resulting molecule. (c) This process continues with a third PEGDA molecule(red), though it should pointed out that if the PEG chain is long enough, the molecules could react with themselves, rather than a new molecule.

bond(see 2-6(a)).[113] The second method of chain termination is through the reaction of the free radical with either a photoinitiator radical, or some other alkyl radical(see 2-6(b)). The photoinitiator molecule will also add through either combination or disproportionation.[113] The choice of combination or disproportionation is usually controlled by steric factors.

The most important external factor which may influence the polymerization process is the presence of molecular oxygen. Oxygen has a habit of scavenging free radicals, both from photoinitiators and from the forming polymer chain. This occurs through the reaction shown in 2-7, forming peroxy radicals which are inactive toward acrylate double bonds.[51] Oxygen reacts extremely quickly with carbon-based radicals ($\geq 10^9 \, M^{-1} \, s^{-1}$), implying that the reaction is limited only by the speed of
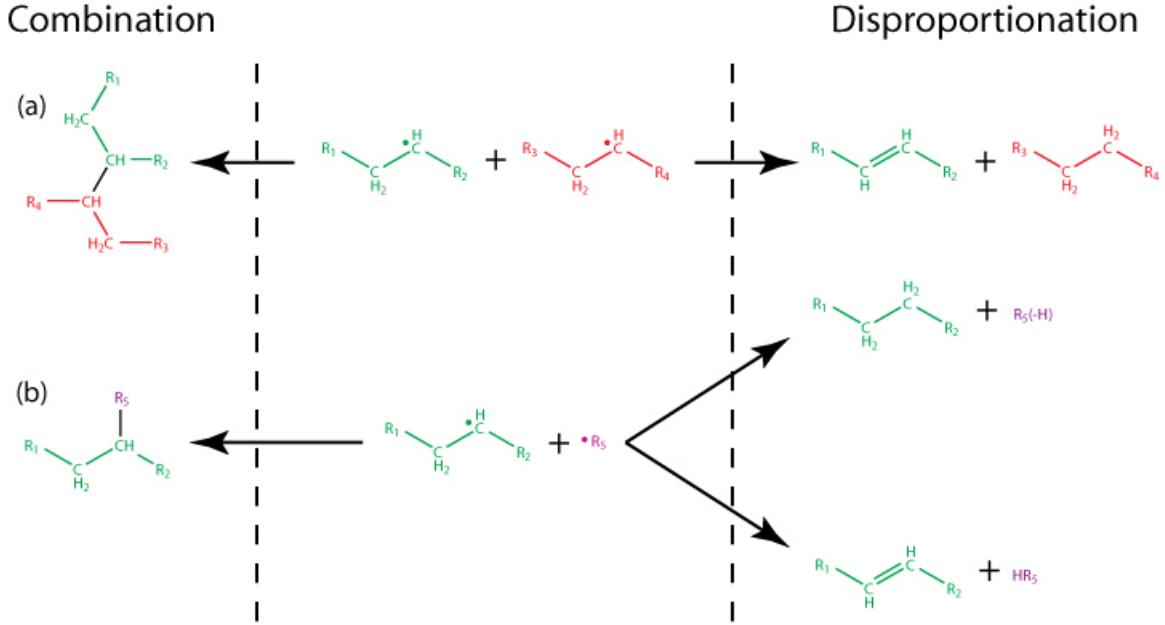
Figure 2-6: Mechanisms of free radical polymerization chain reaction termination. (a) Two PEGDA radicals react with each other, leading to either (left) a stable bond or (right) a stable single bond and a double bond which may react again. (b) A PEGDA radical and a photoinitiator radical. The photoinitiator may add to the polymer(left) or exchange a hydrogel with the PEGDA radical(right)

oxygen diffusion[114].

Considering this problem, the only way that polymerization can proceed is through the elimination of oxygen from the polymerization solution. This is effectively accomplished from the initial burst of photoinitiator radicals, which consume the oxygen dissolved in solution. However, if the layer is too thin or the solution too oxygenated, oxygen will outcompete the monomer for the photoinitiator radicals, and the polymerization will never begin. This problem may be ameliorated by degassing the solution prior to polymerization, or working under an inert atmosphere(N_2, Ar).

2.3.2 Patterns

Using a simple transparency mask, we have been able to create various patterns of this hydrogel. Since the transparency mask can be produced by a standard office printer, this allows for various shapes of sub-millimeter resolution[54] to be produced
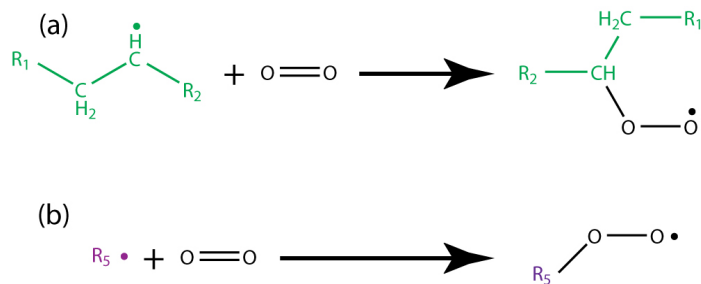
Figure 2-7: Oxygen can interfere with polymerization through the scavenging of free radicals. Either the polymer free radical(a) or the photoinitiator free radical(b) may be changed into peroxy radicals by O_2, which are unreactive in acrylate polymerization.

in a standard biological lab, without any special equipment, using only a standard office printer and a transilluminator or UV lamp. These types of gels might be useful in making cell microarrays.

Another possible method of patterning the hydrogel is the use of a fluorescent microscope. The DAPI filter, often present on biological use microscopes, uses a wavelength which can easily excite biocompatible photoinitiators. The DAPI filter and mercury lamp can be used to gel through the condenser of the microscope, or through the objective, whichever is more convenient. If the microscope is coupled to a motorized stage, patterns may be dynamically drawn in the hydrogel.

2.3.3 Diffusion Measurements

As the pore size of this hydrogel is around 1nm[45], it is difficult to get a direct measurement the distribution of pore sizes, or to understand *a priori* how mass transport will occur in this system. In order to characterize diffusive mass transport in our hydrogel formulation, a simple fluorescence scanning experiment was used to get an empirical estimate for the behavior of a typical small molecule in this hydrogel.

The rate at which a small ($\approx$1nm) fluorescent tracer was able to penetrate a hydrogel spot was measured using laser scanning confocal microscopy. By rapidly scanning through a hydrogel spot during the addition of the tracer, the concentration of the tracer as it diffuses inward may be observed.
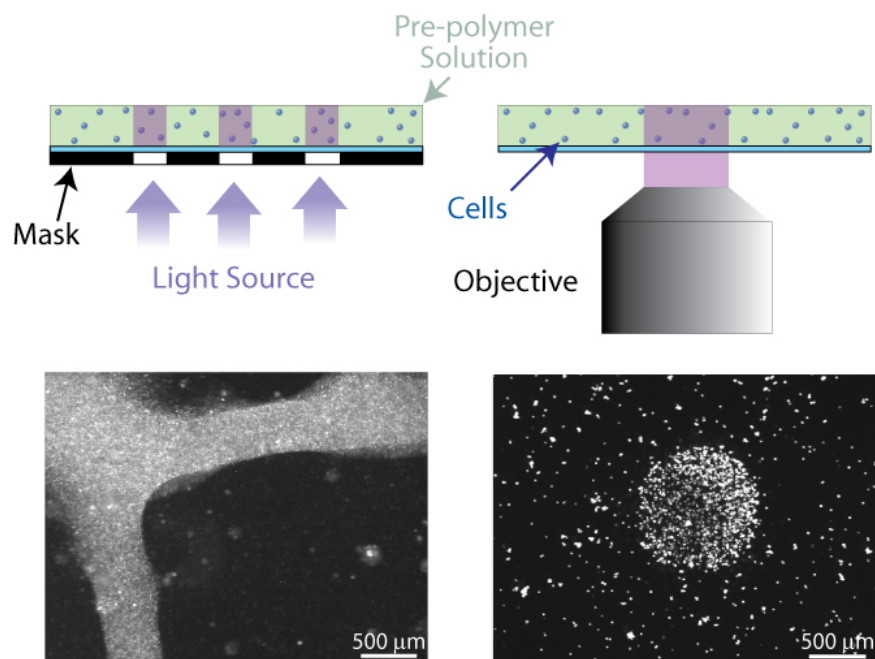
Figure 2-8: Two methods of UV exposure for patterned photopolymerization: (left) masking the UV light, in order to create patterns with a single exposure or (right) using a microscope objective to create a spot, which can build a pattern through subsequent exposures.

A molecule like rhodamine is especially useful, as it is of the same size, and hence transport behavior, as molecules of use for biosensors/signaling behavior, such as glucose, lactose, paraoxon, and AHLs(see 6-7).[146]

Using this fluorescence curve, along with a simple simulation of the hydrogel spot based on the dimensions given from the 3D stack, we are able to get a value for the diffusion coefficient of rhodamine inside the hydrogel spot. Using this analysis, we find that the diffusion coefficient is $4.6 \times 10^{-7} \pm 1.1 \times 10^{(-7)}$ in 5% 575 MW hydrogel and $8.0 \times 10^{-7} \pm 1.4 \times 10^{(-7)}$ in 5% 3400 MW hydrogel.

Others have measured diffusion coefficients of similar size tracers in similar hydrogels, as summarized in 2.1. They have used tracer penetration[146] or diffusion cells[45].
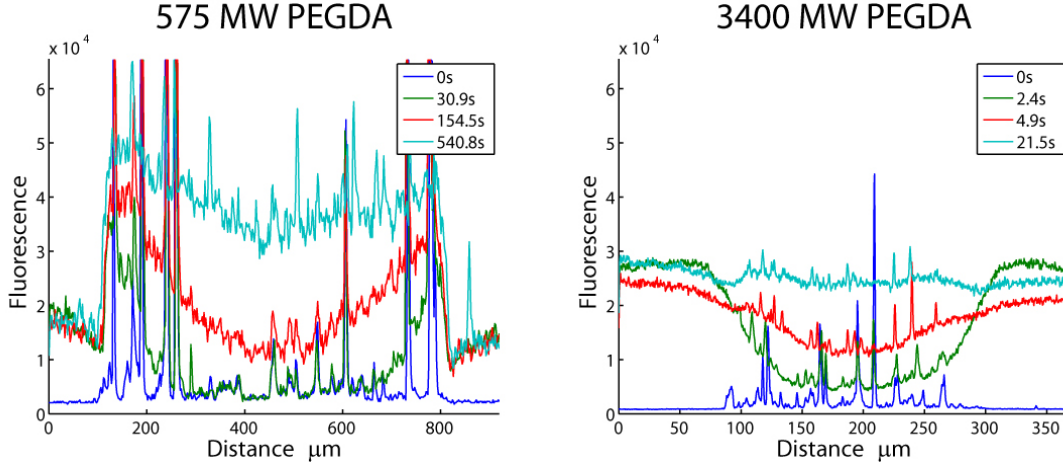
Figure 2-9: These graphs are representitive of the uptake of rhodamine into the hydrogel spot. The hydrogel is, at T=0s, at nearly zero fluorescence, with only the beads encapsulated in the gel spot registering signal. After the rhodamine is added, the concentration surrounding the hydrogel goes up dramatically, as does the edges of the gel. The rhodmaine tracer then diffuses inward, until it reached equilibrium. Traces from both a 5% 575 MW (left) and a 5% 3400 MW (right) hydrogel are shown.

2.3.4 Bacterial Viability

In order to minimize the effect of the hydrogel and its polymerization process on cell behavior, several experiments were done to determine the conditions under which M1 cells produced the most fluorescent protein. We accomplished this by varying two parameters: the formulation of the hydrogel and UV power dosage.

First, the different MW hydrogels, 575 and 3400, were assayed. Altering the

Table 2.1: Diffusion Values in hydrogel, theoretical and measured

Method	Tracer	Gel %	Gel MW	Value (cm^2/s)
Stokes-Einstein	1nm Tracer		Water	2.8×10^{-6}
FCS[79]	Rhodamine	Water/Methanol solution		$2.5 \pm 0.3 \times 10^{-6}$
FRAP[130]	Fluorescein		Water	2.7×10^{-6}
Rhodamine Penetration[146]	Rhodamine	20 % (v/v)	575 Da	3.8×10^{-7}
	Rhodamine	100 % (v/v)	575 Da	2.99×10^{-9}
Stokes Cell[45]	Vitamin B_{12}	10% (w/v)	4000 Da	1.6^{-6}
Timp Measurements				
Rhodamine Penetration	Rhodamine	5% (v/v)	575 Da	4.6×10^{-7}
	Rhodamine	5% (w/v)	3400 Da	8.0×10^{-7}

35
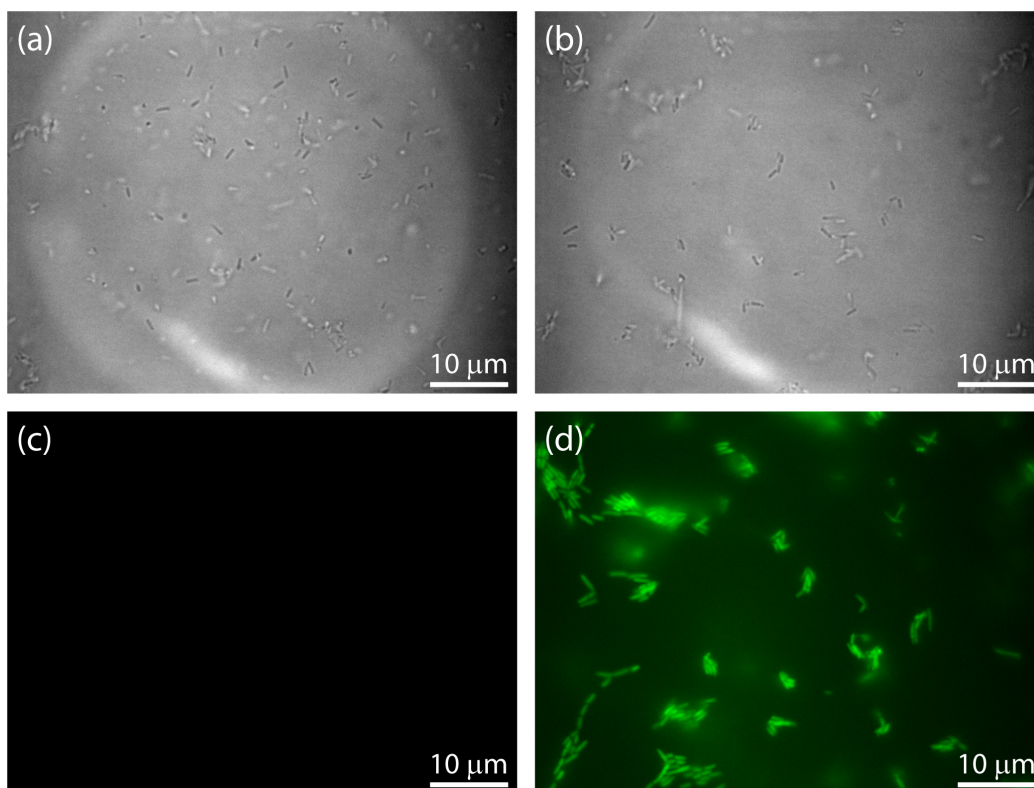
Figure 2-10: Cells encapsulated in lower MW PEGDA demonstrate a lower viability than cells in higher MW PEGDA. (a) shows a transmitted light image from a 575 Da MW PEGDA hydrogel spot, and (c) the corresponding fluorescence after 6 hrs. (b) shows the a transmitted light image from a 3400 Da MW hydrogel spot, and (d) the corresponding fluorescence after 6 hrs.

hydrogel monomer weight should change pore size, stiffness, and overall density of the gel. By encapsulating uninduced, unfluorescent M1 cells within a hydrogel spot, then inducing them with IPTG, we hoped to determine their viability, and utility for applications unambiguously. We found that cells in 575 MW PEGDA displayed no fluorescence after 6 hrs. By comparison, in 3400 MW PEGDA, cells were able to express significant amounts of fluorescent protein, and in fact began to reproduce within the gel.

We then focused more closely on 3400 MW hydrogel, attempting to optimize the amount of power needed for polymerization. Our Exfo metal halide lamp has a power limiting iris installed, which allows us to vary between 12.5%(0.072 mW), 25%(0.146 mW), 50%(0.373 mW) and 100%(0.856 mW) power. Gelling for approximately 1s

36
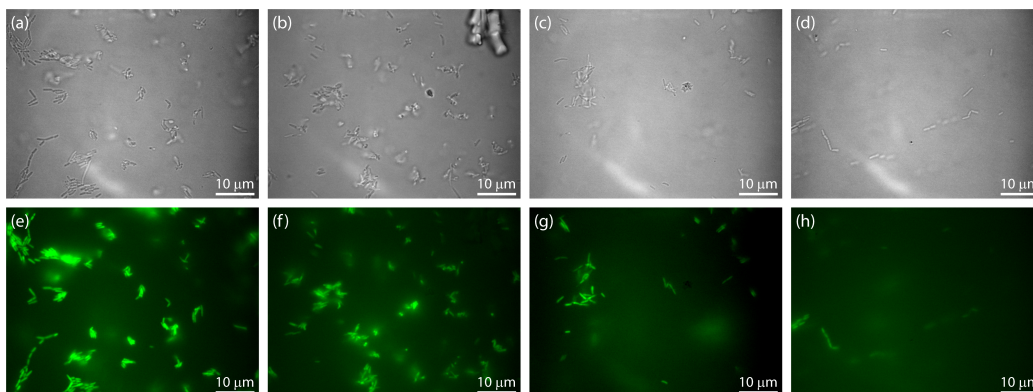
Figure 2-11: Higher power demonstrates lower cell viability: 12% (a) Transmitted (e) Fluorescent, 25% (b) Transmitted (f) Fluorescent, 50% (c) Transmitted (g) Fluorescent, 100% (d) Transmitted (h) Fluorescent.

each time, we found that after 6hrs of induction, cells with the lowest UV dose were glowing brightly. Fluorescence seemed to tend downward with increasing UV power.

2.3.5 Eukaryotic Viability

Initial eukaryotic experiments were done with NIH 3T3 cells using hydrogel spots formed using a microscope. These spots showed a dramatic dependence on the type of photoinitiator used, agreeing with results found in the literature[31]. The smaller and more mobile the photoinitiator free radical, the more harmful to cells.

Calcein AM(LIVE stain;green) provides information on metabolic activity, while propidium iodide(DEAD stain;red) indicates membrane integrity. We are continuing to explore the viability of different eukaryotic cell types. We also hope to create a fluorescent protein reporter for time-resolved viability assays in eukaryotic cells.

2.4 Conclusion

Poly (ethylene glycol) diacrylate hydrogel is a commonly used hydrogel for tissue engineering, drug release and biosensor applications. A full characterization of this hydrogel, with respect to its diffusion behavior for small molecules and the viability of cells encapsulated within, is necessary to use it for these applications. We have demon-

37
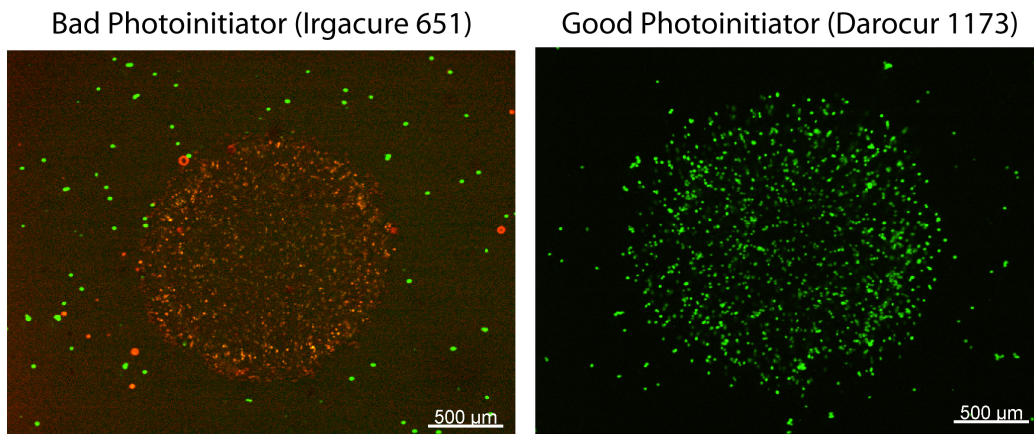
Figure 2-12: Two PEGDA gel spots, one formed with I651 as the photoinitiator, the other with D1179. The gel spots contained S3T3 cells, which were then stained with a LIVE/DEAD kit to show viability

strated that by minimizing the power of the UV light, and using a higher molecular

weight hydrogel, cells are able to live and express fluorescent proteins effectively.

Chapter 3

Optical Trapping of Cells

3.1   Introduction

Synthetic biology is striving to create artificial gene networks to program new cell behaviors.[16] And so, the functionality of a cell is being co-opted for the mass production of proteins; the development of new therapeutic drugs; biochemical and environmental sensing; and even computation.[16, 71, 120, 40, 126, 19, 136, 29, 64] But cells change the pattern of genes they express in response to signals from the environment. In eukaryotes, the extracellular environment plays a vital role in tissue development, differentiation, migration, and cancer. For example, the microenvironment in which cancerous tumor cells reside changes during tumorigenesis.[103] At the molecular level, tumorigenesis translates to different signaling requirements during various stages of growth. Therefore, controlling the environment that fosters and supports tumorigenesis is vital for developing therapies for treating the parasitic growth of a tumor.[103] And like eukaryotes, bacteria show evidence of the use of intercellular signaling to coordinate multi-cellular activity. For example, "quorum sensing" is a type of communication that requires a sufficient number of bacteria in the local environment to secrete a molecular signal, triggering the expression of target genes.[127, 111, 168, 72, 148] And finally, while some cell types express tissue-specific features in a two-dimensional (2D) culture system, it is apparent that a three-dimensional (3D) environment is required by others.[60, 92, 35, 117, 83, 77, 100, 47]

So, to fully exploit synthetic biology and elicit more complex behavior, the microenvironment of the cell has to be harnessed by emulating the social context and the extracellular matrix.

Living cell microarrays, assembled using optical tweezers in a synthetic hydrogel matrix, may provide a suitable platform for exploiting the functionality of the cell. Pioneering work by Ashkin demonstrated that optical tweezers could displace and levitate bacteria and viruses.[7, 8, 10, 12] We show that it is now possible to create heterotypic microarrays of living cells using optical traps for hierarchical control of the cell positions. We can manipulate hundreds of cells simultaneously with submicron precision into 2D and 3D arrays without loss of viability. The cells are positioned using a time-shared holographic array of three-dimensional optical traps produced through a novel combination of two diffractive elements, a spatial light modulator (SLM) and acousto-optic deflectors (AOD). While optical trapping allows for the creation of complex networks of cells resembling tissue, the trapping beam must be held on the cells to maintain the array. To fix the position of the cells permanently, we have supported the organized array with a biocompatible scaffold made from a photopolymerizable Polyethylene glycol diacrylate (PEGDA) hydrogel. PEGDA hydrogels are especially efficacious as a scaffold because the polymerization time can be relatively short ($\sim$3 seconds).[104] PEGDA hydrogels are also pliable, allowing for transport of nutrients to the cell and waste away from it. And they have demonstrated biocompatibility. Using photopolymerizable hydrogels,[104, 110, 94, 44] we have immobilized various cell types without loss of viability.

This is the first time that permanent, living cell arrays of such complexity have been synthesized. Previously, holographic arrays of optical traps have been used to permanently arrange up to 9 *E. coli* in gelatin,[86, 87] but the viability of the bacteria was not demonstrated. The extraordinarily long trapping time required to fix the position of a cell in gelatin ($\sim$60minutes) will adversely affect the viability. Others[104, 94, 2] have recently demonstrated living cell arrays with positional control from millimeters down to 50μm using photolithography or dielectrophoretic forces to form patterns of cells within a hydrogel, but they lack direct control over the density,

cell type, and positioning of individual cells. In contrast, we have assembled hundreds of cells into 2D and 3D heterotypic arrays permanently in a hydrogel scaffold and unequivocally demonstrated viability by measuring membrane integrity, protein production and metabolic activity. Moreover, the stringent accuracy and submicron precision of the cell placement that we achieve with optical trapping, which is preserved in the hydrogel, is an essential requirement for penetrating stochastic biological processes normally buried by bulk (ensemble) measurements. Thus, these complex arrays represent a new tool for the study of gene expression in live cells, affording rigorous control over the three-dimensional microenvironment of the cell.

3.2 Experimental Details

Networks of living cells were assembled with time-multiplexed arrays of optical tweezers formed using a novel combination of two diffractive elements, a spatial light modulator and acousto-optic deflectors, in conjunction with various objectives in an inverted optical microscope (Zeiss Axiovert 200), as illustrated in 3-1. Two different color lasers were used to form the optical traps: a 20W Argon ion laser operated single line at 514nm; and a CW TiSi laser, tunable from λ=850 to 900 nm.

Multiple time-multiplexed traps were generated in three-dimensions by using a combination of AODs (acousto-optic deflectors from AA-Optoelectronic) and an SLM (a spatial light modulator Hamamatsu X8267), which were each optimized for maximum diffraction efficiency at the wavelength of interest. A beam is deflected transverse to the direction of propagation using two orthogonally-mounted AODs to give independent control of the x- and y-positions of a trap, allowing for the creation of a 2D network of traps. The beam is time-shared between different positions in the 2D array: i.e. it is scanned rapidly from one trap position to the next, dwelling at the desired position in the array just long enough to illuminate an optical trap and fix the location of the cell. When the AOD deflects the beam to the next trap location in the array, cells that are not illuminated will diffuse from the target location and disperse. To prevent dispersal, the rate of deflection between trap positions is properly chosen
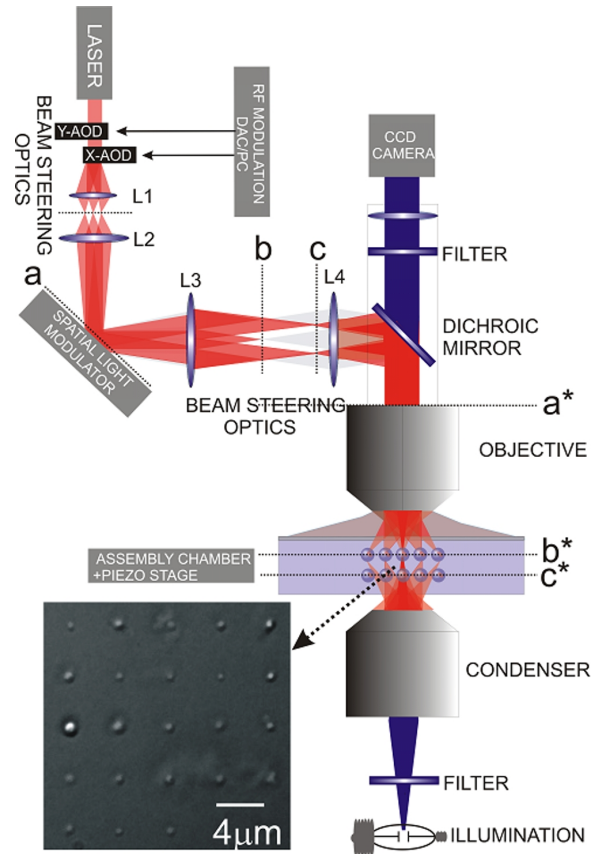
Figure 3-1: Schematic diagram of a time-shared holographic optical trapping apparatus. Trap arrays are formed using a high NA objective in a commercial optical microscope in conjunction with two acousto-optic deflectors and a spatial light modulator (SLM) to produce a time-shared (3D) array of optical traps. The plane of the SLM, **a**, is imaged into the microscope objective entrance aperture (OEA) **a***, and the corresponding planes **b** and **c** are imaged into the focal region of the microscope. The same microscope that is used to produce the cell traps is also used for viewing (via the blue beam). The inset in the lower left shows an example of a 2D 5x5 array of P. Aeruginosa formed using this apparatus and subsequently embedded in hydrogel. The distances are: AODs-L1=165 mm; L1-L2= 650 mm; L2-SLM =332 mm; SLM-L3=421 mm; L3-L4=1400 mm; and L4-OEA =493 mm, where the focal lengths are L1=150mm, L2=500mm, L3=1000mm, L4=400mm.

relative to the time the cell spends in the dark. The maximum allowable dark time depends on the diffusivity of the cell, the size of the array, the scan rate and dwell time.[116] The laser beam was deflected between trap positions at 100 kHz or 10 sec between traps. The dwell time of the trap over a particular position is variable, but is at least 10 sec.

42

Relay lenses were used to project the 2D array onto an SLM to create a 3D array. The SLM is an optically addressed nematic liquid crystal device configured to act as a phase hologram, using 256 gray levels. It has near-VGA resolution without sharp pixilation, which gives first-order diffraction efficiencies of approximately 40%. Effectively, the SLM was used to introduce phase shifts to implement a diffraction grating, offsetting the array transverse to the beam, and Fresnel lenses to offset the array along the optical axis.

The novel combination of an SLM with AODs has practical implications for assembling large arrays of living cells. Ostensibly, a time multiplexed strategy might preserve cell viability by minimizing beam exposure and the ensuing photodamage. Minimizing the photodamage is a prerequisite for producing viable living cell microarrays. It has been proposed that photodamage in the trap beam results from local heating,[106] two-photon absorption[22, 96] and photochemical processes leading to the reactive chemical species.[33, 118, 160, 161] Using temperature sensitive dyes in micron-scale liposomes, Berns and co-workers have eliminated local heating by a tightly focused CW laser as a photodamage mechanism. Berns measured a temperature rise of only 1.25°C per 10^7 W/cm^2 at λ=1064nm. On the other hand, Block showed that *E. coli* viability depends crucially on wavelength[118]-a change of 20nm in the wavelength from 850 to 870nm can affect the lethal dose by a factor of 3. To diminish damage, lasers in the near-infrared band are usually employed since a "biological window" for light exists in tissue for near-infrared wavelengths between 700-1500 nm. Light attenuation is governed primarily by scattering processes there.[160]

We hypothesize that minimizing the duration of exposure to the beam by time-multiplexing the optical trap will preserve viability (possibly even at shorter wavelengths). While continuous wave computer-generated holographic optical traps can be formed using an SLM[143, 133], the dynamical control required for time-multiplexing optical traps is limited by the slow refresh rate. A dynamic array can be created by encoding different holographic patterns into a reconfigurable SLM and time-sharing between patterns. But slow switching times characteristic of nematic liquid crystals

(~12Hz for the Hamamatsu) slows the refresh rate of the SLM. Therefore, the switching speed of the SLM affects the light/dark time spent on each dielectric comprising the array, which in turn limits the number of elements in the array and potentially affects photodamage. The switching speed also adversely affects the time required to steer dielectrics elements into an array since the speed of the particle's movement is not limited by the depth of the trap (relative to the Stokes drag). These constraints, combined with the relatively low diffraction efficiency (40%) and incident power limitations, may adversely affect the size and complexity of the array. In contrast with the SLM, AODs have a high diffraction efficiency (>70%) and permit high-speed (100kHz) dynamic control over the position of individual cells in an array while minimizing exposure to the beam. And due to the stability of the AODs, the position of each trap can be controlled with ±19nm precision.

So, we used the AODs to time-multiplex the position of the optical traps in a 2D array to take full advantage of the high-speed dynamics, while encoding a static phase grating on the SLM to introduce additional spatial variations in intensity (required to produce 3D arrays, for example.) To determine the phase distribution in the SLM plane (plane a in 3-1) required to produce the desired intensity distribution in the trapping plane, we used the Gerchberg-Saxton (GS) algorithm.[153] The GS algorithm, implemented in LabView 7.1 on a standard Pentium4 PC, uses an iterative technique to find a phase distribution that transforms a light field in a transverse plane a in 3-1 into the desired intensity distribution I_b^0 in another plane b in the far field. Starting with a beam with an intensity profile I_a with a uniform phase in plane a, which corresponds to a complex amplitude A_a, the complex amplitude of the beam at plane b is simply the Fourier transform. If the intensity distribution at b, namely $I_b = |A_b|^2$ is not the desired I_b^0, then the intensity distribution at b is replaced by I_b^0 without adjusting the phase in the plane of b. This change affects A_a-the inverse Fourier transform of A_b-and so the intensity distribution at a is no longer I_a. The intensity at a is subsequently replaced with the actual beam profile while retaining the new phase, and then the procedure iterates until it converges on the phase distribution at a that transforms the input beam with intensity I_a in plane

a through a phase hologram to an approximation of I_b in plane b.

Relay lenses were used to image the pattern emerging from the SLM onto the back aperture of the objective. The optical systems comprised of lenses L1 and L2, and L3 and L4 are both afocal: i.e. a collimated incoming beam will emerge collimated. The focal length of the lenses L1, L2, L3 and L4 and the separation between them are chosen so that a small deflection of the beam by the AOD results in a change only in the direction of the laser beam at the objective entrance aperture, without any change in position.[63] Typically, the trapping was done 5μm from the surface of the coverslip to minimize spherical aberrations from the aqueous media.

Three types of cells were incorporated into microarrays: two rod-shaped bacteria, *Pseudomonas aeruginosa* and *Escherichia coli*, and mouse fibroblasts, Swiss 3T3. *P. aeruginosa* is a gram-negative pathogen. Desiccated *P. aeruginosa* obtained from (ATCC# 17468) were rehydrated in *P. aeruginosa* selective broth (Fisher# MHA000P2P). The bacteria was cultured at a temperature of 26°C and passaged every 1-2 days. Samples were prepared by mixing 200 μL of bacteria solution with 800 μL of 1X PBS, and centrifuging at 10,000 x g RPM for 15 minutes. The supernatant was aspirated, and the pellet resuspended in 1 mL PBS, to remove cellular debris and dead bacteria from the sample solution. The samples contained about 5000 bacterium/μL.

E. coli ($DH5\alpha$) was transformed with the plasmid pFNK-203 (3739bp) to express the luxR gene of Vibrio fischeri following Weiss et al.[167] The bacteria were plated on LB+Kan and samples grown at 37°C in M9 minimal media (0.2% casamino acids, 200 μM thiamine, 1 mM MgSO$_4$, 100 μM CaCl$_2$) with antibiotics (50 μg/ml kanamycin) until the log-growth phase is reached showing an OD$_{633}$=0.3. The plasmid incorporated into the *E. coli* contains the lux operon, exerting positive control on the synthesis of a variant of the green fluorescent protein (GFP-LVA), in response to an acryl-homoserine lactone (AHL) signal. AHL diffuses through the cell membrane and is bound by LuxR, an AHL-dependent transcriptional regulator that activates the expression of Lac repressor. We found that AHL concentrations of 7-10nM induces detectable amounts of GFP-LVA. The LVA tag on the C-terminal end of the GFP

marks it for proteolytic digestion. With a half-life of about 40 minutes, the intensity of green fluorescence will diminish without constant production[6].

The Swiss 3T3 (ATCC# CCL-92) cells were cultured at 37°C and 5% CO_2 in Dulbecco's Modified Eagle Medium (DMEM) with 10% fetal bovine serum (FBS) and 1% penicillin/streptomycin. Mammalian cell samples were created by first detaching cells from the flask surface with a .05% trypsin/EDTA solution. The resulting solution was centrifuged at 5000 x g for 5 minutes, and the cells resuspended at a concentration of 400 cells/μL in PBS.

To impede cell adhesion to the surface, we deposited a polyelectrolyte multilayer on the culture dishes following Berg et al.[21] Briefly, MatTek dishes were treated with poly(allylamine hydrochloride) at acidic pH. The dishes were then treated with alternating solutions of poly(acrylic acid) and polyacrylamide for a total of 6 layers. Finally, the dishes were baked overnight at 80°C, to thermally crosslink the polyelectrolytic layers. This treatment effectively prevents protein adhesion to the surface and inhibits cell adhesion.

Though optical trapping allows for complex and precise assembly of cellular arrays, it is still impractical for long-term experiments. Over time, constant exposure to the laser beams may prove harmful to living cells. Trapping also requires that the array be kept on the optical trapping setup at all times, which limits its portability. To solve these problems, we used a hydrogel matrix prepared from poly(ethylene glycol) diacrylate. This gel only requires a short (<10 s) burst of UV light to polymerize, which limited the amount of time the cells were held in the trap.

To form the hydrogel, we used a pre-polymer mix consisting of poly(ethylene glycol) diacrylate (MW=400) mixed with HEPES buffered saline to make a 20% (v/v) solution. This solution was combined with the cell suspension to create the final desired concentration of PEGDA. The photo-initiator 2-Hydroxy-2-methylpropiophenone (Sigma #405655) was added to the cell/PEGDA solution to a 0.1 % (v/v) concentration immediately before trapping. Finally, the cell/PEGDA suspension was pipetted onto MatTekő dishes and placed on the microscope. After the array was assembled, the pre-polymer solution was exposed to light from a filtered 100W Hg lamp to form the

gel. A beam of UV light in the band λ=360$\pm$20nm with a waist of 2.1mm and a total power power of 6-7mW was stop-down to a 600μm diameter spot that exposed the hydrogel for 3-5sec. The exposure was minimized to ensure clonal efficiency and avoid cell damage. We found that cell proliferation was adversely affected for UV exposures >20sec. The hydrogel was able to adhere to the polyelectrolyte layers, due to the acrylate base of both chemistries.

To explicitly illustrate the 3D aspects of the microarrays fixed in hydrogel, samples were imaged using a laser scanning confocal microscope (Leica SP2) with a 63X, 1.32NA objective and a pinhole size of 1.001 Airy unit. Mammalian cells were stained with Calcein AM and propidium iodide, and bacterial cells with SYTO 9 and propidium iodide. Images were deconvolved with Huygens (SVI) and iso-surfaces constructed with Imaris software (Bitplane). We estimate a typical lateral and axial resolution to be $0.61 \times \lambda/(NA) = 235nm$ and $2\lambda/(NA)2 = 779nm$, respectively.[129]

3.3   Results

We first formed living cell microarrays of a prototype cell, *P. aeruginosa*, to evaluate the system performance of the apparatus shown in 3-1. 3-2 shows the optical system performance, demonstrating the capacity to form a 21x21-2D array of 441 *P. aeruginosa* bacteria formed with a 100X, 1.25NA oil immersion (Zeiss Plan-Apo) objective in a time-shared trap using λ=900nm. The total laser power delivered to the sample was 800mW, giving a time-averaged power per trap of <2 mW. This is the largest array of living cells assembled using optical trapping to date. The array was filled either by the diffusion of bacteria into the capture range of a trap or by the use of an additional "shepherd" beam formed with the same laser to move individual bacterium to the trap positions. The maximum size of the array is limited by the dark time, the diffusion of the cell from the area of the trap, by the objective, and by the laser power delivered through it.

The minor axis of the rod shaped bacteria ($\approx$ 1μm) is close to the size of the diffraction limited laser spot, which means that bacteria in the array can be brought
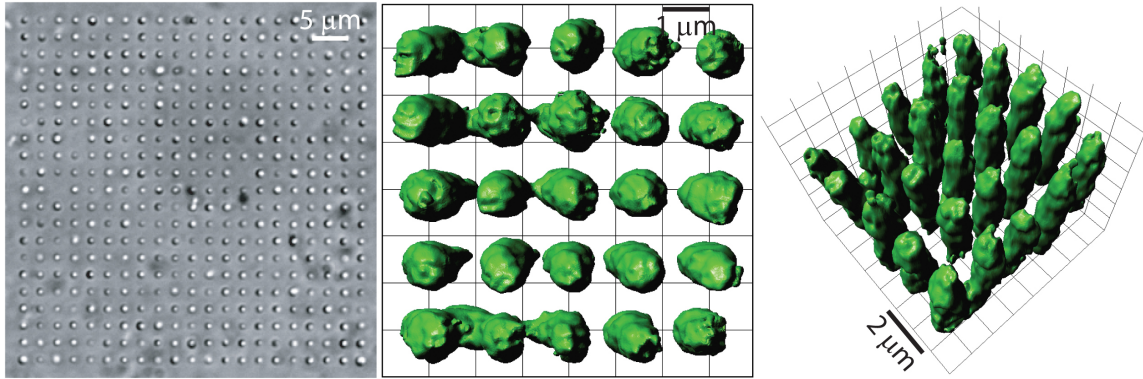
Figure 3-2: Optical micrographs showing 2D microarrays of *P. aeruginosa* bacteria. (a) A transmission micrograph of a 21x21-2D microarray of *P. aeruginosa* formed with a 100X, 1.25NA oil immersion (Zeiss Plan-Apo) objective at λ=900nm using <2mW per trap. (b) A false-color iso-surface was generated from volumetric data obtained from deconvolved confocal images of a 5x5 microarray of *P. aeruginosa* assembled with a 100X, 1.3NA oil immersion (Zeiss Plan-Apo) objective at λ=514nm using <2mW per trap, and embedded in hydrogel. The average center-to-center distance is 1.52±0.06μm and average space between each bacterium is 354±134nm. (c) A 3D representation of (b)

nearly into contact. To test the positional control over the cells in the array, we reduced the inter-cell spacing until the array collapsed(see 3-3). 3-2 also shows laser scanning confocal images of a 5x5-2D array formed using 514nm light with a time-averaged power per trap of <2 mW to ensure viability. This array has a spatial period of 1.52±0.06 m with a separation between cells of only 354±134nm on average. This is the first time that living cells have been assembled into a pattern with such high resolution. Below a period of 1.1 μm with 370nm between the bacteria, the array tends to collapse, presumably because of limitations associated with the intensity profile in the trap at a power <2mW. We have found that it is possible to produce an array with a 0.7 μm period using longer wavelength light λ=900nm with a time-averaged power per trap of <15 mW, but viability is compromised for powers >9mW (see 3-4). These observations suggest that mode structure of the beam (not the wavelength) used to form the trap, and the local electromagnetic environment presented by multiple bacteria in such close proximity may affect the minimum separation that can be maintained.

Figure 3-3: Reducing Array Spacing. Maximum intensity projection(MIP) of deconvolved confocal images of *P. aeruginosa* microarrays assembled with a 100X, 1.3NA oil immersion (Zeiss Plan-Apo) objective at λ=514 nm using <2mW per trap, and embedded in hydrogel. (a) 1.5 μm spacing array, as seen in Figure 2. (b) 1.25 μm spacing array. (c) .8 μm spacing array - the array here has collapsed.

Using this apparatus, trap arrays are not limited to planar configurations. If the beam entering the objective lens is slightly divergent, then the entire pattern of traps comes to focus at a different point along the optical axis.[49] This divergence can be introduced using a Fresnel lens encoded into the phase grating of the SLM. This functionality can be implemented by adding the phase modulation associated with the lens to the existing phase grating computed for the desired 2D pattern so that plane a in 3-1 can be imaged to planes b and c at the same time. We have tested this idea with 1 μm diameter latex microspheres and determined that an out-of-plane motion $>\pm$10 m is easily accessible.

3-5 shows a 3D array comprised of three overlapping 2D-5x5 arrays of *P. aeruginosa* separated along the optical axis by 3 μm and fixed in hydrogel. The array was formed with a 100x, 1.3NA oil immersion (Zeiss Plan-Apo) objective at λ=514nm using <1mW time-average power per trap. In the transmission optical micrograph shown in 3-5, the corner vertex of each of the three arrays is highlighted by a (blue, green and red) circle. Notice that the three arrays are shifted by 4 μm along both the x- and y-axes to facilitate imaging. The three-dimensional nature of the array is indicated by the focus conditions. The camera focal plane is coplanar with the central (green) array so that the top array (blue), which is under-focused, appears bright in the image while the under-focused bottom array (red) appears dark. However, the

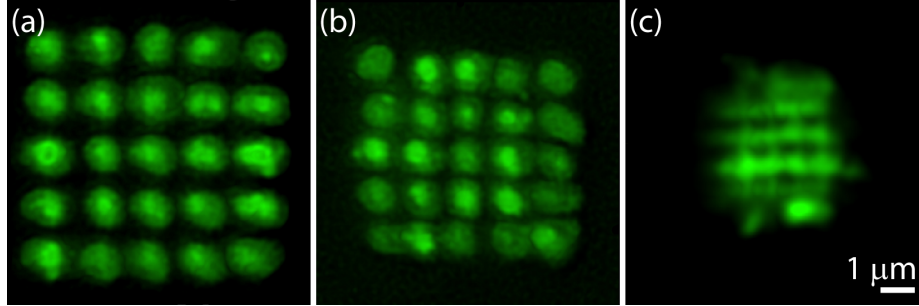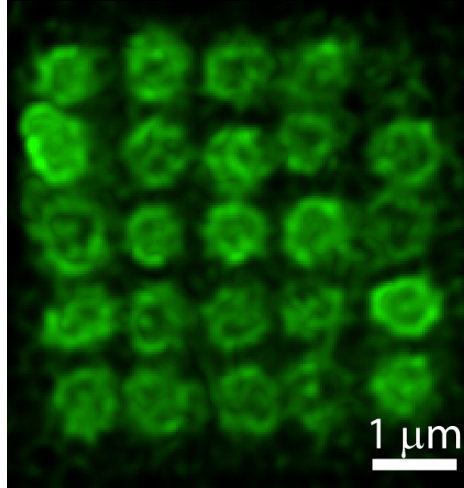Figure 3-4: Using IR to Reduce Array Spacing. Maximum intensity projection(MIP) of deconvolved confocal images of a *P. aeruginosa* microarray assembled with a 100X, 1.3NA oil immersion (Zeiss Plan-Apo) objective at λ=900 nm using <13mW per trap, and embedded in hydrogel. The array has a spacing of 850nm.

transmission micrograph is an ambiguous illustration of the 3D hierarchy within of the array. On the other hand, the false-color iso-surfaces reconstructed from confocal images of the same array illustrate unequivocally the top(blue), middle(green), and bottom (red) arrays separated by 3 μm. From the confocal images, we observe that multiple bacterium frequently populate the same trap unless they are loaded carefully-one at a time.

To elicit tissue-specific features, the microarray should mimic not only the three-dimensional character of tissue, but also the heterotypic micro-environment of the cell. For example, heterotypic systems are needed to model cell-type specific responses to infection by *P. aeruginosa*.[41] Several methods[25, 24, 124] have already been explored for co-culturing different cell-types onto a single substrate in 2D, which involve patterning resists that allow cells to attach only to selected regions of a substrate. A second cell type is subsequently attached once the resist is removed to reveal the underlying surface.

Using arrays of time-shared, holographic optical traps, we have assembled 3D, heterotypic living cell micro arrays in hydrogel without loss of viability, while accounting for variations in the size of the cells. We explored two strategies for trapping large
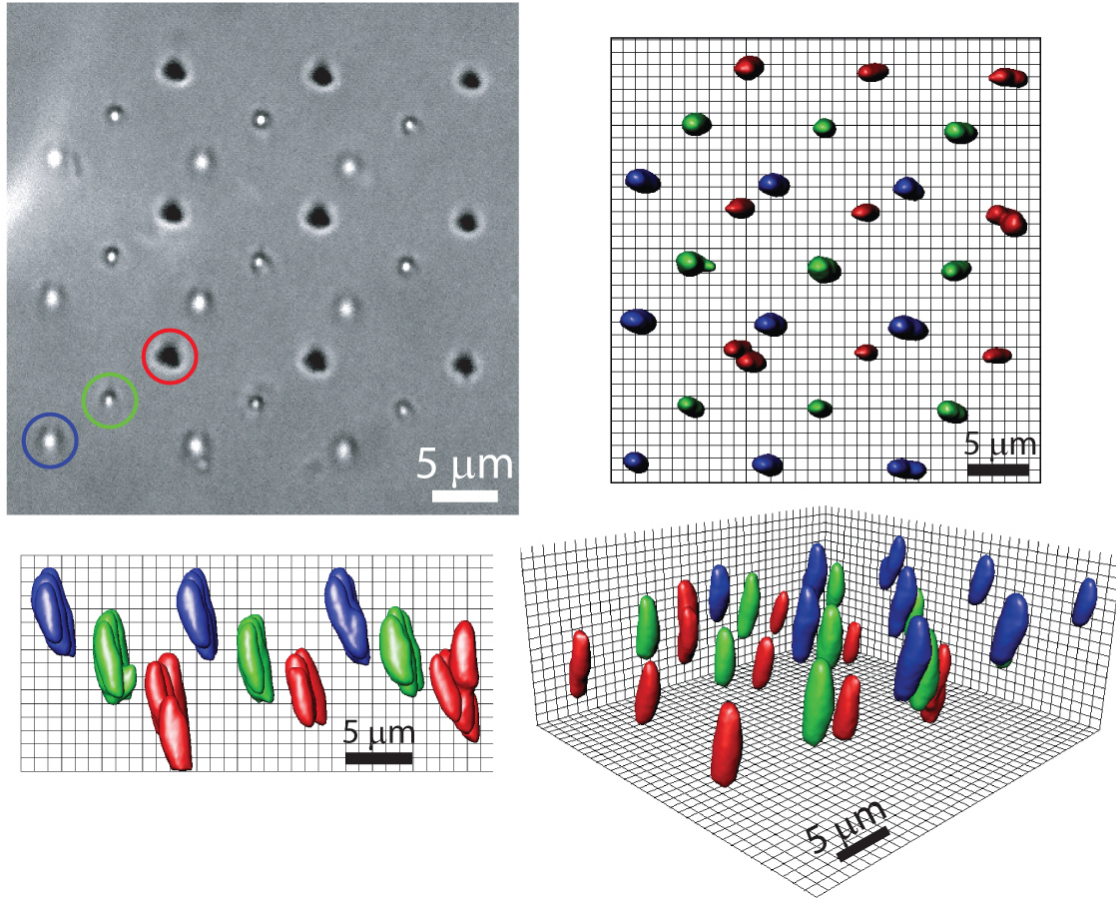
Figure 3-5: A 3x3x3-3D array of *P. aeruginosa* bacteria. (a) A transmission micrograph of three overlapping 3x3 arrays of *P. aeruginosa*, shifted by 3μm from each other along the optical (z)-axis and embedded in hydrogel. The arrays are formed with a 100X, 1.3NA oil immersion (Zeiss Plan-Apo) objective using 514nm light with <1mW per trap. The corner vertex of each of the arrays is highlighted by a blue, green and red circle in the figure. The focus is coplanar with the middle of the three arrays so that the under-focused top array (blue) appears bright while the over-focused bottom array (red) appears to be dark relative to the center array (green). The three arrays are shifted by 4μm along both the x and y-axes to facilitate imaging. (b) A false-color iso-surface, reconstructed from volumetric data obtained from a series of confocal images, showing the offset along x and y-axes with the xy-projection. (c) Reconstructed (false color) iso-surface xz-projection, illustrating the 3 m separation along z-axis. (d) A false-color iso-surface perspective reconstruction illustrating the top(blue) middle(green) and bottom (red) arrays separated by 2μm.

mammalian cells: (1) assigning a high-power single trap to each cell regardless of size or (2) dedicating an array of low-power multiple traps to each cell where the number of beams in the array is determined by the cell size. While both strategies can be used

successfully, the latter avoids photo-damage of a disproportionately small cell due to high power. 3-6(a) shows a homotypic, 2D array of 9 trapped Swiss 3T3 fibroblasts with only one trap assigned to each cell. The traps were formed using a Zeiss Neo-Fluor 40X, 0.9NA objective at λ=514nm with a time-averaged power per trap at the sample of 20 mW. In contrast, the heterotypic array comprised of 3T3 fibroblast and 16 *P. aeruginosa* bacteria shown in 3-6(b) and (c) was formed using 100X, 1.3NA objective at λ=900nm with multiple (9) 2mW beams trapping the mammalian cell, while only a single 2mW beam was dedicated to each bacterium. The confocal images shown in 3-6(b) and (c), which were taken about 4 hours after the formation of the hydrogel, explicitly demonstrate the facility we have for simultaneously assembling cells of differing sizes and types into an arbitrary 3D array. Apparently, because of the small mesh size associated with PEG of this molecular weight, ($\sim$1nm)[45] the position of the cells is rigidly fixed within the array. This is the first time that a permanent, heterogeneous network of cells has been assembled with such precision. Notice that the bacteria are encircling the waist of the 3T3 cell, imitating the onset of infection. According to Rocha et al.,[142] infection is supposed to begin with the adherence of *P. aeruginosa* to host cells through pili and nonpilus mechanisms.[132] Living cell microarrays may provide an opportunity to study infection through control of colonization and the biochemical library in the microenvironment of a cell.

Generally, for every cell type that we manipulate into an array in hydrogel, we have to assess: 1. photodamage;[106, 22, 96] 2. cytotoxicity/cytocompatibility of the photoinitator;[31] and 3. biocompatibility in the hydrogel. The viability of the cells in this array was assessed using two nucleic acid stains: SYTO9 and propidium iodide. SYTO9 permeates the membrane of a living cell and labels nucleic acids with green fluorescence, while membrane-impermeant propidium iodide labels the nucleic acids of membrane-compromised cells with red fluorescence. 3-6(b) and (d) illustrate the results of the assay: i.e. the bright green fluorescence shown in 3-6(b) observed in conjunction with a lack of red fluorescence in 3-6(d) indicates that both cell types remain viable. However, after exposure of the same cells to ethanol the fluorescence is intensely red as shown in 3-6(e).
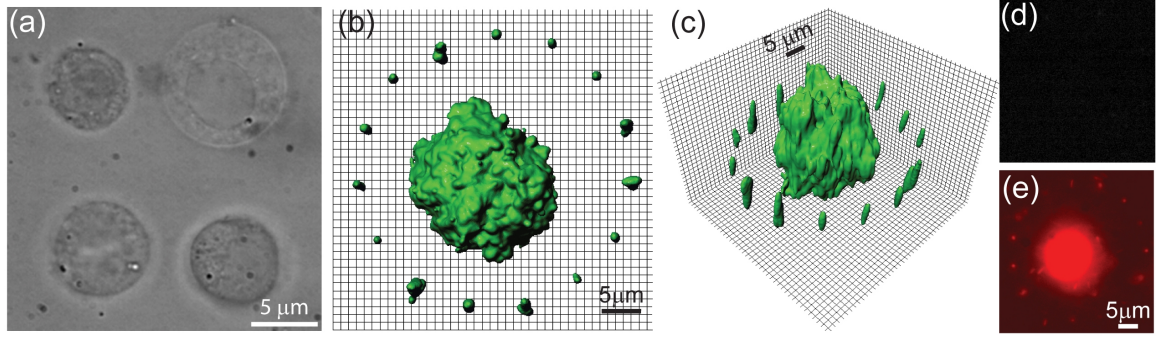
Figure 3-6: Heterotypic microarray of Swiss-3T3 mouse fibroblast and *P. aeruginosa* bacteria. (a) Swiss-3T3 mouse fibroblasts trapped in a 3x3 2D array formed at λ=514nm using a 40X objective with 20mW per trap. (b) A false-color iso-surface reconstruction obtained from a confocal image of a Swiss-3T3 cell trapped with 100X objective using 9-2mW beams at λ=900nm, surrounded by a ring of 16 *P. aeruginosa* with each bacterium trapped using a single 2mW beam. This image was obtained by exciting SYTO 9 labels with 488nm. (c) The same microarray as in (b) rotated to reflect the 3D aspects of the array. (d) (e)Viability assay of the same heterotypic microarray showing an image obtained by exciting propidium iodide labels with 488nm. The lack of red fluorescence in (d) indicates viability, but after killing the cells with ethanol the fluorescence is intensely red (e).

While assays of viability using these dyes have been found to correspond to about 90% clonal efficiency,[118, 62] they only measure membrane integrity. We want to assess viability of the optically patterned, hydrogel encapsulated cells as a function of time. To facilitate a comparison to previous characterizations of the photodamage caused by optical trapping on *E. coli* metabolism, we monitored protein production directly by observing the production of GFP in response to chemical induction using an AHL signal. 3-7(a) shows a transmission micrograph of a 5x5-2D array of *E. coli* bacteria formed in hydrogel with a 100X, 1.25NA oil immersion (Zeiss Plan-Apo) objective in a time-shared trap using λ=900nm, taken immediately after gelation. (The time-averaged power per trap of <2 mW.) The array is then incubated at room temperature. 37 hours later, we induced GFP production with 500nM AHL, and we observe green fluorescence 5.5 hours later. 3-7(b) shows the green fluorescent signal obtained from the same array after exposure to 500nM of AHL, 43 hours after assembly using 470nm excitation. Every element of the array is fluorescing green indicating that every cell is producing GFP(LVA). Also notice that the position of

each cell in the array has not changed after 43hours indicating that the bacteria have been immobilized.
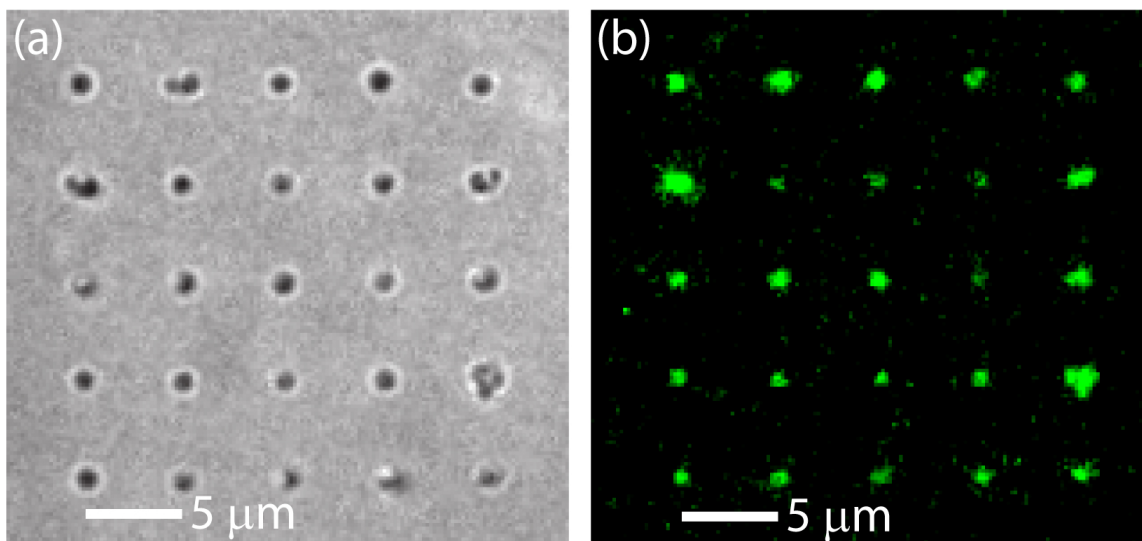
Figure 3-7: A 5x5-2D array of *E. coli* bacteria incorporating the receiver plasmid pFNK-203. (a) A transmission micrograph of a 5x5 array of *E. coli* embedded in hydrogel. The array is formed with a 100X, 1.3NA oil immersion (Zeiss Plan-Apo) objective using λ=900nm with <2mW per trap. (b) A green fluorescent image of an the same array obtained using 470nm excitation, after inducing the production of GFP within the *E. coli* with 500nM of AHL 43 hours after gelling. Every element of the array is fluorescing green. These images indicate metabolic activity and cell viability up to 43 hours after fixing the array in hydrogel.

That fluorescence is inducable 43 hours after fixing the array is an unambiguous measure of protein production and metabolic activity in the bacteria, and the perfect viability of the elements of the array. For reference, in a minimal media like M9, a culture of this strain (that is not constrained by the hydrogel) doubles about every 2hours, while in rich media, a culture doubles every 20-30 minutes. We have measured protein production, or an operational lifetime, of 48hours after fixing the array in hydrogel. The efficacy of whole cell-based environmental sensors relies on similar measures of the operational lifetime and shelf life.[28] For comparison, Kuang et al.[99] recently reported an operational life span of a single cell, *E. coli* genotoxin biosensor of more than 6hrs under ambient conditions with a shelf-life of two weeks when stored at 4°C.

3.4 Summary

It is now possible to assemble hundreds of living cells into three-dimensional heterotypic microarrays with submicron resolution without loss of viability using time-shared, holographic optical traps. In an attempt to preserve cell viability, the optical traps are implemented using a novel combination of two diffractive elements: an SLM and AOD. The viability we observed at λ=514nm and for λ>850nm is an indication of the promise of this strategy. This laser-guided technique is superior to lithographic and DEP cell patterning because it offers three-dimensional placement with high precision and selectivity, limited only by the diffusion of the cell during the dark time and photodamage.

The development of living cell microarrays brightens the prospects for synthetic biology and tissue engineering. Although single cells are currently the crucible for testing synthetic biology, to fully exploit it and elicit more complex regulatory behaviors, the microenvironment surrounding the cell must be harnessed, as well. Signals between cells can be transmitted through extracellular space by molecular diffusion, through receptor proteins in the cell membrane or directly through gap junction proteins that provide a communication link between the cytoplasm of adjacent cells. Cells can acquire positional information by sensing a chemical gradient that is interpreted according to specific genetic instructions, depending on developmental history. Or the position could be specified by lateral inhibition in which differentiating cells secrete an inhibitory signaling molecule that acts on the nearest neighbors to prevent them from developing similarly.

The fluorescent array shown in 3-7 demonstrates unequivocally the manipulation of gene expression through the broadcast of a biochemical signal. Using the same methods, we should be able to explore gene expression in live cells using only a few signaling molecules at a time by controlling the position of cells transmitting and receiving the signals. Thus, the potential exists for manipulating 3D biochemical gradient communication with physiologically relevant concentrations and gradients using living cell microarrays. More complex microarrays offer a more diverse library

of biochemical signals and at the same time afford us stringent control over the three-dimensional microenvironment of every cell in the array; making it useful in studies of tissue development and differentiation in eukaryotes, as well as cancer.

3.5 Acknowledgements

Chapter 4

Trapping Viability

4.1 Introduction

Optical micromanipulation in biological systems has undergone a revolution.[75] Twenty years ago, pioneering work by Ashkin demonstrated that light pressure forces could displace and levitate bacteria and viruses, and even manipulate organelles within living cells.[8, 10, 12, 9, 11] He used a single-beam gradient force optical trap-now commonly referred to as optical tweezers-produced by focusing a single TEM00 laser beam of wavelength to the diffraction-limit with a high numerical aperture (NA) microscope objective. Although the trapping force is weak ($\sim$1 nN), cells have a miniscule mass (a red blood cell weighs $\sim$1 pN), allowing optical tweezers to be effective for micromanipulation of living tissue. Now, with the development of evanescent-wave traps,[90, 140, 39] holographic arrays of traps,[1, 133, 116, 49] and multi-functional traps,[160] optical tweezers can be used to exert a wide range of forces and torques at many points in space and time with sub nanometer and sub millisecond resolution.[121, 163]

Two or more optical traps arrayed together can be especially useful for manipulating living cells,[1, 87] and several beam-steering strategies have already been employed to produce them. For example, using these strategies we have recently demonstrated the ability to assemble three-dimensional, heterotypic microarrays of living cells that resemble tissue.[1] The cells are positioned using a time-shared holographic array of

three-dimensional optical traps produced through a novel combination of two diffractive elements, a spatial light modulator (SLM) and acousto-optic deflectors (AOD). Multiple traps were created by time-sharing the beam between different positions in the array, scanning rapidly from one trap position to the next faster than the relaxation time for Brownian motion, then dwelling at the desired position in the array just long enough to form an optical trap and fix the location of the cell.

Minimizing the photodamage in the trap beam is vital for manipulating living cells. It has been suggested that photodamage results from local heating,[106] two-photon absorption[22, 96, 33] and photochemical processes leading to reactive chemical species.[95, 98, 118] Optical tweezers work because of refraction-too much absorption can lead to excessive heating and an ineffective trap. To avoid absorption, lasers in the near-infrared band are usually employed for trapping since a "biological window" exists in tissue for wavelengths between 700-1500 nm where attenuation is governed primarily by scattering processes.[160] For optical wavelengths less than λ=700 nm, attenuation is dependent on absorption from chromophores like hemoglobin and melanin. At wavelengths longer than λ=1300 nm, attenuation is primarily governed by absorption from water. Due to the emergence in recent years of high-intensity, continuous wave (CW) Ti:sapphire (Ti:Sap) lasers, we can now avail ourselves of light sources with continuous tuning in the wavelength range 700-1500 nm with $\sim$1 W of power.

The irradiance at a diffraction-limited focus[95, 118](with an Airy disc diameter $7/8\lambda$) for a λ=900 nm, 100 mW laser beam is: $I = 1.03 \times 10^7 \, W/cm^2$. Despite the high power density, it seems unlikely that photodamage is associated with non-specific heating.[118, 74] Liu[105] and Peterman[131] have eliminated local heating as a mechanism for photodamage by measuring the change in temperature using dyes in micrometer-scale liposomes or power spectrum of trapped microspheres. Liu measured a temperature rise of only 1.25°C per $10^7 \, W/cm^2$ near the focus for λ=1064 nm, while Peterman measures only 0.8°C. Both measurements indicate that the heat is rapidly conducted away probably because of the small volume at the focus. And even this estimate for the temperature rise may be exaggerated according to Schönle and

Hell.[151] Instead, resonant absorption (by chromophores), specific photochemistry or even electric-field induced denaturing of the protein mechanisms within the cell seem more likely causes of photodamage.[118]

Neuman et al.[118] and Liang et al.[102] have reported wavelength-specific adverse effects of optical trapping on viability with CW exposure. In particular, Neuman showed that a change in the wavelength from 930 nm (most damaging) to 830 nm (least damage) affects the lethal dose for E. coli by about a factor of 5. Neuman monitored the rotation rate of cells tethered to a glass cover slip by means of a single flagellum, as the rotation rate is proportional to the transmembrane potential. Assays like this for proton pumping, for respiration, or uptake of substrates are used to measure metabolic activity. These assays may not discriminate effectively between live and dead cells (especially for bacteria) since the activity of the cells may be below the threshold for detection. The most effective assays for cell viability use protein production or secretion to dynamically monitor cell metabolism.[73] In fact, even cells that cannot reproduce may still exhibit metabolic activity.[14] Another possible viability assay that uses LIVE/DEAD stains to test membrane integrity has been found to correspond to about 90% clonal efficiency.[62]

We hypothesize that minimizing the time-averaged power delivered to the cell by the laser beam in an optical trap will preserve viability from single photon damage. To test this hypothesis, we followed the gene expression of eGFP in E. coli organized into two-dimensional (2D) 5x5 microarrays using both time-shared and CW optical traps. Gene manipulation and regulation of gene expression is easily accomplished in this prokaryote. And so, to monitor cell metabolism in real time, we incorporated a reporter gene into the bacteria, encoding eGFP in response to an inducer. To track the activity of individuals for up to 12 hours after exposure, we (semi-permanently) fixed the position of the cells in a scaffold made from a photopolymerized polyethylene glycol diacrylate (PEGDA) hydrogel. PEGDA hydrogels are especially effective as a scaffold because they have demonstrated biocompatibility: i.e. bacteria and eukaryotes can remain viable for weeks encapsulated in a hydrogel environment.[28, 81] So, for each bacterium that we manipulate into an array in hydrogel, we are actu-

ally assessing not only photodamage, but also cytotoxicity/cytocompatibility of the photoinitator;[31] and biocompatibility in the hydrogel. In what follows, we show that time-sharing the optical traps by dwelling only 10 μs-1 ms on each cell increases the survivability of E. coli expressing eGFP relative to CW exposure with the same peak power in the beam. We find a linear dependence of viability on power, which implies that photodamage is dominated by single photon absorption. We also find a wavelength dependence that is unlike prior work on E. coli: i.e. λ=870 nm shows the most damage and λ=900 nm the least, though the variation in viability is only about 30% across the entire band. The photodamage in a time-shared trap does not seem to strongly depend on the dwell time provided that the time-averaged power is the same. When it is related to the time-averaged power, the viability observed for a time-shared optical trap follows the same wavelength and power dependence observed for a CW trap.

4.2 Experimental Methods

4.2.1 Trapping

To acquire statistical data about the viability of a cell population, we tracked the time development of the individual cells in 5x5 arrays that had been fixed in hydrogel scaffolds. As illustrated in 4-1, the arrays are formed with optical tweezers produced from a CW Ti:Sap laser beam and a Zeiss Achroplan 100x oil immersion objective (1.25NA) held in an inverted optical microscope (Zeiss Axiovert 200M). We used two different methods to produce multiple traps that employed either acousto-optic deflectors (AODs) to create time-shared traps, or a spatial light modulator (SLM) to produce CW, holographic optical traps (HOT). To form multiple, time-multiplexed optical traps we used the AODs (from AA-Optoelectronic) with the SLM acting like a mirror. In this configuration, the CW Ti:Sap beam is deflected transverse to the direction of propagation using two orthogonally-mounted AODs to give independent control of the x- and y-positions of a trap. The beam is time-shared between different

positions in the 2D array: i.e. it is scanned rapidly from one trap position to the next, dwelling at the desired position in the array just long enough to form an optical trap and fix the location of the cell.[116] Typically, the laser beam was deflected between 25 trap positions in a 5x5 array at a 4 kHz rate with a dwell time of the trap over a particular position of 10 μs. The inset to 4-1 shows a microarray of bacteria produced under these conditions. We formed similar arrays by generating CW, HOTs with the SLM (Boulder Nonlinear Systems) instead of using time-shared optical traps. The SLM is an optically addressed nematic liquid crystal device configured to act as a phase hologram with 256 gray levels. It has near-VGA resolution without sharp spatial pixelation, which gives first-order diffraction efficiencies larger than 90%. Effectively, the SLM was used to introduce phase shifts to implement a 2D diffraction grating. To determine the phase distribution in the SLM plane required to produce the desired intensity distribution in the trapping plane, we used the Gerchberg-Saxton algorithm, described in detail elsewhere.[153]

Relay lenses were used to image the beam emerging from the AOD or SLM onto the back aperture of the objective. The optical systems comprised of lenses L1 and L2, and L3 and L4 are both afocal: i.e., a collimated incoming beam will emerge collimated. The focal length of lenses L1, L2, L3 and L4 and the separation between them are chosen so that a small deflection of the beam results in a change only in the direction of the laser beam at the objective entrance aperture, without any change in position.[63] Typically, the cells were trapped about 5μm above the surface of the coverslip to minimize spherical aberrations from the media. We measured the power incident on the back aperture of the 1.25NA 100x objective for each wavelength and then corrected for the transmission through the objective using transmission curves provided by Zeiss.[34] The transmission over the wavelength range $840 \leq \lambda \leq 930$ nm was approximately 73%.

We chose to assess the viability of the prokaryote E. coli DH5 (Invitrogen #18258-012) because genetic manipulation and regulation of gene expression are easily accomplished. The E. coli strain was transformed with a plasmid coded GFP-M1 and selected by ampicillin resistance. The GFP-M1 plasmid, shown in 4-2(a), uses the

61
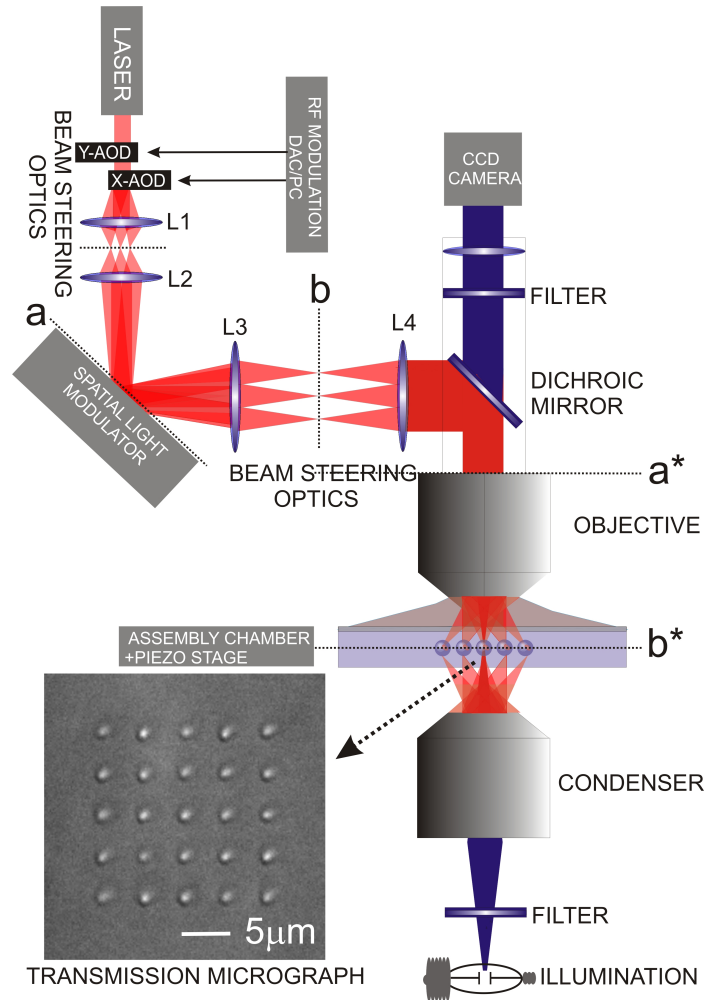
Figure 4-1: Schematic diagram of a time-shared/holographic optical trapping appa-
ratus. Two-dimensional (2D) trap arrays are formed using a Zeiss Achroplan high
NA objective (100x/1.25NA) commercial Axiovert 200M optical microscope in con-
junction with either one of two diffractive elements: i.e. two acousto-optic deflectors;
or a spatial light modulator. The same microscope that is used to produce the cell
traps is also used for viewing (shown with the blue beam). The inset in the lower left
shows an example of a 2D 5x5 array of E. coli formed using this apparatus and sub-
sequently embedded in hydrogel. The distances are: AODs-L1=400 mm; L1-L2=800
mm; L2-entrance pupil=400 mm; L3-L4=800 mm; and L4-OEA=420 mm, where the
focal lengths for L1, L2, L3, L4 are 400mm.

pBR322 origin of replication providing 15-20 plasmid copies per cell. It contains a

gene encoding eGFP under the control of the lac operon. lac is a catabolite-regulated

operon responsible for obtaining energy from β-galactosides such as lactose. During

normal growth in an LB medium, the lac repressor (lacI) is bound to the operator

region of the lac operon preventing transcription[157]. However, in the presence of an inducer, the repressor protein binds the inducer and is rendered incapable of interacting with the promoter region of the operon. We induced the transformed cells using IPTG (Isopropyl β-D-thiogalactopyranoside), a molecule which mimics allolactose, but unlike allolactose it is not hydrolyzable by the cell so it is not degraded. IPTG binds to the repressor protein and allows transcription, reported through the production of green fluorescent protein. Thus, a fluorescent signal from the cell indicates gene expression and an active cell metabolism.

The threshold IPTG concentration for induction in GFP-M1 transformed bacteria was determined by measuring fluorescence of single bacteria taken from log-phase culture (OD_{633}=0.33±0.08 at T=25°C). The transformed bacteria were grown from culture in M9-Glycerol minimal media consisting of: 0.2% (v/v) glycerol, 42 mM Na_2HPO_4, 22 mM KH_2PO_4, 19 mM NH_4Cl, 9 mM NaCl, 1 mM $MgSO_4$, 100 μM $CaCl_2$, 200 μM thiamine hydrochloride, and 0.2% (w/v) casamino acids with ampicillin (100 μg/ml) (Sigma Aldrich A5354) as a selection marker. Fluorescence data was collected by using a Cytomation MoFlo MLS flow cytometer/cell sorter at a low flow rate, exciting the GFP with a 488 nm argon laser and detecting fluorescence using a 515-545 nm emission filter. Green fluorescent microspheres (Invitrogen) were used to calibrate the flow cytometer; determining fluorescence sensitivity and size measurements. For each concentration of IPTG, a fluorescent measurement of gene expression was obtained from one culture. Two measurements were made for each culture: $\sim$ 23,000 induced cells with $\sim$ 23,000 uninduced cells used as a control. The introduction of a scattering filter normalizes the cellular size and morphology variability, providing a better basis for comparison. 4-2(b) shows the number of active (expressing GFP) and inactive (not expressing GFP) bacteria as a function of IPTG concentration. The threshold for inactive bacteria was set by the autofluorescence associated with uninduced bacteria. The threshold concentration, defined as the IPTG concentration at which expression is 50% of maximum, was determined to be 24 μM of IPTG at 25řC. At 10mM, 81% of the bacteria are expressing GFP.

While optical trapping can be used to create vast networks of cells resembling tis-
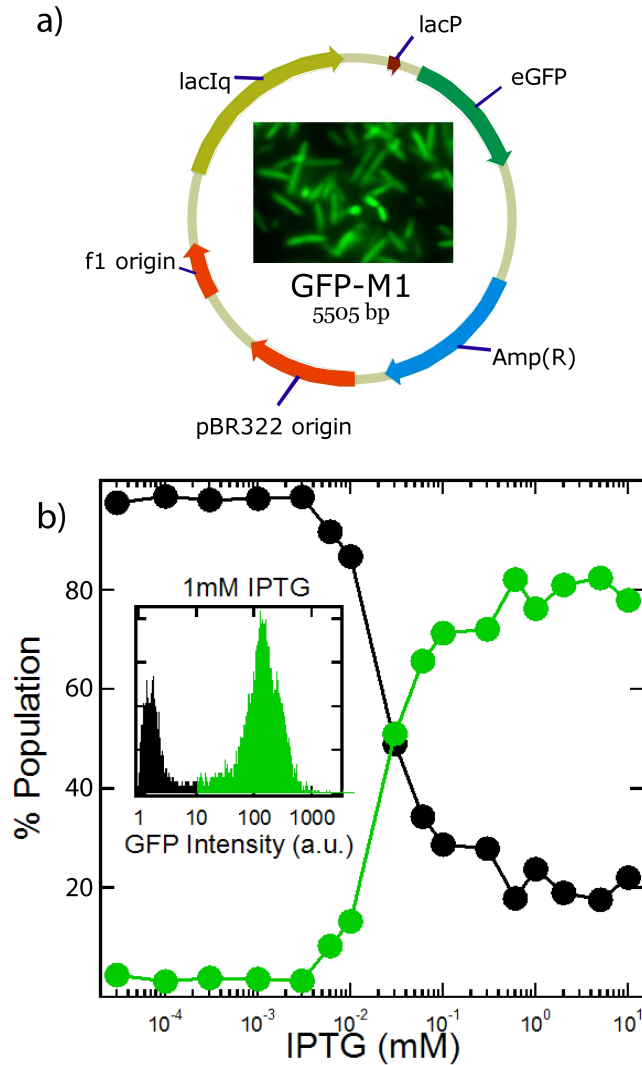
Figure 4-2: (a) The receiver plasmid, GFP-M1, is the focus of this work. It combines the lac operon with green fluorescent protein (GFP). Induction by IPTG initiates GFP production. The resulting fluorescence is used to indicate an active cell metabolism. (b) Threshold for induction of M1's by IPTG at 25°C. Bacteria count measured using laser cytometry for 23,000 E. coli cultured at 25°C. A typical distribution as a function of the fluorescent intensity obtained for 1mM IPTG is shown in the inset. The active cell count indicated by green fluorescent is shown in green, and the inactive is shown in grey. The IPTG threshold estimated from a fit to the data is 24 μM. Only about 80% of the cells are active even at high IPTG concentration. The number of inactive cells (showing no fluorescence) observed at high concentrations indicate that the value for the molecular induction threshold (and response times) are not deterministic, but stochastic.

sue, the trapping beam must be held on the cells to maintain the array. To fix the position of the cells semi-permanently[86, 87] and subsequently follow the GFP production in individuals we have supported the array with a biocompatible scaffold made from a photopolymerizable polyethylene glycol diacrylate (PEGDA) hydrogel.[1] PEGDA hydrogels are especially effective as a scaffold because photopolymerization time can be relatively short ($\sim$ 1-3 seconds).[2] Hydrogels are also porous,[45] allowing for transport of nutrients to the cell and waste away from it.[119] Hydrogels have been shown to maintain viability and activity of bioluminescent E. coli for up two weeks without a change in the dose dependent induction.[91]

We formed the hydrogel from a pre-polymer mix consisting of poly (ethylene glycol) diacrylate (MW=3400 Da) dissolved in M9 minimal media without the thiamine and casamino acids) to yield a 5% (w/v) final concentration. 1 mL samples of bacteria grown in M9 overnight at 25°C were centrifuged 3 times for 5 min at 800g. Between each spin cycle the supernatant was aspirated, and the bacterial pellet re-suspended in 1 mL of M9-Glycerol media. Finally, a pre-polymer mixture comprised of 3400 Da MW PEGDA (Nektar Therapeutics) dissolved at 5% (w/v) in M9-Glycerol along with photoinitiator, 2-hydroxy-2-methyl-priophenone at a concentration of 0.2% (v/v) was vigorously vortexed for 1 minute, and then combined with the cell suspension to create the desired concentration of PEGDA immediately before trapping. The cell/PEGDA suspension was 100 μL pipetted onto MatTek dishes and placed on the microscope.

A microarray was assembled using optical tweezers to manipulate the bacteria in a MatTek dish. Typically, it takes less than 2 minutes to form an array, but to be consistent and make contact with earlier work,[118] each bacterium in the array was held in the trap for 7-8 minutes prior to photopolymerizing the hydrogel. The pre-polymer solution was then exposed to light from a filtered 100 W Hg lamp to form the gel. A beam of UV light in the band λ=360$\pm$20 nm with a waist of 2.1 mm and a total power of 4-5 mW was stopped to a 600 μm diameter spot that exposed the hydrogel for 1-6 s. The exposure was minimized to ensure clonal efficiency and avoid cell damage. We found that E. coli proliferation was not adversely affected for UVA exposures less than 60 s. However, it has been reported that cell death based on

non-thermal, photochemical reactions like photo-oxidation can occur with $1\ J/cm^2$ to UVA (320-400 nm) for an interval of less than 1 minute with the λ=365 nm line of a 100 W xenon arc lamp through a 0.55NA condenser.[62, 97] The encapsulated array was then washed with M9 media to remove residual cells and pre-polymer.

Subsequently, the microarrays in hydrogel were placed in a M9+ampicillin solution containing 10 mM of IPTG, which is more than enough to saturate the promoter activity at 25°C. A time-lapsed fluorescence image of a typical array formed using P=140 mW at λ=900 nm is shown in 4-3(a). These images, obtained using a 12-bit CCD camera (Hammamatsu ORCA-ER) camera, were used to follow the development of green fluorescence from the bacteria in the array, indicating that GFP is being produced in the trapped cells after induction by IPTG. The fluorescence is an unequivocal measure of the cell metabolism after being subjected to the trap beam. In this case, 23 of the cells in the array (92%) expressed GFP. In contrast, GFP expression in M1 bacteria used as a control, which had been encapsulated in PEGDA but not exposed to the trapping beam, was 90±3%. Approximately 10 hours after induction, the fluorescence tended to saturate the camera. At that time, we used 1 μg/mL propidium iodide (Invitrogen: P3566) to test membrane integrity and subsequently report the red fluorescent cells as dead. It was apparent that most of the cells shown in 4-3 remained viable despite encapsulation in hydrogel because they started to proliferate after 12 hours.

The change in fluorescence with time indicates a viable cell with an active metabolism. So we monitored the fluorescence, extracting the intensity from the time lapse images like those shown in 4-3(a) using MATLAB (V7.2, MathWorks) along with the Image Processing Toolbox (V5.2, MathWorks). The images were recorded as 16-bit grayscale TIFFs, and subsequently read into two-dimensional numerical arrays containing the intensity values of each pixel in the image. The images were manually cropped around the cell array to facilitate automatic cell detection. The cropped images were filtered using a Gaussian bandpass filter to eliminate the low frequency background and high frequency pixelation noise. To detect the location of the cells expressing fluorescence, a 90% threshold value was used to mask the image. A wa-
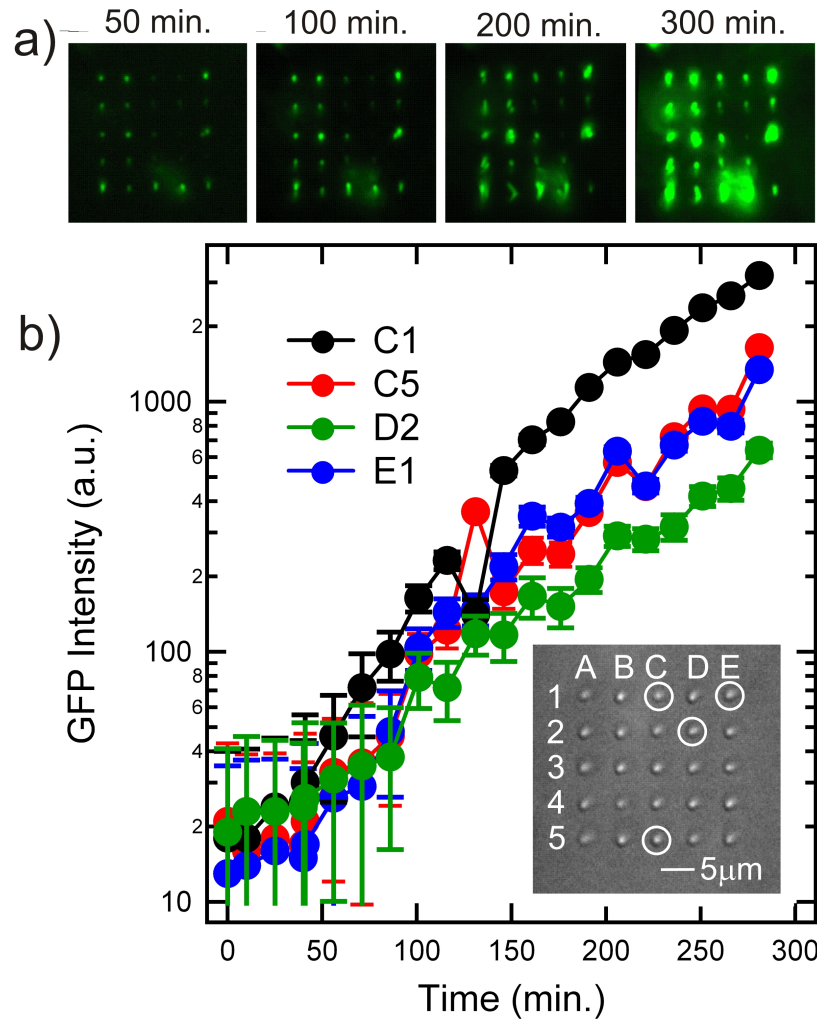
Figure 4-3: Genetically identical cells express GFP differently due to interpopulation variance. (a) Time evolution of green fluorescence in a 5x5 microarray of M1 bacteria following the induction using 10mM IPTG at t=0. The bacterial array was assembled using time-shared optical traps formed using a beam with P=140 mW at λ=900 nm. The array was held for about 8 minutes prior to gelling. We can follow the development of the fluorescence associated with each cell in the array as a function of time. (b) A summary of the time development of the fluorescence measured on five cells in the array. The fluorescence usually saturates after about 5hrs.

tershed algorithm[70] was then used to separate the fluorescent pixel regions. The coordinates associated with the centers of each of these regions were recorded yielding the individual cell centers. Finally, the 90th percentile of the unfiltered intensity values of these regions was recorded and plotted. The corresponding fluorescence of selected bacteria is summarized in 4-3(b). 4-3(b) reveals a distribution of response

67

times associated to individuals in the cell array-information like this is usually obscured in bulk measurements of the fluorescence that cannot monitor the same cell at different times.

4.3   Results and Discussion

We are motivated to determine conditions suitable for optically trapping E. coli without adversely affecting viability. To study the wavelength and power dependence of the lethal dose of IR radiation, we assembled 5x5 microarrays of the E. coli bacteria using optical traps at wavelengths λ=840, 870, 900 and 930 nm and with time-averaged optical power ranging from about 5 to 20 mW (after the objective) using a dwell time of 10 sec and a duty cycle of 1:25. 4-4(a) represents the bacteria score corresponding to the cells in a 5x5 microarray 5 hours after exposure to a time-shared trapping beam. (The number of cells for each data point in the histogram is given in Table S1 in the supplementary materials.) The number of active cells, evident from the expression of eGFP are represented by green; the number of inactive bacteria with no gene expression, but an intact membrane are represented by grey; and the number of bacteria lacking membrane integrity are shown in red. The power in the beam is either ∼140 mW, 280 mW and 490 mW with a duty cycle of 1:25 corresponding to time-averaged power levels of 5.6 mW, 11.4 mW and 19.6 mW respectively. With increasing power in the beam, we find a monotonic decrease in the viability measured by the green bacteria score-notice that the number of active cells drops by about a factor of 2 when the power doubles, regardless of the wavelength. A simplified model for the photodamage proposed by Neuman[118] relates the sensitivity, S, to the power, P, delivered to the specimen: $S(P) = A + BP^n$, where A is the control sensitivity and B is the wavelength-dependent sensitivity. For a single photon process this relationship is linear (n=1). S(P) is defined as the reciprocal of the glowing (gene expression) to total number of the bacteria in the array. We also assume that the control sensitivity vanishes since presumably photodamage by the laser is the only factor contributing to loss of viability. As shown in the supplementary materials, fitting the data yields

an index n for time-shared traps. For the time-shared traps we find: n= 1.34±0.04 at 840 nm; n= 0.93±0.14 at 870 nm; n= 1.1±0.1 at 900 nm. Since the exponent for time shared traps is about n=1 this suggests a linear relationship indicating that the photodamage is predominately due to a one-photon process induced via absorption.

4-4(a) also scores the sensitivity of E. coli to the wavelength of the optical trap. We find that the spectrum for photodamage exhibits only weak minima at λ =870 nm and 930 nm with $\sim$ 20% degradation in activity between the peak at 900 nm (92%) to the minimum at 870 nm (65%), while the M1 bacteria used as a control showed about 90% viability. (Corresponding to 4-4 we provide a table representing the same data in supplementary materials.) The error associated with the determination of the number of active cells reflects a 68% confidence level. If this assay is related to single photon absorption, then biological activity might reflect the absorption spectrum of the molecule causing the photochemical effect. Within the error, the spectrum of 4-4(a) does not resemble the absorption spectrum of free water absorption,[125] or E.Coli in sM9 media.[118, 18] Moreover, the observed spectrum is at variance with Neuman[118] and Liang[102]-we found the least damage at λ=900 nm, while they found most damage there. But Liang and Neuman were both measuring something different: Liang was monitoring the clonal efficiency of a eukaryote, Chinese hamster ovary (CHO) cells; and Neuman used a different measure of viability for a different strain of E. coli.

Another clue to the origin of the photodamage follows from viability tests on cells that were induced prior to trapping. Using GFP-M1 E. coli that were already induced with 2mM IPTG to express eGFP, we assembled 5x5 arrays using time-shared optical traps formed from a beam with a peak power ranging from 112 to 329 mW at λ=900 nm, holding the cells in the array for only 90 s. These conditions on power, wavelength and hold time generally promote viability in bacteria induced after trapping-typically, we find >90% active for a peak power of $\sim$ 110mW-but when induced cells are trapped the viability collapses As illustrated in the supplementary materials, viability is less than 20% when the cells are induced prior to trapping. We attribute the collapse in viability to an increase in (two-photon) absorption associated with the fluorescent
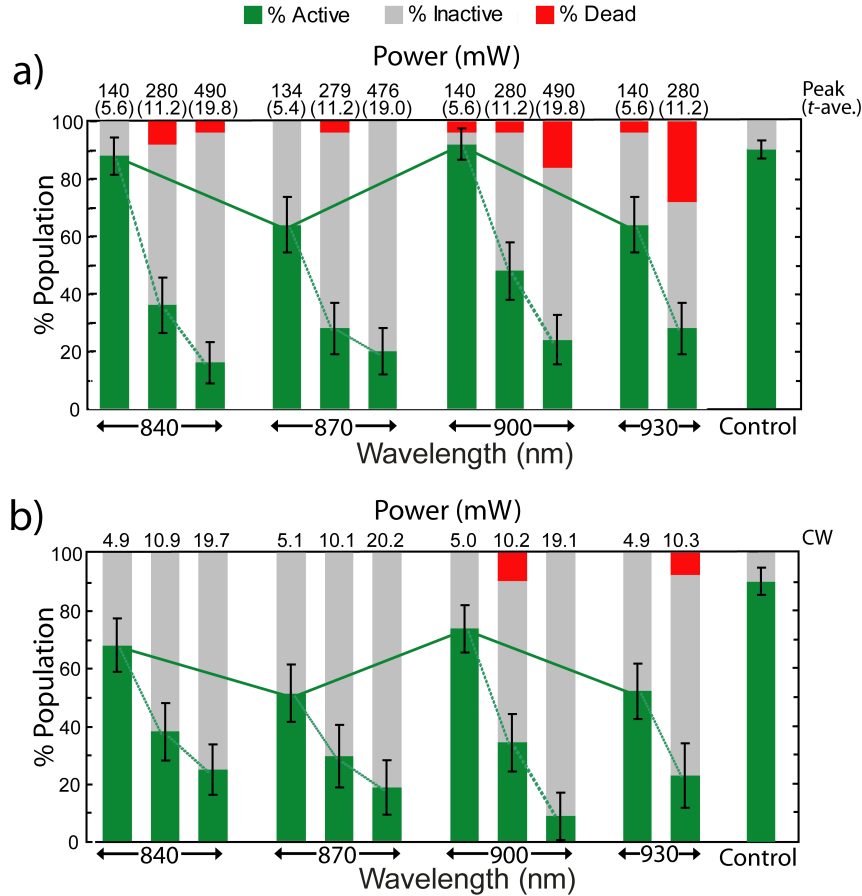
Figure 4-4: Viability as a function of wavelength and power for both time-shared and continuous wave optical traps. (a) A 5x5-2D array of E. coli bacteria incorporating the plasmid GFP-M1 were assembled using a time-shared optical trap with the specified wavelength and power. In each case the cells in the microarray were held for ≈ 8 minutes prior to gelling. The peak power is indicated along with the corresponding time-averaged power in parenthesis. The bar graph represents viable, active bacteria (green); inactive bacteria (gray) and dead bacteria (red) for each wavelength and power. Viability decreases nearly linearly with increasing power, and peaks at $\lambda=840$ nm and 900nm. (b) Similar to (a) but now using a CW beam to form the 5x5-2D array of E. coli. The static (CW) in optical traps ranges from about 5 mW to 20 mW at the specified wavelength. Again, in each case the cells in the microarray are held for ≈ 8 minutes prior to gelling. The CW viability tracks that found for the time-shared trap at about the same time-averaged power. The right side of the corner shows control bacteria, untrapped but encapsulated in the hydrogel spot.

protein. The complex photophysics of GFP gives rise to a broad one-photon excitation spectrum that peaks near $\lambda=489$ nm.[154] The two photon excitation spectrum is even more complex, due to different selection rules and the effects of vibronic coupling, and

70

peaks near λ=950 nm. So, we expect that cells induced prior to trapping produce eGFP that absorbs in near λ=900 nm with a deleterious effect on the reporter or cell metabolism.

4-4(a) indicates that minimizing the peak power delivered to the cell by the laser beam in an optical trap preserves viability from single photon damage. A comparison of this data with that obtained for CW traps suggests that minimizing the time-averaged power is actually what is important for viability. 4-4(b) shows the viability obtained at continuous exposure of 25 E. coli cells to approximately 5, 10 and 20 mW trapping beams in an array formed using the SLM for wavelengths ranging from 840 $\leq \lambda \leq$ 930 nm. These powers correspond approximately to the same time-average powers used in 4-4(a). The power and wavelength dependence of the surviving bacteria score for the CW traps track the dependence of the time-share trap with approximately the same corresponding time-averaged power. The bacterial viability in CW traps is only slightly degraded from the time-shared traps. For example, the number of active cells (18 out of 25) at 5 mW CW power for λ=900 nm approaches (within 20%) the viability exhibited by the time-shared trap at the same time-averaged power and wavelength. The viability is adversely affected by increasing power. For the CW traps, we find that n=0.73±0.04 at 840 nm; n= 0.73±0.01 at 870 nm; n=1.6±0.1 at 900 nm. Higher power in a CW trap beyond the range shown in 4-4(b) is especially deadly. Neuman[118] found a LD$_{50}$, the time necessary to reduce the tethered cell rotation rate by 50%, for an 80 mW CW trap of 520±20 s. So, we tested similar conditions by maintaining a CW trap over several cells before gelling as indicated in Methods. We found a dearth of active cells at 80 mW even for an exposure of only 300 s-observing green fluorescence at λ=900 nm in only 20% of the population. Moreover, we did not observe green fluorescence at 80 mW power with 300 s exposure at any of the other wavelengths. (See supplementary materials)

Finally, the dependence on dwell-time supports the conclusion that the time-averaged power is the dominate factor affecting viability. 4-5 shows the dependence of viability on dwell time measured in a 5x5 array formed using a 140 mW time-shared beam at λ=900 nm. With a duty cycle of 1:25, the dwell time ranges from 10

μs to 1 ms per trap with corresponding scan frequencies that range from 40 Hz to 4 kHz. The M1 bacteria used as a control for this series of experiments showed about 90±6% viability. Under these conditions, the time-average power, which is 5.6 mW, is independent of the dwell time-it depends only on the duty cycle. 4-5 shows that the viability is practically independent of dwell time over the range, provided that the time-average power is unchanged.
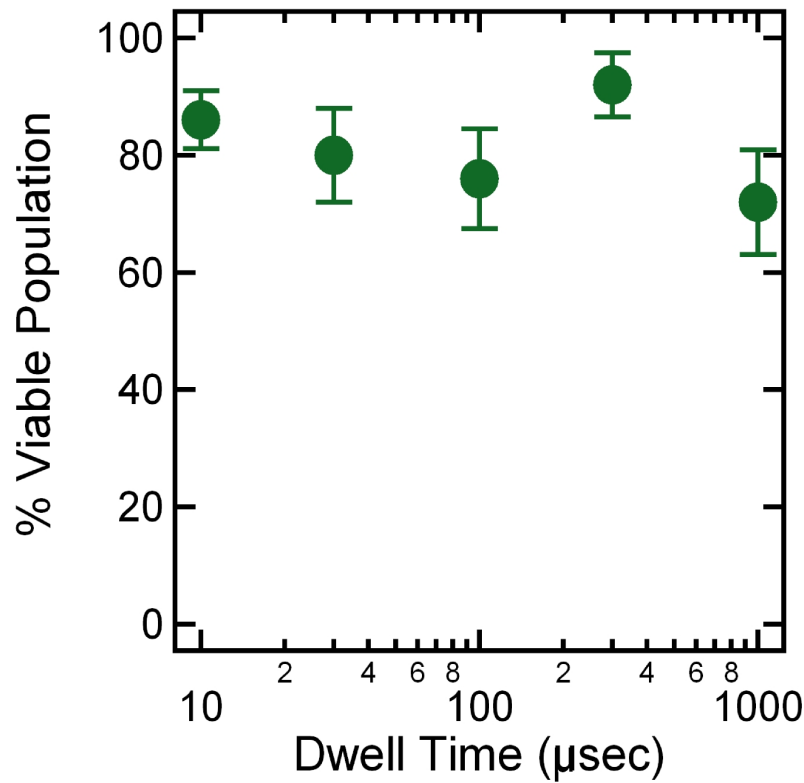
Figure 4-5: Viability as a function of dwell time for time-shared optical traps. A 5x5-2D arrays of E. coli bacteria incorporating the plasmid GFP-M1 are assembled using time-shared optical traps at λ=900nm with a power of 140mW in the beam. In each case the cells in the microarray are held for $\approx$8 minutes prior to gelling. The percentage of the population that is viable (i.e. expressing GFP) after trapping is shown as a function of dwell time for a 1:25 duty cycle scan. Since the duty cycle is the same, the time average power is independent of the dwell time. So, the viability is independent of dwell time over the range studied here.

4.4 Conclusion

We have established that time-sharing optical traps in the near IR improves viability of E. coli measured by the gene expression of green fluorescent protein after trapping relative to continuous wave (CW) exposure with the same power. Like CW traps, the photodamage in a time-shared trap only depends weakly on wavelength, but depends approximately linearly on power, which implies an effect induced by single photon absorption. Generally, the photodamage seems to be related to the time-averaged power. We observe that exposures of >8 minutes using a >100 mW beam pulsed at a 1:25 duty cycle adversely affects expression of eGFP in E. coli. But viability is not affected by the dwell time in the range from 10 μs to 1 ms with the duty cycle of 1:25. Finally, we notice that viability is adversely affected by two-photon absorption in cells induced to produce eGFP prior to trapping at λ=900 nm, indicating the phototoxicity of the fluorophore.

Chapter 5

Microfluidics

5.1 Introduction

The combination of optical trapping and photopolymerizable hydrogel provides a method for the assembly of three dimensional cell patterning, even of different types of cells.[1]3-6 However, in order to place the different types of cells in the correct locations relative to each other, a method for identifying them is needed.

If the cells have a morphological difference, this is an trivial undertaking, as with cells of vastly different size or shape(as in 3-6). While trapping cells of the appropriate type may be selected and brought into position. It is also possible - though more difficult - to organize the cells if they have different fluorescent markers. With the aid of a color CCD and appropriate excitation - fluorescent markers can allow for cell selection and positioning.

These solutions are not very flexible or robust, requiring that the cells have certain aforementioned characteristics in order to pattern them. In addition, we have shown (see 4.3 that trapping cells which are expressing fluorescent proteins can be hazardous to their health. A better solution would allow for cell selection by spatial or temporal isolation of the different cell populations. A method of separating various cell populations by either *when* or *where* they are introduced to the assembly area will allow for simple determination of which cell type is which. A good method for doing this is to feed a small assembly area with microfluidics, allowing various cell

populations to be introduced in a well controlled manner.

Microfluidics have recently come into vogue for cellular sorting and analysis.[170, 67, 159] One of the primary advantages of working at microscale is the domination of Stokes flow, a regime where viscous effects are dominant over inertial effects. This allows for the precise control of spatial and temporal populations necessary for our application.

Other benefits are also granted through the introduction of microfluidics into the apparatus. Microfluidics allow for thorough flushing of the assembly area after polymerization. This allows for the complete removal of residual cells, an important factor when attempting more sensitive measurements. Cells encapsulated in the hydrogel will be isolated and protected from this cleansing flow.

Microfluidics also allow for precise control over the chemical microenvironment. Chemicals may be introduced and cleared rapidly, allowing fine temporal control. The shape of gradients within the hydrogel can be altered by changing the velocity of flow past the hydrogel spot.

Finally, microfluidics allows for a consistent readout of the chemical output of the system. By using a constant flow, and collecting the output of the microfluidic, the chemical production of the cellular array may be studied. The resulting fractions collected from the microfluidic may be run through a varied of assays and tests such as FPLC or mass spectrometry to determine metabolic usage, as well as signal production rates.

5.2   Methods

5.2.1   Replica Molding

Poly (dimethylsiloxane)

For this project, poly (dimethylsiloxane) was chosen as the chip material. It is a silicone polymer, with relatively long chains of $Si(CH_3)_2O$ repeats. It is well crosslinked, leading to good mechanical stability, though the formulation used in this experiment

still yields high flexibility and elasticity ($E = 0.5 - 4\,MPa$). PDMS was obtained from Dow Corning, under the commercial name of Sylgard 184[58].

PDMS is optically transparent in the range of 300 to 1200 nm. Thus fluorescently tagged species may be easily detected in the channel, without concern of signal loss through absorbance. PDMS also has little to no natural fluorescence, ensuring a low signal to noise ratio for sample detection. The index of refraction of PDMS elastomer is 1.43[58], which is not far from that of common Pyrex brand glass of 1.47citeCorning1. This indicates that standard lenses and objectives could be used for observation of a silicone chip under a microscope. However, the scattering which results from PDMS layer of sufficient thickness usually precludes using this optical property.

PDMS elastomers are intrinsically hydrophobic, as might be expected from its methyl side chains. As a result, it is unreactive to both sample and gel chemistry, ensure an inert surface. This can be changed, at least temporarily, by reaction in oxygen plasma, causing the surface to become oxidized, reactive, and extremely hydrophilic, with a contact angle of approximately 10°[169]. Basically, the plasma oxidation causes the surface of the silicone to behave like silica, allowing for silyanization. This change also allows for irreversible bonding to a glass or silica substrate, which can be extremely useful if strong adhesion becomes necessary.

One property of PDMS which is important to note is its permeability to oxygen. O_2 can easily diffuse through PDMS, keeping any solution in a PDMS microfluidic well oxygenated[43].

Microchannel Creation

The easiest was to create microchannels in PDMS is by a mold casting technique. To apply this technique, a master mold is needed. It comprises the topographic structure, from which all of the successive iterations of silicone chips will be fabricated. Its only requisite properties are mechanical stability, chemical stability, and topographic information. In this case, the topographic information was generated through off-site stereolithography based on a CAD file we designed (FineLine Prototyping). The

mold is made of a DSM Somos ProtoTherm 12120, a strong, high temperature tolerant plastic.

The mold is first coated with a fluoropolymer in order to make it easier to detach the PDMS from the mold without tearing. This was accomplished through a vapor deposition of Tridecafluor-1,1,2,2,-Tetryhydrooctyl)-1-Trichlorosilane. Essentially, a few drops of this fluorosilane were placed in a vial, and the vial and mold were placed in a vacuum oven at 75°C and 20Hg vacuum for 2 hrs.[38]

The silicone polymer which was used to create the chips is commercially available as Sylgard 184, a two part polymer mix. The two parts were mixed throughly at a 1:5 ratio of curing agent:base. The mixture was then degassed at house vacuum for 30 minutes. This mixture was poured into the master mold, then cured at 75°C for $\geq$2 hrs. After cooling, the plastic, which has hardened to a rubber like consistency, was peeled away from the mold, yielding a piece of silicone with the inverse pattern of the master mold.
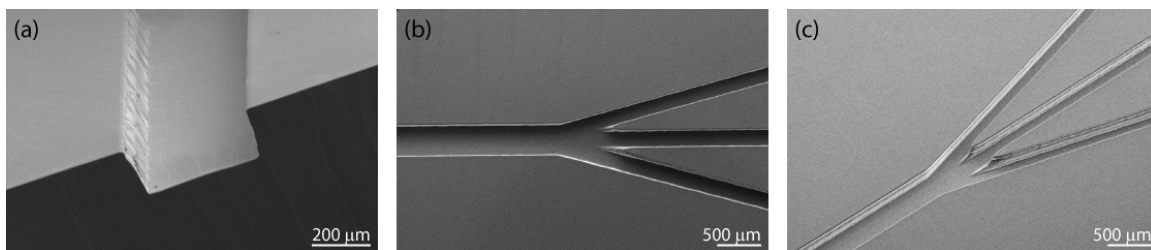
Figure 5-1: (a) Cross-sectional SEM image of unbonded PDMS channel (b) Top down SEM image of the "peace symbol" channel design (c) Tilted SEM image of channel design

These microfluidic channels must be connected to external sources of pressure and fluid reservoirs. In order to accomplish this, a fluidic interconnect is needed. Using a blunt syringe needle, a hole is punched in the silicone chip at the input and output ports, marked for alignment by 2 mm diameter circles.

To complete the chip, the bottom of the PDMS must be sealed. Though PDMS is transparent to most interesting wavelengths of light, our microfluidic chip is thick, and light scattering through it will attenuate intensity dramatically, effectively preventing optical access through the top of the chip. So, the bottom should be chosen based

on the necessity of optical access. Accordingly, we decided to use a piece of #1 cover glass.

Though PDMS will reversibly bind to any flat plastic effectively, this is not a permanent or high-pressure seal. In order to tightly bond the PDMS microfluidic to the coverslip bottom, a covalent bond between the PDMS and glass is formed using an oxygen plasma. The oxygen plasma generates silanol(Si-OH) groups on the surface of PDMS, which react with silanol groups on the glass surface to form an Si-O-Si bond.

The chip was first cleaned by the application of scotch tape to "delint" the PDMS, cleaning the surface quite effectively. The coverslip was blown clear of particles using a air gun. The PDMS and coverslip were then placed, bonding-face up, on a scotch tape covered slide, and into a Harrick plasma cleaner (PDS-32G). After pumping chamber, a small air leak was introduced through a needle valve, and the RF coils turned on to high, to ignite a plasma. The plasma was monitored to ensure a bright, purplish color, and left on for 45 s. The RF coils were turned off, and the chamber vented. Finally, the PDMS chip was gripped by the sides, and placed in contact with the coverslip. Gentle, uniform pressure was applied for 10s, as the bond was forming. Tygon tubing was then inserted into the pre-bored holes, completing the chip.

5.2.2   Chip Pretreatment

In order to enhance hydrogel adhesion and prevent bacterial adhesion, it is advantageous to treat the internal surfaces of the microfluidic device. To that end, we use a methacrylate silane treatment, which will crosslink with the hydrogel.[73, 94] Acrylate coatings have also been shown to prevent bacterial adhesion in previous work.[109]

A 2 % (v/v) solution of 3-(trimethoxysilyl) propyl methacrylate was made in 10 mL of 95% ethanol. The solution was adjusted to a pH of 5 using 50 μL of glacial acetic acid. 500 μL of this solution was pushed through the microfluidic chip using a 1 mL syringe, and incubated for 5 minutes at room temperature. The chip is then flushed out with 5 mL of deionized water. Finally, the chip is placed in an oven overnight at 85°.

5.2.3 Cell Genetics

Two different plasmids were transformed into the same E. Coli strain, DH5α, in order to illustrate the ability of this technique to pattern cells which differ only genotypically. The two types were known as "sender" cells, which fluoresce red, and "receiver" cells, which fluoresce green.

The sender plasmid has two genes controlled by the lac operon, mCherry a RFP, and luxI, the AHL producing protein. Essentially, the repressor protein lacI, constitutively expressed in this E. Coli strain (DH5α), binds to the lac promoter, preventing expression of the genes controlled by the lac operon. Upon addition of allolactose, or its analog IPTG, the repressor is unbound from DNA, allowing expression of the genes. In the case of this plasmid in DH5α E. Coli, the threshold concentration of IPTG was found to be approximately 38 μM, with a Hill coefficient of 2.1.
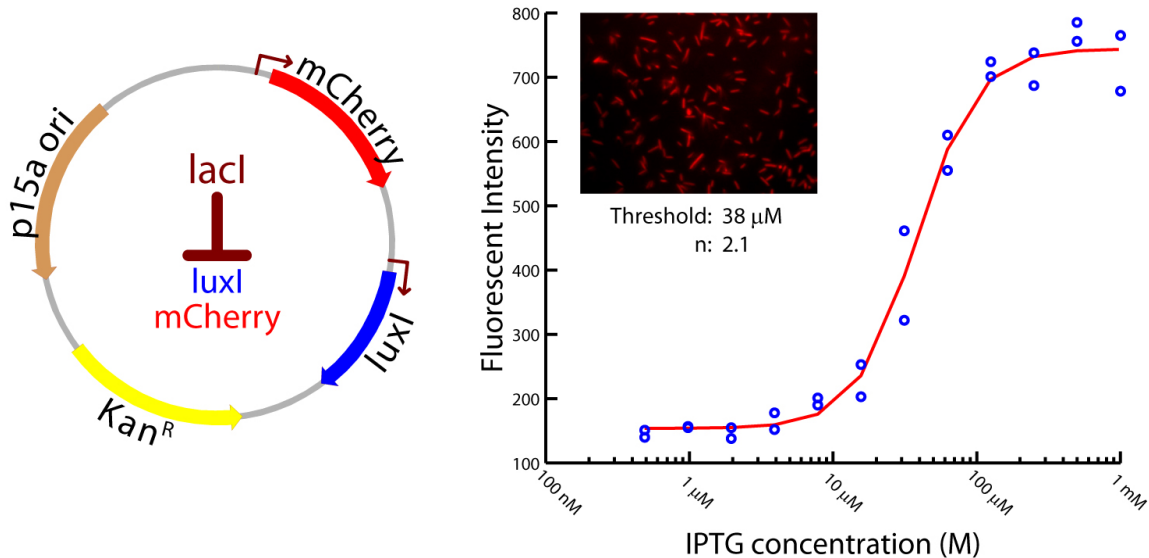
Figure 5-2: (Left) Sender plasmid map (Right) Plate reader data of various IPTG dilutions(blue circles) and a Hill equation fit to the data(red line) (Right inset) Fluorescence microscopy image of cells transformed with sender plasmid.

The receiver plasmid has the luxR gene, the AHL binding protein, controlled by the luxP(L) promoter. It has the GFP-LVA gene, a degradable form of GFP[6], controlled by the luxP(R) promoter. As described elsewhere(see 6-1) luxR binds AHL and dimerizes, binding to DNA at the lux promoter region. It downregulates

the luxP(L) promoter, controlling luxR production, and upregulates the luxP(R) promoter, controlling GFP-LVA production. In the case of this plasmid in DH5α E. Coli, the threshold concentration of AHL was found to be approximately 4.7 nM, with a Hill coefficient of 2.1 It should be noted that the noise in this plasmid was especially low, probably due to the degradation tag on the C-terminal end of GFP. This degradation tag also causes the bacteria to be very sensitive to temporal changes in the AHL concentration, i.e. if the AHL concentration drops, the fluorescence of the cells will drop rapidly in response.

Figure 5-3: (Left) Receiver plasmid map (Right) Plate reader data of various AHL dilutions (blue circles) and a Hill equation fit to the data (green line) (Right inset) Fluorescence microscopy image of cells transformed with receiver plasmid.

The plasmids both have the same backbone, a p15a origin of replication with a kanamycin resistance gene. The origin of replication controls the number of plasmid copies in a given bacterial cell, usually giving 10-12 copies per cell.[137] The kanamycin resistance gene is constitutively expressed, modifying kanamycin and preventing its binding to the 70S ribosomal subunit. This allows bacteria containing the plasmid to survive.[152]

5.2.4 Cell Culture

For prokaryotic cell experiments, Escherichia Coli cells of the DH5α strain were used. Chemically competent cells of this strain were purchased(Invitrogen # 18258-012) and transformed with either the 111 or the 203 plasmid(see 5.2.3). These cells were cultured on LB-agar plates using kanamycin as a selection marker, and grown up in M9-Glycerol media. M9-Glycerol is composed of : 0.2% (v/v) glycerol, 42 mM Na_2HPO_4, 22 mM KH_2PO_4, 19 mM NH_4Cl, 9 mM NaCl, 1 mM $MgSO_4$, 100 μM $CaCl_2$, 200 μM thiamine hydrochloride, and 0.2% (w/v) casamino acids. 100 μg/mL ampicillin is added to the media for use as a selection marker.

5.2.5 Hydrogel Solution

The hydrogel solution was composed of a pre-polymer mix consisting of poly (ethylene glycol) diacrylate (MW=3400 Da) dissolved in M9 minimal media (without the thiamine and casamino acids) to yield a 5% (w/v) final concentration. 1 mL samples of bacteria grown in M9 overnight at 25°C were centrifuged 3 times for 5 min at 800g. Between each spin cycle the supernatant was aspirated, and the bacterial pellet re-suspended in 1 mL of M9-Glycerol media. Finally, a pre-polymer mixture comprised of 3400 Da MW PEGDA (Nektar Therapeutics) dissolved in M9-Glycerol along with photoinitiator, 2-hydroxy-2-methyl-propiophenone was vigorously vortexed for 1 minute, and then combined with the cell suspension for a final concentration of 5% (w/v) PEGDA and 0.2% (v/v) photoinitiator.

5.2.6 Pumping Apparatus

Syringes are loaded into one of two Pico Plus (Harvard Apparatus) syringe pumps: one syringe pump is for syringes which feed the left and right channels, containing cell suspensions, and the second syringe pump is for the sterile center channel, containing M9/PEGDA only. The pumps are computer controlled through an RS232 interface, with code written in LabView.

5.2.7   Optics Setup

As illustrated in 5-4, the arrays are formed with optical tweezers produced from a CW Ti:Sap laser beam and a Zeiss Achroplan 100x oil immersion objective (1.25NA) held in an inverted optical microscope (Zeiss Axiovert 200M). We used a unique combination of two diffractive elements, acousto-optic deflectors (AODs) to create time-shared traps in 2D and a spatial light modulator (SLM) acting as a Fresnel lens to give control of the Z-dimension.
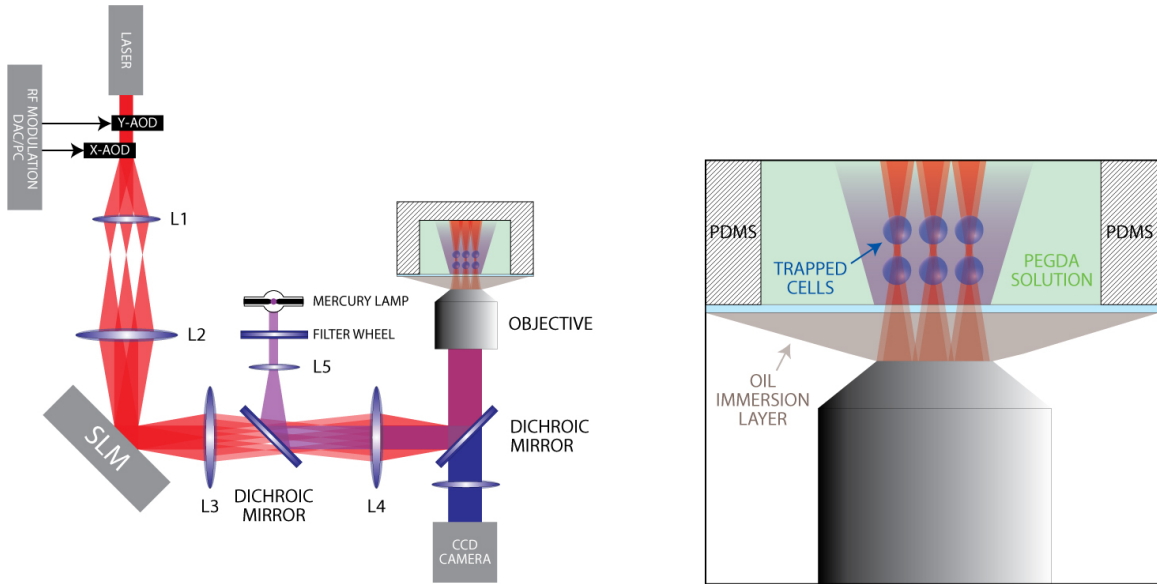
Figure 5-4: Schematic diagram of a time-shared holographic optical trapping apparatus. Trap arrays are formed using a high NA objective in a commercial optical microscope in conjunction with two acousto-optic deflectors and a spatial light modulator (SLM) to produce a time-shared (3D) array of optical traps.

In this configuration, the CW Ti:Sap beam is deflected transverse to the direction of propagation using two orthogonally-mounted AODs to give independent control of the x- and y-positions of a trap. The beam is time-shared between different positions in the 2D array: i.e. it is scanned rapidly from one trap position to the next, dwelling at the desired position in the array just long enough to form an optical trap and fix the location of the cell.[116]

The SLM was then used to introduce phase shifts to implement a diffraction grating, offsetting the time-shared array transverse to the beam, and Fresnel lenses

to offset the array along the optical axis. This allows for duplication of the array along Z, with an offset in X and Y, if desired. To determine the phase distribution in the SLM plane required to produce the desired intensity distribution in the trapping plane, we used the Gerchberg-Saxton algorithm, described in detail elsewhere.[153]

Relay lenses were used to image the beam emerging from the AOD or SLM onto the back aperture of the objective. The optical systems comprised of lenses L1 and L2, and L3 and L4 are both afocal: i.e., a collimated incoming beam will emerge collimated. The focal length of lenses L1, L2, L3 and L4 and the separation between them are chosen so that a small deflection of the beam results in a change only in the direction of the laser beam at the objective entrance aperture, without any change in position.[63] Typically, the cells were trapped about 5μm above the surface of the coverslip to minimize spherical aberrations from the media. We measured the power incident on the back aperture of the 1.25NA 100x objective for each wavelength and then corrected for the transmission through the objective using transmission curves provided by Zeiss.[34] The transmission over the wavelength range $840 \leq \lambda \leq 930$ nm was approximately 73%.

In order to polymerize the hydrogel in a microfluidic device, it was necessary to bring the UV light in through the microscope objective as well. The reason for this was twofold: it is desirable to have a small hydrogel spot in microfluidics, easily possible with a high NA objective, and the PDMS created too much scattering for efficient gel polymerization through the top.

To generate the UV light, a metal halide lamp(Exfo X-Cite 120) was used, filtered with a 360/50 nm filter held in a shuttered Ludl filter wheel. The light was brought to the main light path using a dichroic mirror which allowed IR light to pass while reflecting UV light. This allowed the UV light to be introduced to the optical path right before the beam entered the back of the Zeiss 200M microscope. Lenses were used to ensure that the IR beam and UV beam were confocal. A secondary advantage of this setup was the ability to employ the shuttered filter wheel to acquire epifluorescent images from the sample.

5.2.8   Array Formation

To assemble the arrays, hydrogel solutions as described above are prepared: two solutions containing different cell types and a third solution containing PEGDA but barren of cells. The solutions are loaded using a syringe pump into the microfluidic chip, at an initial rate of 20 μL/min. After the bacterial solution have reached the chip and the flow has stabilized, the pumps are slowed to 0.02-0.05 μL/min, to allow for trapping. Any faster flow rate prevents trapping at the low trapping power (<5mW time-averaged power) we use to ensure viability. Cells are trapped from one bacterial flow, then the stage is moved to the other side of the microfluidic, holding the cells in the traps the entire time. The other type of cells are then added to the array of traps, completing the array. The array is then moved into the sterile channel and a burst of UV light (<4s) is used to polymerize the heterotypic array.

5.3   Results

5.3.1   Initial Hurdles

Moving our trapping/hydrogel system[1] into a microfluidic posed some challenges. First was polymerization of the hydrogel inside the microfluidic. As has been previously mentioned2-7, PEGDA polymerization is strongly inhibited by oxygen.[53] Since PDMS allows oxygen to diffuse freely[43], a reservoir of oxygen has effectively been placed at the PDMS/liquid interface, inhibiting gel formation. This forces constraints on the microfluidic design - the desired location of the gel must be a sufficient distance away from all PDMS surfaces. It was also empirically determined that flowing argon through the chip for 2-3 hrs before use aided in consistent gel polymerization, effectively degassing the chip.

The other problem was attempting to trap cells under microfluidic flow. Optical traps provide only weak forces($\sim$nN), which are proportional to the power of the laser beam used. As we are trying to minimize power for cell viability concerns(see 4), the traps are relatively weak. The force of fluid applied to the cells is dependent on flow

speed - this essentially gives a constraint on using low flow on trapping, of less that 0.1 μL/min.

5.3.2 Heterotypic Arrays

To test our technique, we first assembled a simple 4x5 array in 2D, with the left two columns composed of cells capable of expressing red fluorescent protein ("senders";RFP), and the right two columns composed of cells capable of expressing green fluorescent protein ("receivers";GFP). We then chemically induced the cells to express these proteins using 1 mM IPTG and 1 μM AHL. The resulting fluorescence after 4 hrs is shown in 5-5, demonstrating the ability to form simple heterotypic arrays. It also reveals another feature of microfluidics - the ability to deliver various chemicals and observe the resulting behavior.

Further, we wanted to test our ability to make three dimensional arrays in the microfluidic. There was some concern that the flow rate higher in the channel would preclude the formation of arrays too far from the coverslip bottom. This was not the case, as seen in 5-6. A 2x2 array of red cells was placed in the center plane, with 2x2 arrays of green cells placed above and below by about 15μm.

This image also illustrates the structure of the gel spot in the microfluidic chip. When gelling from the objective, the gel spot forms a roughly cylindrical structure, in this case 100 μ in diameter by 60 μ tall. Such a small gel spot allows for fine control of the chemical profile by properly adjusting the flow and chemistry of its surroundings using the microfluidic.

5.4 Conclusion

Combining our previous photopolymerization technique with microfluidics opens the door to the creation of heterotypic arrays. These arrays may be useful for the study of cell signaling, tissue engineering, or biosensor applications. The microfluidics provide an ancillary benefit in that they allow control of the ability to pulse chemical signals to the encapsulated cells, and watch the ensemble response. Resistance or tolerance
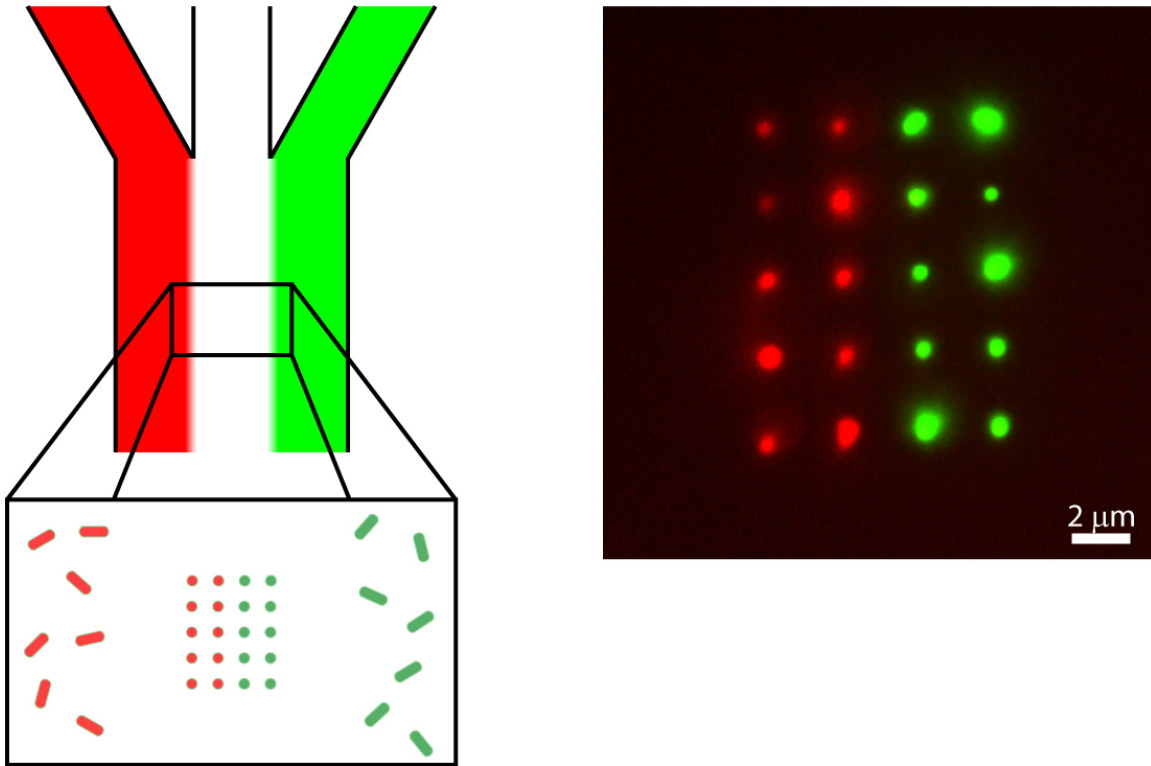
Figure 5-5: In order to pattern two genotypically different cells, a 3-way microfluidic was used. Essentially, one cell type(red) was flowed in one side channel, another cell type(green) in the other side channel. The center channel was pumped with sterile solution, in order to keep the two populations of bacteria well separate. Using optical trapping in combination with a motorized stage, cells from each flow could be captured and patterned into arrays, as shown in the image on the right. The left half of the array contains cells expressing RFP1 and the right half has cells expressing GFP.

to drugs, study of the time-dependent response, and many other options become open with this new development.
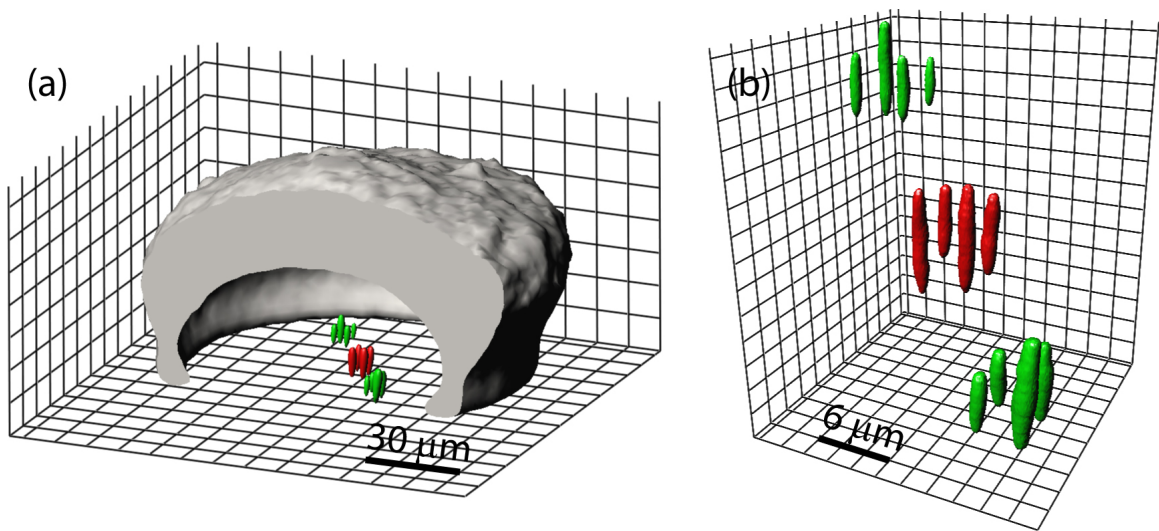
Figure 5-6: 3D Heterotypic array formed in a microfluidic device with optical trapping. The bacterial cells were stained with SYTO9 and the gel spot stained with rhodamine to increase signal to noise. The spot was then scanned with a Leica SP2 laser scanning confocal microscope. (a)Iso-surface reconstruction of gel spot and array; the gel spot has been cross-sectioned in order to display the array clearly. (b) Iso-surface reconstruction of higher-mag image stack taken of array

Chapter 6

Cell Signaling

6.1 Introduction

Quorum sensing (QS) is a regulatory mechanism that has evolved in bacteria as a means for launching a coordinated response to environmental cues.[15, 72, 69, 68] It has been implicated in the regulation of diverse physiological processes such as bioluminescence, swarming, and swimming. It also plays a significant role in pathogenesis, allowing bacteria to reach high populations before producing virulence factors that elicit an immune response in the host.[15] According to the quorum sensing hypothesis, bacteria count their numbers by producing, releasing, and detecting small signaling molecules called autoinducers (AI). At low population density, the AI-synthase gene expresses at a low basal-level, producing a small amount of AI that diffuses out of the cell and is diluted in the environment without effect. An increase in the population results in a local accumulation of AI in and around the cells that eventually activates a transcription regulator protein by binding to it. The activated regulator-AI complex interacts with the target operon, providing positive feedback by upregulating the AI-synthase gene and inducing certain AI-regulated phenotypes in the population. How many bacteria constitute a quorum? It is likely that the answer is influenced by the social-environmental context as it affects signaling.[82, 139, 61] Most of the experiments used to test QS are done in a shaken culture flask. In a culture flask, the QS signal accumulates to a threshold concentration at a specific

point in the growth curve. The cell population is actively mixed, being constrained only by the size of the (large) culture vessel, so that the AI is dispersed among the population (although the population itself is not necessarily dispersed.) However, the diffusion, mixing and flow of autocrine-paracrine signals in the microenvironment of a cell in vivo is difficult to emulate in a culture flask. Bacteria naturally coexist in open, multi-kingdom communities where intraspecies, interspecies, and bacteria-host communications occur simultaneously, with a signal concentration that depends on: 1. the production rate of the signal; 2. the half-life or degradation of the signal; 3. the rate of diffusion between cells; and 4. mass-transfer to a surrounding fluid.[82] An especially noxious example of such a community is the biofilm. A biofilm is comprised of microcolonies of bacteria encapsulated in a hydrated matrix of polysaccharides, proteins and exopolymeric substances. The mass transport in a biofilm exhibits gross deviations from Brownian diffusion-in some cases the diffusion coefficient is 50 times smaller than in aqueous solutions.[76] Consequently, the chemistry (pH, dissolved oxygen, etc.) in a biofilm can vary drastically over a short (100 μm) distance, which can have a profound effect on the signal production rate and half-life, and antibiotic resistance.[82]

A living cell microarray affords us unprecedented control over cell-to-cell communications. Cells act like transmitters and receivers of chemical signals. Heterogeneous microarrays provide us with a diverse library of these biochemical signals through control of the constituent cell types, and at the same time allow us to stringently control the diffusive flux of signals through manipulation of the relative positions of the cells. In preliminary work (presented below), we have shown that it is possible using optical tweezers in conjunction with a microfluidic network to create a heterogeneous, 3D microarray of bacteria that either transmit or receive QS signals, and then follow the space-time development of fluorescent reporters associated with the individual cells comprising the array. We have also shown that it is possible to influence the signaling between transmitters and receivers by controlling the external hydrodynamics of the overlying fluid. Now, we intend to discover the physical, chemical and biological parameters governing QS by engineering bacteria that both transmit and receive

the same signals with a functionally linked fluorescent reporter; array the mutants on a bio-compatible scaffold that limits diffusion, just like in a biofilm; and then follow the spatio-temporal development of QS genes.

Optical tweezers and hydrogels are linchpins of this proposal, enabling a study of the spatio-temporal development of QS in the individuals that comprise a vast array of bacteria (and eukaryotes). The micromanipulation of biology by light has recently undergone a revolution.[75] Twenty years ago, in pioneering work Ashkin demonstrated that light pressure forces could displace and levitate bacteria and viruses, and even manipulate organelles in living cells.[8, 10, 12] He used a single-beam gradient force optical trap-now commonly referred to as optical tweezers-that is produced by focusing a single TEM_{00} laser beam of wavelength λ to the diffraction-limit with a high numerical aperture (NA) microscope objective. Although the trapping force is weak ($\sim$ 1nN), micrometer-scale objects like cells have a minuscule mass (a red blood cell weighs $\sim$ 1pN) so optical tweezers can be effective for micromanipulating living tissue. Now with the development of evanescent-wave[90, 140] and holographic arrays,[133, 49] and multi-functional traps[39, 108], optical tweezers can be used to exert a wide range of force and torque at many points in space and time with subnanometer and submillisecond resolution.[121, 163] While optical trapping allows for the creation of complex arrays, the light still has to be held on the cells to maintain the array. So, to fix the position of the cells (semi-)permanently, we use a scaffold made from a photopolymerizable hydrogel. Hydrogels are used prevalently as a scaffold for tissue engineering[94, 93, 135, 4, 138, 45, 104, 162] to mimic the extra-cellular matrix (ECM). Hydrogel is a network of hydrophilic polymers capable of absorbing and holding large amount of water (over 90% of water in most cases). Polymers such as PLA, poly(N-isopropyl acrylamide, PEG, poly(hyaluronic acid) and poly(sodium alginate) have been used in hydrogel synthesis. A hydrogel may be polymerized through many different mechanisms; cross-linking either through covalent bonding or through physical interaction of hydrophobic segments. To form a scaffold to support the biofilm, it is crucial that gelation occur in the presence of cells, and so a relatively benign inducer such as temperature, pH or UV, are required.

One of the more prevalent and practical hydrogel processes is photopolymerization of poly(ethylene glycol) diacrylate (PEGDA), pioneered by Hubbell and coworkers. The resulting PEGDA hydrogels have excellent biocompatibility and hydrophilicity, and can be tailored to have adjustable porosity and mechanical properties by varying the PEG chain length. Bacteria and eukaryotes can remain viable for weeks encapsulated in a hydrogel environment.[28, 81]

6.2 Methods

6.2.1 Bacterial Signaling

We have chosen to examine the quorum sensing system of *Vibrio fischeri*. Essentially, *V. fischeri* is an aquatic bacteria that has a symbiotic relationship with *Euprymna scolopes*, the Hawaiian bobtail squid[145]. *V. fischeri* lives in one of two states: as a highly concentrated(10^10 cells/mL), homotypic culture within a "light" organ of the squid, producing light via bioluminescence, or swimming within the oligotrophic seawater at a low cell density.[69] With *V. fischeri* acting as a diffuse light source, *E. scolopes* directs the light downward, removing their shadow and making them invisible to predators below, as a sort of advanced stealth technique.[68]

As light production is an *extremely* energetically demanding process, and produces nothing of direct value for the bacteria. So, if not present within the light organ of the squid, this effect is turned off. These genes are regulated, as seen in 6-1, by the local concentration of an autoinducer molecule, N-(3-oxohexanoyl)homoserine lactone, an acyl-homoserine lactone (AHL). AHL is produced by the protein luxI, which is leakily expressed by the luxP(R) promoter.

When a large number of *V. fischeri* are in a enclosed, transport hindered area, AHL is able to accumulate, and turn on the lux promoter further. The positive feedback causes this reaction to snowball, turning on the entire lux operon, expressing genes required for luminescence luxCDABEG.[69]

Using BioBricks^TM, we have been able to construct plasmids which contain the
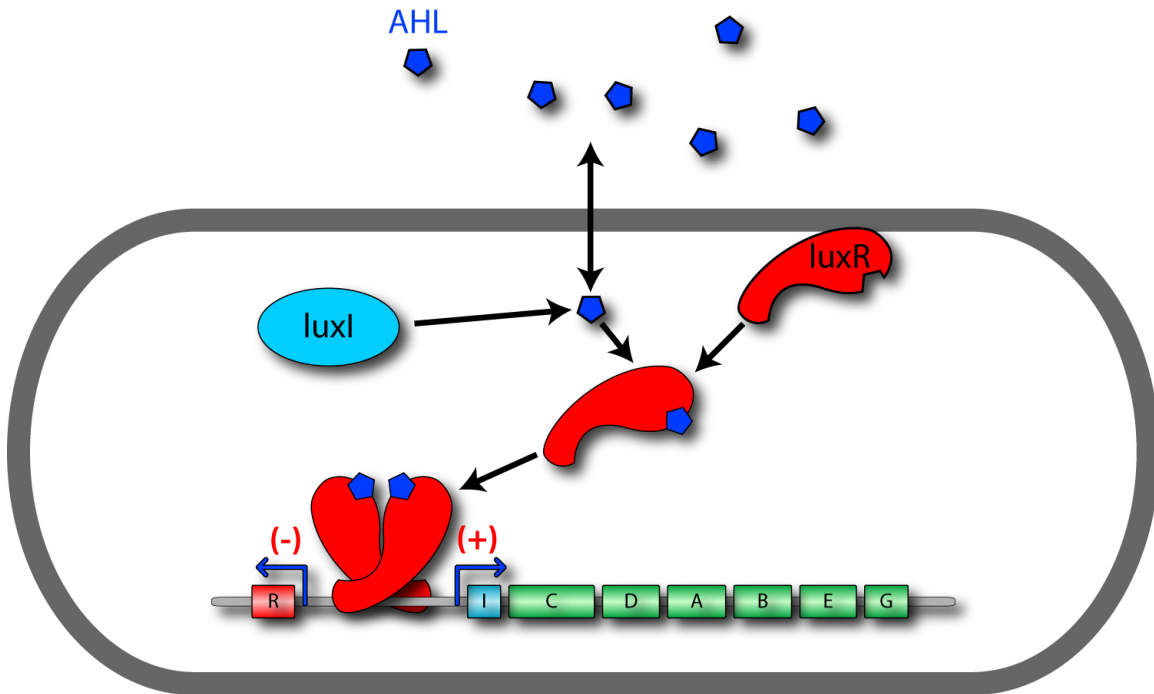
Figure 6-1: The operation of the quorum sensing system of *Vibrio Fischeri*. luxI, present through leakage of the lux operon, produces the autoinducer molecule AHL, which builds up in the environment until it reaches a critical concentration. luxR binds AHL, dimerizes and binds the lux promoter region, upregulating production of luxI, providing positive feedback, as well as luxCDABEG, required for light production. luxR is downregulated by the same binding.[69]

AHL producing and AHL detecting portions of the *V. fischeri* genome(see 6-2.[16]

Essentially, the "sender" cells, under control of the lac operon, produce luxI and red fluorescent protein (RFP). luxI produces AHL, which then diffuses out of the cell, and is detected by the "receiver" cells. These receiver cells, in response to AHL, produce green fluorescent protein (GFP). These plasmids are then transformed into chemically competent *E. Coli* cells.

In order to find the transfer function of these plasmids, we used a 96-well fluorescent plate reader to observe E. Coli transformed with these plasmids, and induced with various dilutions of IPTG or AHL.

The sender plasmid has two genes controlled by the lac operon, mCherry, a RFP, and luxI, the AHL producing protein. Essentially, the repressor protein lacI, constitutively expressed in this *E. Coli* strain (DH5α), binds to the lac promoter, preventing
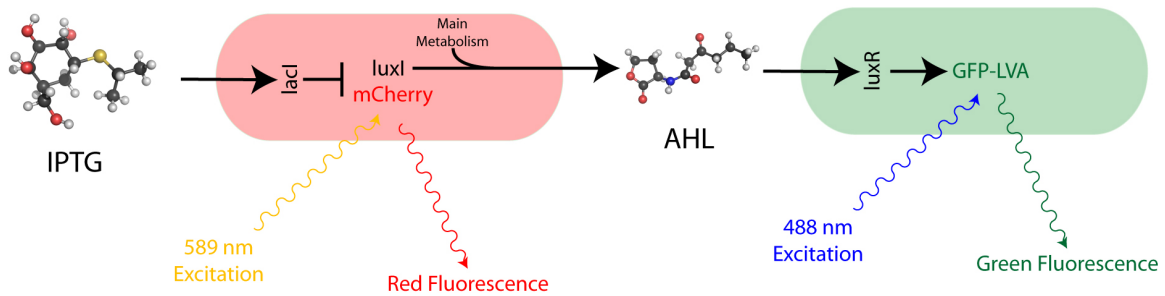
Figure 6-2: Bacterial signaling model: Sender cells fluoresce red and produce AHL in response to IPTG; Receiver cells fluoresce green in response to AHL

expression of the genes controlled by the lac operon. Upon addition of allolactose, or its analog IPTG, the repressor is unbound from DNA, allowing expression of the genes. In the case of this plasmid in DH5α *E. Coli*, the threshold concentration of IPTG was found to be approximately 38 μM, with a Hill coefficient of 2.1.
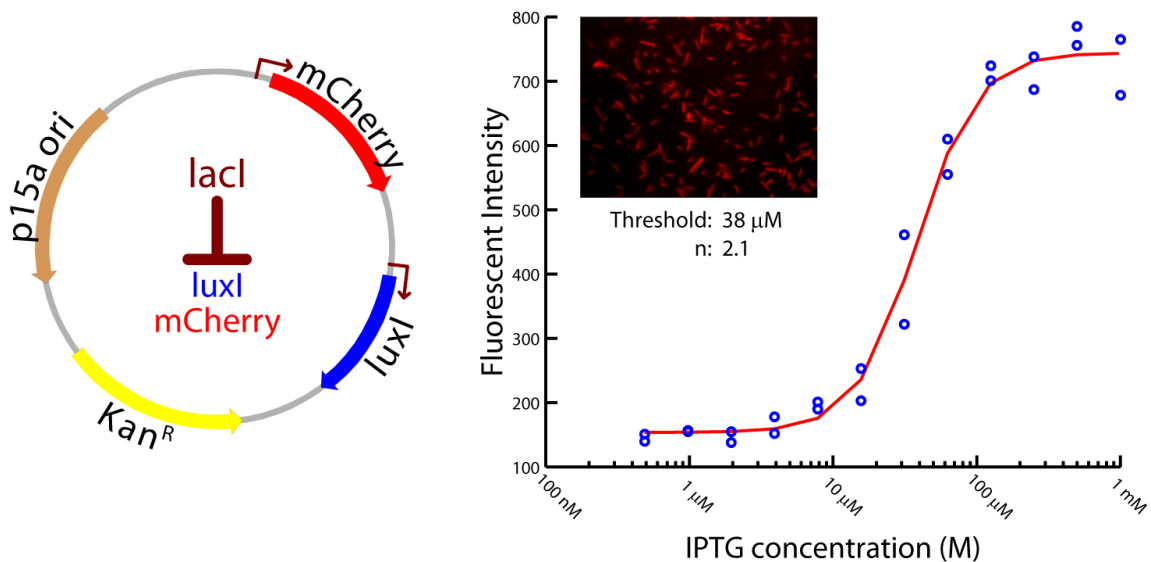
Figure 6-3: (Left) Sender plasmid map (Right) Plate reader data of various IPTG dilutions(blue circles) and a Hill equation fit to the data(red line) (Right inset) Fluorescence microscopy image of cells transformed with sender plasmid.

The receiver plasmid has the luxR gene, the AHL binding protein, controlled by the luxP(L) promoter. It has the GFP-LVA gene, a degradable form of GFP[6], controlled by the luxP(R) promoter. As described elsewhere(see 6-1) luxR binds

AHL and dimerizes, binding to DNA at the lux promoter region. It downregulates the luxP(L) promoter, controlling luxR production, and upregulates the luxP(R) promoter, controlling GFP-LVA production. In the case of this plasmid in DH5α E. Coli, the threshold concentration of AHL was found to be approximately 4.7 nM, with a Hill coefficient of 2.1 It should be noted that the noise in this plasmid was especially low, probably due to the degradation tag on the C-terminal end of GFP. This degradation tag also causes the bacteria to be very sensitive to temporal changes in the AHL concentration, i.e. if the AHL concentration drops, the fluorescence of the cells will drop rapidly in response.

Figure 6-4: (Left) Receiver plasmid map (Right) Plate reader data of various AHL dilutions (blue circles) and a Hill equation fit to the data (green line) (Right inset) Fluorescence microscopy image of cells transformed with receiver plasmid.

The plasmids both have the same backbone, a p15a origin of replication with a kanamycin resistance gene. The origin of replication controls the number of plasmid copies in a given bacterial cell, usually giving 10-12 copies per cell.[137] The kanamycin resistance gene is constitutively expressed, modifying kanamycin and preventing its binding to the 70S ribosomal subunit. This allows bacteria containing the plasmid to survive.[152]

6.2.2   Microfluidics

Microfluidic design and setup are described in detail elsewhere (see 5.2).

Essentially, a chip is constructed using replica molding of (dimethyl siloxane) (PDMS) from a CAD designed mold with three separate feed channels. The mold is created using off-site stereolithography (FineLine Prototyping) and coated with (Tridecafluor-1,1,2,2-Tetrahydrooctyl)-1-Trichlorosilane to aid in PDMS delamination. Sylgard 184 at a 1:5 ratio of curing agent:base is used as the PDMS formulation, and cured at 75°C for ≥ 2 hrs.

After cooling, the PDMS is removed from the mold, holes are punched in it for fluidic access, and it is plasma bonded to a #1 glass coverslip. Tubing is connected to the PDMS chip, and a coating solution of 3-(trimethoxysilyl) propyl methacrylate was added to limit bacterial adhesion and increase hydrogel adhesion.

6.2.3   Optics Setup

As illustrated in 6-5, the arrays are formed with optical tweezers produced from a CW Ti:Sap laser beam and a Zeiss Achroplan 100x oil immersion objective (1.25NA) held in an inverted optical microscope (Zeiss Axiovert 200M). We used a unique combination of two diffractive elements, acousto-optic deflectors (AODs) to create time-shared traps in 2D and a spatial light modulator (SLM) acting as a Fresnel lens to give control of the Z-dimension.

In this configuration, the CW Ti:Sap beam is deflected transverse to the direction of propagation using two orthogonally-mounted AODs to give independent control of the x- and y-positions of a trap. The beam is time-shared between different positions in the 2D array: i.e. it is scanned rapidly from one trap position to the next, dwelling at the desired position in the array just long enough to form an optical trap and fix the location of the cell.[116]

The SLM was then used to introduce phase shifts to implement a diffraction grating, offsetting the time-shared array transverse to the beam, and Fresnel lenses to offset the array along the optical axis. This allows for duplication of the array

Figure 6-5: Schematic diagram of a time-shared holographic optical trapping apparatus. Trap arrays are formed using a high NA objective in a commercial optical microscope in conjunction with two acousto-optic deflectors and a spatial light modulator (SLM) to produce a time-shared (3D) array of optical traps.

along Z, with an offset in X and Y, if desired. To determine the phase distribution in the SLM plane required to produce the desired intensity distribution in the trapping plane, we used the Gerchberg-Saxton algorithm, described in detail elsewhere.[153]

Relay lenses were used to image the beam emerging from the AOD or SLM onto the back aperture of the objective. The optical systems comprised of lenses L1 and L2, and L3 and L4 are both afocal: i.e., a collimated incoming beam will emerge collimated. The focal length of lenses L1, L2, L3 and L4 and the separation between them are chosen so that a small deflection of the beam results in a change only in the direction of the laser beam at the objective entrance aperture, without any change in position.[63] Typically, the cells were trapped about 5μm above the surface of the coverslip to minimize spherical aberrations from the media. We measured the power incident on the back aperture of the 1.25NA 100x objective for each wavelength and then corrected for the transmission through the objective using transmission curves provided by Zeiss.[34] The transmission over the wavelength range $840 \leq \lambda \leq 930$ nm was approximately 73%.

97

In order to polymerize the hydrogel in a microfluidic device, it was necessary to bring the UV light in through the microscope objective as well. The reason for this was twofold: it is desirable to have a small hydrogel spot in microfluidics, easily possible with a high NA objective, and the PDMS created too much scattering for efficient gel polymerization through the top.

To generate the UV light, a metal halide lamp(Exfo X-Cite 120) was used, filtered with a 360/50 nm filter held in a shuttered Ludl filter wheel. The light was brought to the main light path using a dichroic mirror which allowed IR light to pass while reflecting UV light. This allowed the UV light to be introduced to the optical path right before the beam entered the back of the Zeiss 200M microscope. Lenses were used to ensure that the IR beam and UV beam were confocal. A secondary advantage of this setup was the ability to employ the shuttered filter wheel to take epifluorescent data of the sample.

6.2.4   Array Assembly

To assemble the arrays, hydrogel solutions as described above are prepared: two solutions containing different cell types and a third solution containing PEGDA but barren of cells. The solutions are loaded using a syringe pump into the microfluidic chip, at an initial rate of 20 μL/min. After the bacterial solution have reached the chip and the flow has stabilized, the pumps are slowed to 0.02-0.05 μL/min, to allow for trapping. Any faster flow rate prevents trapping at the low trapping power ($<$5mW time-averaged power) we use to ensure viability. Cells are trapped from one bacterial flow, then the stage is moved to the other side of the microfluidic, holding the cells in the traps the entire time. The other type of cells are then added to the array of traps, completing the array. The array is then moved into the sterile channel and a burst of UV light ($<$4s) is used to polymerize the heterotypic array.

6.2.5   Fluid Simulation

In order to determine the convective flow profile in the microfluidic device, we chose to simulate it using a finite element method. This was implemented using COMSOL Multiphysics(COMSOL). The microfluidic structure was created in 3D, exactly as specified in the design file for the stereolithography mold. This geometry correlated well with the SEM results found of the PDMS chip previously(see 5-1). Empirical measurements of the location and dimensions of the hydrogel spot were used to place a cylinder approximating its shape in the microfluidic channel(see 5-6).

The boundary conditions for the walls of the microfluidic and the surface of the hydrogel spot were set as a no-slip condition, i.e. velocity of flow must be zero at a solid surface. spot. Entry points of the microfluidic were defined to have parabolic flow given by:

$$\boldsymbol{u} = \boldsymbol{n} \cdot 4U_{max}(1 - s_1)(1 - s_2) \tag{6.1}$$

where $\boldsymbol{u}$ is the velocity vector, $\boldsymbol{n}$ is the vector normal to the entry port, s_1 and s_2 are values from 0 to 1 which range along the length of either axis of the square entry port. U_{max}, the maximum velocity of the flow, is given by:

$$U_{max} = \frac{Q_{in}\,\mu L/min}{60\,s/min} \times \frac{1\,m^3}{10^9\,\mu L} \times \frac{36}{A_{entry}} \tag{6.2}$$

with Q_{in} the volume rate of input flow set by the syringe pump, and A_{entry} the cross-sectional area of the entry port. The exit port allows the flow to freely exit from this interface.

The geometry was automatically meshed, with a vertex density set by the smallest features in the geometry. The hydrogel spot, and the accompanying high resolution areas within it, were excluded entirely from this simulation, acting only as a no-slip boundary for the microfluidic.

As any flow perturbation had a faster transient than any other element in our system, and the fluid flow is kept generally constant for the experiment, the flow was solved for a steady-state situation. The governing equation for the simulation was

given as:

$$\rho(\frac{\partial \boldsymbol{v}}{\partial t} + \boldsymbol{v} \cdot \nabla \boldsymbol{v}) = -\nabla P + \eta \nabla^2 \boldsymbol{v} \tag{6.3}$$

assuming an incompressible fluid:

$$\nabla \cdot \boldsymbol{v} = 0 \tag{6.4}$$

We assume that the M9 solution has a similar viscosity $\eta = 1 \times 10^-3\,Pa \cdot s$ and density $\rho = 1g/cm^3$ to that of water.

6.2.6   Signal Transport Simulation

With a good idea of the fluid flow profile, the next step is to attempt to simulate the mass transport of the signal through both advection and diffusion, in the microfluidic and through the hydrogel spot.

To prevent the problem from becoming computationally intractable, only the small section of the microfluidic 100 μm up and downstream of the hydrogel spot was simulated. Bacteria were placed at their proper positions inside the hydrogel spot using cylinders 1 μm x 3 μm to approximate their size.

This area was simulated with a finite element model of advection/diffusion (COMSOL Multiphysics), with the mesh set automatically, though with guidance to be tightly spaced around the bacteria. In order to accomplish this, a smaller encapsulating cylindrical mesh region was placed around the bacteria, as can be seen in 6-6(right).

The concentration at the upstream face was set to be 1 mM [IPTG] and 0 [AHL], and at the downstream face, the boundary condition was set to allow convective transport of material outward. All other microfluidic faces were set to be a zero flux condition, i.e. that no material could transmit through. Despite the porous, somewhat absorbing nature of PDMS, this was thought to be a reasonable assumption.

An estimation of the free solution diffusion coefficients of IPTG and AHL was
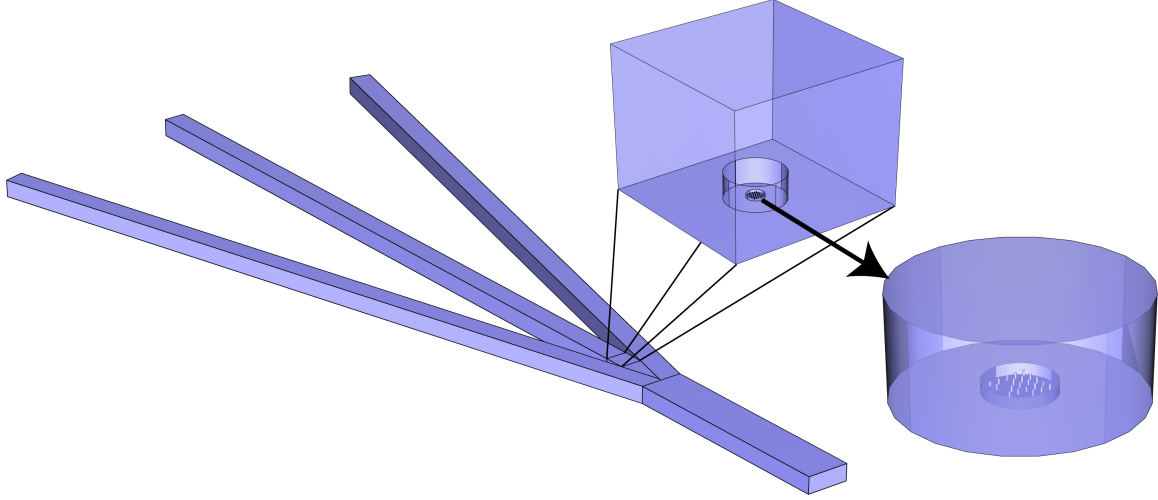
Figure 6-6: (Bottom left) Geometry of microfluidic simulation (Middle) Section of microfluidic fully simulated for signal transport (Right) Closer view of hydrogel spot, with bacteria contained within

given by the Stokes-Einstein equation:

$$D = \frac{k_B T}{6\pi \eta R_0} \tag{6.5}$$

with D as the diffusion coefficient, k_B Boltzmann's constant, η the solvent viscosity and R_0 the radius of the solute[50]. This estimate is usually accurate to within 20%. Using 1nm as the size of the molecules(see 6-7), a value of $2.2 \times 10^{-6} \, cm^2/s$ is used for the initial simulation values.

Inside the hydrogel, diffusion is hindered as it is a porous matrix. The speed of solute motion through the hydrogel is limited by the size and chemistry of the pores. The value of this hindered diffusion coefficient is given by:

$$D_{hydrogel} = \epsilon \frac{D_{free}}{\tau} \tag{6.6}$$

with D_{free} the diffusion in free solution, ϵ the fraction of hydrogel composed of solvent(water), and τ the tortuosity of the hydrogel. As a hydrogel is composed primarily of water, we expect ϵ to be between 0.8 and 1. The tortuosity usually ranges between 2 and 6 for hydrogels, with an average of about 3. Based on measurements
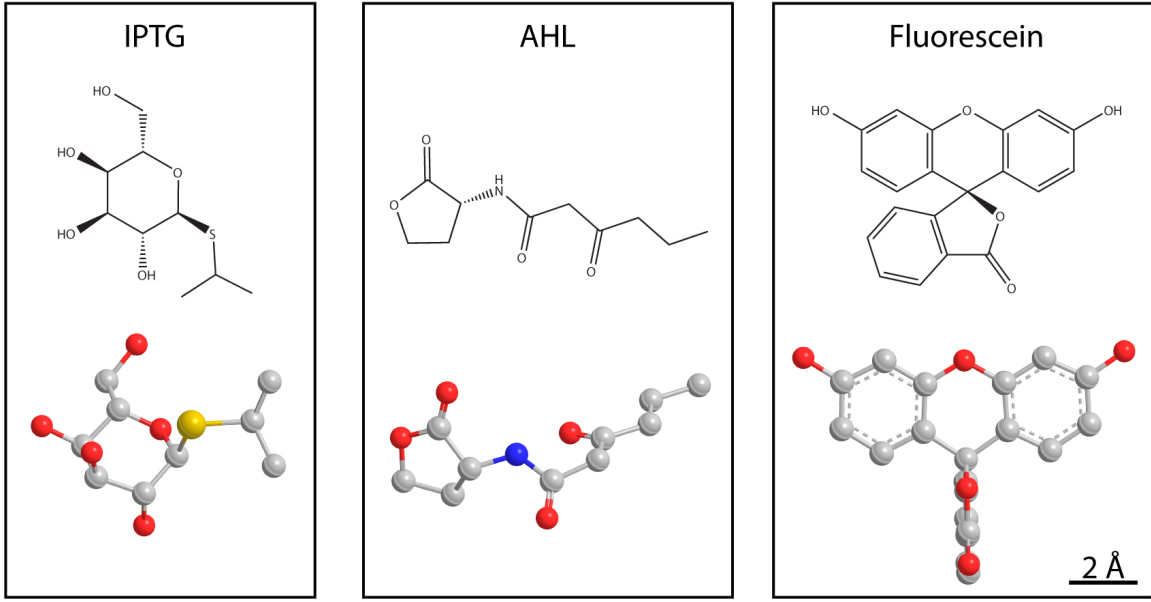
Figure 6-7: Chemical structure and 3D reconstruction of the molecules used in simulation and experiments; scale bar is 2 Å

made previously (see 2.3.3) we find a diffusion coefficient of fluorescein for our 3400 MW hydrogel of $8.0 \times 10^{-7} \, cm^2/s$. With other measurements, this gives a ϵ of 0.9 and a τ of 3. These values were used to estimate initial values for the ratio of diffusion coefficient in hydrogel to that in free solution.

AHL generation in the hydrogel is given by the solution to the bacterial ODEs (see 6.2.7). Essentially, this gives a concentration of luxI, the AHL producing protein, within the sender bacteria. This concentration is used to define a production rate of AHL within the volume defined by the sender bacteria. An experimentally determined initial value of $0.3 \frac{\text{molecules AHL}}{\text{molecules luxI·min}}$ is used to convert concentration of luxI to a rate of AHL production. The maximum production rate was determined biochemically by Schaefer et al as $1.1 \frac{\text{molecules AHL}}{\text{molecules luxI·min}}$.[150]

6.2.7 Bacterial Protein Simulation

Now that the fluid and signal transport problems have been solved, it is necessary to couple the bacterial behavior into these models. We have taken a simplistic view of the bacterial behavior/response to signals, simulating the behavior with mass-action

kinetics.

Cells regulate protein production through a series of transcription networks[5]. The details of operation of transcriptional networks are described elsewhere, but may be modeled as controlling the rate of protein production through the concentration of inducer. The governing equation for this behavior is called the Hill function, and appears like a monotonic, sigmoidal function described by:

$$\text{Protein Production Rate} = \frac{\beta[\text{Inducer}]^n}{K^n + [\text{Inducer}]^n} \tag{6.7}$$

with β the maximum rate of protein production, K the threshold concentration of inducer which causes half-max production, and n, the Hill coefficient, which controls the steepness of the function.

Even within our hydrogel, the bacteria are reproducing, and at the very least, their protein production capacity is increasing. This is encapsulated in the term:

$$\beta = \beta_0 2^{t/\nu} \tag{6.8}$$

where β_0 is the max protein production rate per cell, and ν the cell doubling time. The degradation rate of the protein is usually assigned as a half-life, given by :

$$\text{Protein Degradation Rate} = \alpha[\text{Protein}] \tag{6.9}$$

Where $ln(2)/\alpha$ is the half-life of the protein.

If we assume deterministic, mass-action kinetics occur in the bacteria, a protein production differential equation looks like:

$$\frac{\partial[\text{Protein}]}{\partial t} = \text{Production Rate} - \text{Degradation Rate} \tag{6.10}$$

$$= 2^{t/\nu} \frac{\beta_0[\text{Inducer}]^n}{K^n + [\text{Inducer}]^n} - \alpha[\text{Protein}] \tag{6.11}$$

Some of the proteins in our simulation, specifically RFP and GFP, have an additional post-translational modification not covered by 6.11. These fluorescent proteins

(FPs) are initially non-fluorescent; they must have their fluorophores oxidized before displaying fluorescent properties.[80] This introduces a new term for the rate of autoxidation, γ:

$$\frac{\partial[\text{FP}_{\text{unox}}]}{\partial t} = 2^{t/\nu} \frac{\beta_0[\text{Inducer}]^n}{K^n + [\text{Inducer}^n]} - (\alpha + \gamma)[\text{FP}_{\text{unox}}] \tag{6.12}$$

$$\frac{\partial[\text{FP}_{\text{ox}}]}{\partial t} = \gamma[\text{FP}_{\text{unox}}] - \alpha[\text{FP}_{\text{ox}}] \tag{6.13}$$

Using these base equations, the protein production for our sender cells is described as:

$$\frac{\partial[\text{RFP}_{\text{unox}}]}{\partial t} = 2^{t/\nu_r} \frac{\beta_{r0}[\text{IPTG}]^n_r}{K_r^{n_r} + [\text{IPTG}^{n_r}]} - (\alpha_r + \gamma_r)[\text{RFP}_{\text{unox}}] \tag{6.14}$$

$$\frac{\partial[\text{RFP}_{\text{ox}}]}{\partial t} = \gamma_r[\text{RFP}_{\text{unox}}] - \alpha_r[\text{RFP}_{\text{ox}}] \tag{6.15}$$

$$\frac{\partial[\text{luxI}]}{\partial t} = 2^{t/\nu_r} \frac{\beta_{r0}[\text{IPTG}]^{n_r}}{K_r^{n_r} + [\text{IPTG}^{n_r}]} - \alpha_r[\text{luxI}] \tag{6.16}$$

$$\tag{6.17}$$

and for the receiver cells as:

$$\frac{\partial[\text{GFP}_{\text{unox}}]}{\partial t} = 2^{t/\nu_g} \frac{\beta_{g0}[\text{AHL}]^{n_g}}{K_g^{n_g} + [\text{AHL}^{n_g}]} - (\alpha_g + \gamma_g)[\text{GFP}_{\text{unox}}] \tag{6.18}$$

$$\frac{\partial[\text{GFP}_{\text{ox}}]}{\partial t} = \gamma_g[\text{GFP}_{\text{unox}}] - \alpha_g[\text{GFP}_{\text{ox}}] \tag{6.19}$$

$$\tag{6.20}$$

6.3 Results and Discussion

6.3.1 2D Signaling

To elicit tissue-specific features, a microarray should mimic not only the three-dimensional character of tissue, but also the heterotypic microenvironment of the cell. Using a microfluidic network to both sort and convey cells toward time-multiplexed holographic optical tweezers, we can produce heterotypic microarrays in hydrogel. These microarrays, in conjunction with fluorescent reporters, provide us with the opportunity to follow the spatial and temporal gene expression within the array in response to environmental cues associated with various cell products. Genetically engineered cells juxtaposed with bacteria within the microarray, along with the microfluidic network, can be used to supply a diverse library of biochemical signals to the array, affording us stringent control over the microenvironment of each cell.

In order to determine the parameters used for signaling, we first attempted to construct a simple pattern consisting of a small array of sender cells in the center, surrounded by two concentric rings of receiver cells. This array, termed a "snowflake" after its appearance - was used to determine the threshold and production rates of AHL from the sender cells. By varying the number of sender cells at the start, we can find parameters controlling AHL production. As an approximation, the sender cells can be thought of as a point source, with the receiver cells in the ring receiving the same concentration of AHL at any given time.

The results of this experiment are seen in 6-8. The sender cells are expressing significant amounts of RFP within 6 hrs after induction by IPTG, as seen in 6-8(b, e). However, after 12 hrs, only the microarray which started with 4 sender cells has been able to induce GFP production in the receiver cells. The array which was initialized with 1 sender cell was unable to induce fluorescence.

It should be pointed out that, though the cells are initially set extremely precisely in place, the separation distance begins to vary due to cell reproduction within the hydrogel. Though this reproduction is an unambiguous display of cell viability and normal behavior, it does present difficulties in interpretation of the data.
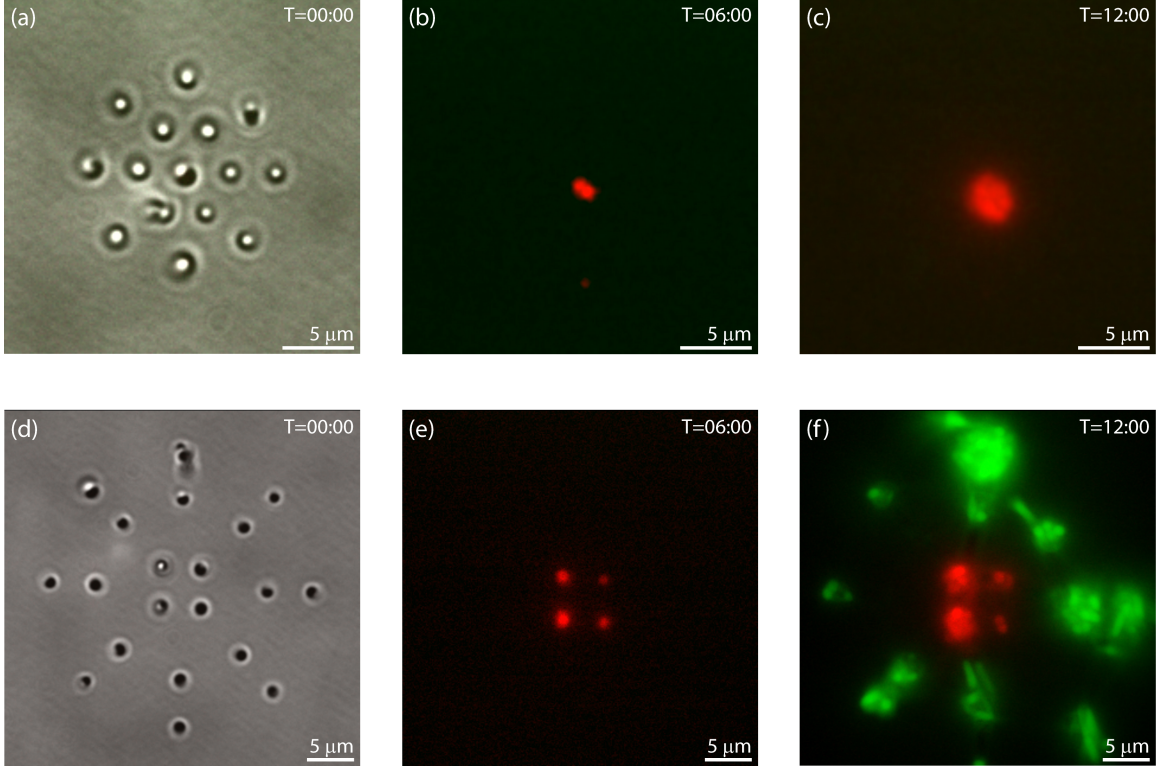
Figure 6-8: Varying sender cell quantity to assay production of AHL: (a-c) Time course of 1 initial sender cell array; (d-f) Time course of 4 initial sender cell array; Initial image has no fluorescent signal, so transmitted light image was substituted. Images were taken at 100X with Zeiss Achroplan 100x objective(1.25NA)

In order to verify our early determinations of diffusion coefficient in the hydrogel(see 2.1), we repeated the 4 sender cell experiment, but with a large difference between the two concentric rings of receiver cells. The expectation was that the receiver cells would light up at different times, which allows for a estimation of the shape of the AHL concentration profile with respect to time.

With an inner ring of receivers placed at a small radius near the senders (5 μm) and an outer ring further out (12 μm), we see the expected behavior(6-9). However, it is important to point out that, if this was a diffusive motion of the concentration front, the time scale is far too slow. With the average diffusion time given by

$$t = \frac{L^2}{2D} \tag{6.21}$$

106

For a distance of 7 μm, with a diffusion coefficient of 2.2×10^{-6} cm^2/s, the time for diffusion is approximately 1/10 second. So, the difference in induction of cells in the inner and outer rings must be due to the increased AHL production from the sender cells as a function of time. Put a different way, the Damköhler number in this system, a measure of diffusion rate versus reaction rate approaches zero.
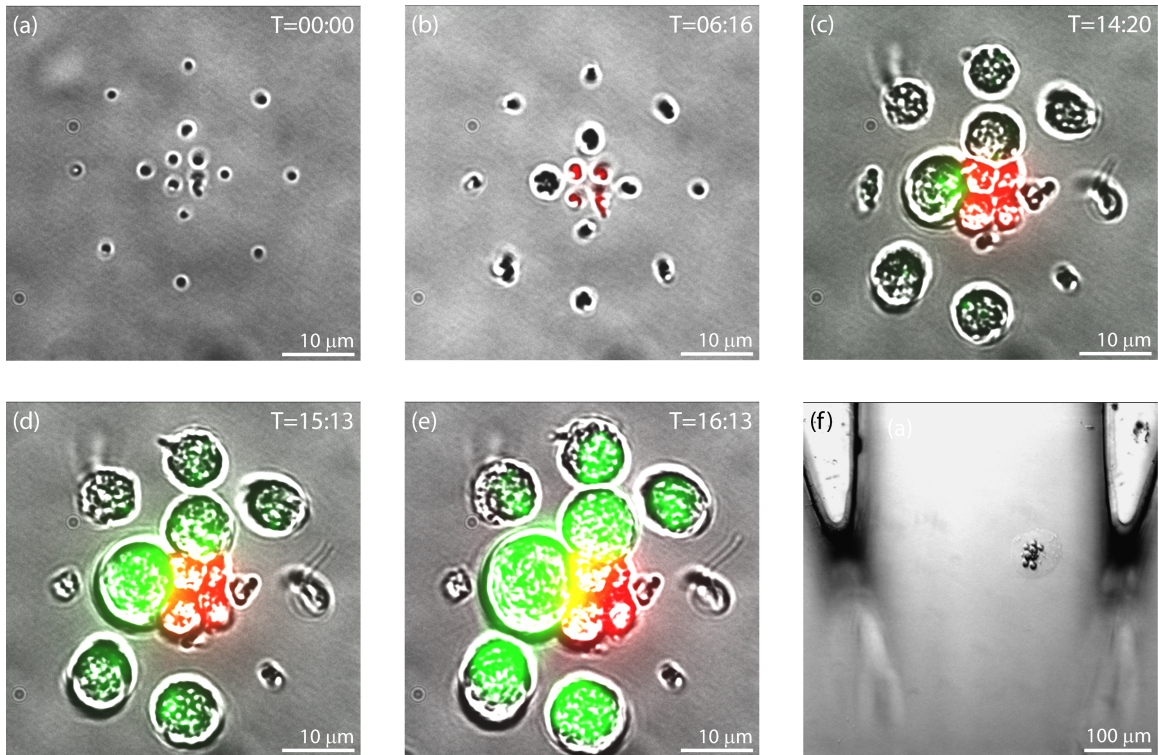
Figure 6-9: An experiment to show "wave"-like behavior - watching the threshold concentration front expand with time. Transmission images are overlaid onto fluorescent images taken of the same microarray. The microarray is organized with a 2x2 array of senders in the central core with a 2.1 μm radius with the first ring of 4 receivers located at a radius of 5 μm and the second concentric ring of 8 receivers at a radius of 12 μm. The inner ring of receivers begins fluorescing at 14hrs(c) around 1 hr before the outer ring begins fluorescing(d).

6.3.2 3D Data

Since the reproduction of E. Coli seems to occur mainly along the long axis - that is - the majority of E. Coli remain coplanar, a 3D array should allow for determination of the signaling behavior without as much interference from cellular reproduction. That

is to say, the distance separation between the bacteria in Z remains essentially the same, despite cellular reproduction and subsequent remodeling of the hydrogel.

To that end, a 3D array was constructed out of 3 2x2 arrays of cells, spaced 9 μm apart in Z(6-10). These arrays were also shifted 3 μm in X and 5 μm in Y, to allow for easy visualization. The bottom two arrays were made of senders, and the top array made of receivers.
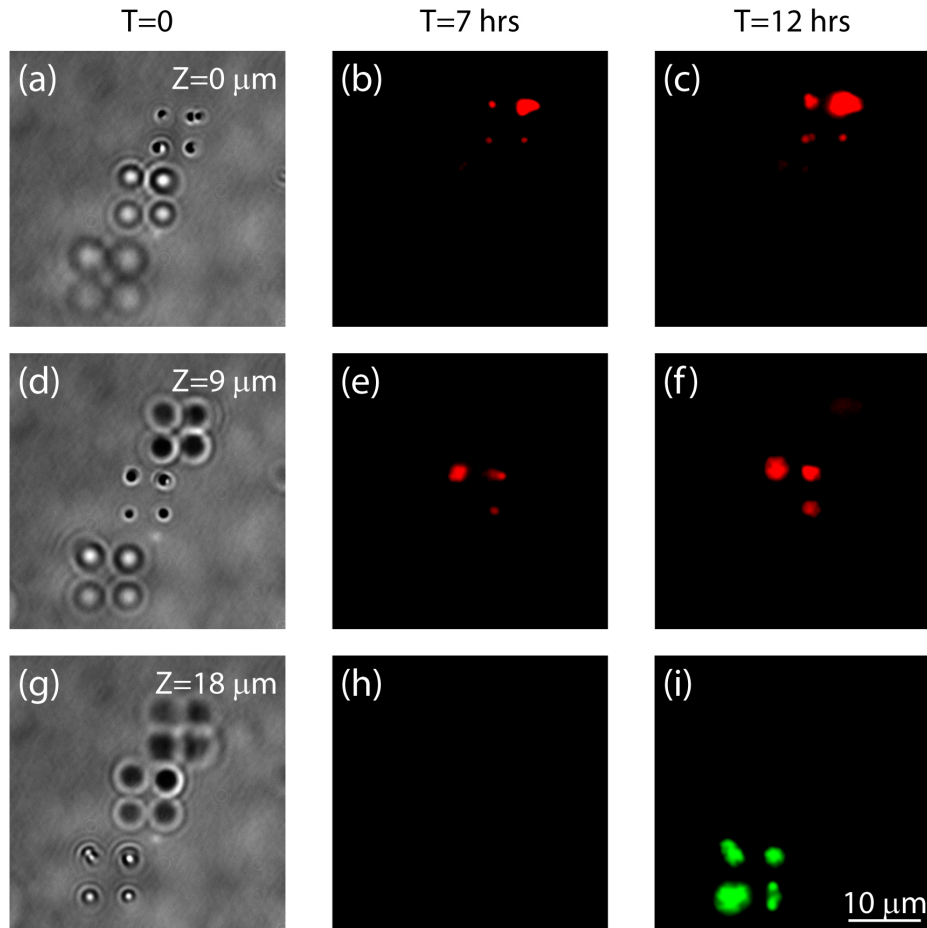
Figure 6-10: . A 2x2x3 3D microarray of sender and receiver cells. (a,d,g) are transmission images with the focus at Z=0 μm, 9 μm and 18 μm respectively observed at t=0, just prior to induction. When an IPTG is broadcast to the array, the senders rapidly perceive IPTG in their microenvironment beyond a threshold and RFP production has reached a clearly detectable level by 7 hours(b,e,h). Finally, after 12 hours, the sender cells have a high enough production rate of AHL to cause the receiver cells to be induced, producing GFP(c,f,i).

The rate of flow in the microfluidic also affects the concentration profile inside the

hydrogel. Essentially, there is a layer around the hydrogel spot where the flow is small enough that the dominant mode of mass transport is still diffusion. This phenomena is guided by the Péclet number, given by:

$$Pe = \frac{LU}{D} \qquad (6.22)$$

where L is the length scale, U the velocity of flow and D the diffusion coefficient. The thickness of this diffusive dominant region is determined by the velocity of the flow in the channel. As the velocity increases, the thickness of this layer decreases. So, with a fast enough flow, the concentration at the surface of the hydrogel is 0.

This means that the concentration profile can be altered dynamically by adjusting the flow rate past the hydrogel spot. Using a 3x2x2 array, similar to the one previously discussed, the effect of flow on the concentration profile was assayed. Essentially, a 2x2 array of sender cells was placed in the center Z-plane, with a 2x2 array of receivers placed both above and below it.

By adjusting the flow from 0.2 μL/min to 0.6 μL/min and back again, it is possible to modulate the fluorescence response of the receiver cells. After the sender cells induce both the top and bottom receiver arrays, we turned up the flow, expecting that the fluorescence of the arrays would go down as the flow drew away more AHL. As noted earlier, due to the proteolytically sensitive form of GFP we are using(GFP-LVA)[6], the receiver cells are responsive to a loss of inducing signal, losing their fluorescence rapidly.

With the higher flow rate, the fluorescence of the top receiver array decays to almost nothing, and the bottom receiver array decays slightly. It should be pointed out that the receiver array at the top is more sensitive to the changes in flow rate than the array at the bottom, as the bottom has a zero convective flux boundary(glass coverslip) compared to the top of the hydrogel, which has the fluid flow rushing past, drawing away the AHL.

Finally, upon readjusting the flow back downward to 0.2 μL/min, both the top and bottom arrays regained their fluorescence, as the concentration of AHL locally
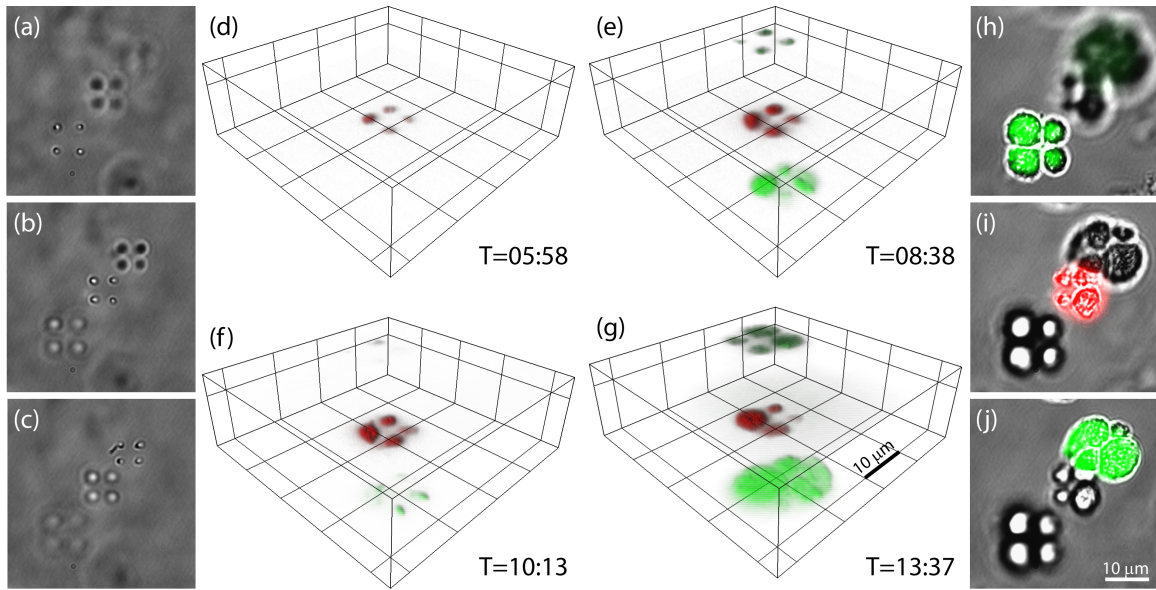
Figure 6-11: External flow affects cell signal concentration in a 3D microarray. (a-c) illustrates the initial setup of the array, comprised of 3 2x2 arrays offset by 9 μm in Z. The arrays are also offset by 6 μm in X and Y for ease of visualization. The center 2x2 array is constructed from sender cells, and the 2 flanking arrays from receiver cells. Figures (d-g) show perspective images of the 3D microarray illustrating the fluorescence in three planes reconstructed from time-lapse data. The normal time-development of the fluorescence can be modulated using the rate of flow in the microfluidic network. With 1 M IPTG in M9 flowing at 0.2 μL/min (d) red fluorescence is observed at t≈6hrs indicating the production of AHL. (e) Both flanking arrays begin to fluoresce at t≈8.5hrs but it should be noted that the top green array shows weaker fluorescence than the bottom probably due to the signal gradient in the hydrogel, considering that the convective flow is nearer the top array. Immediately after (e), the flow rate is changed to 0.6 μL/min so that (f) at t≈10hrs the intensity of the fluorescence in the bottom green array has weakened, while the fluorescence associated with the top green array has almost disappeared. Finally, at t≈10.5 hrs the 0.2 μL/min flow is re-established, and as shown in (g) both green arrays recover fluorescence by t=13.5hrs.

surged upward due to the expanded low Péclet number region.

6.3.3 Simulation

To help to design these experiments, as well as to demonstrate the dominant mechanisms at work in this system, we established a simple simulation to described our cell signaling behavior. The microfluidic fluid flow is simulated, then used, coupled

to mass-action kinetics for protein production, to describe the concentration profile of the AHL signal in the hydrogel. Details of the simulation are described in the methods section.

Estimates for the parameters involved in the simulation were determined empirically, or with support from literature. The threshold for induction of receiver and sender cells (K) as well as the Hill coefficient (n) were determined from fluorescent plate reader data taken of the cells in question (see 6.2.1). The rate of fluorescent protein oxidation γ was given from literature, given as 12 minutes for RFP[84] and 25 minutes for GFP-LVA[6]. Rate of protein degradation (α) for non tagged proteins (RFP, luxI) is set to zero - as proteins in bacteria are normally very stable, only being diluted by cell division. Rate of protein degradation of tagged proteins (GFP-LVA) was found by Andersen et al. to be $\approx$40 min[6].

A other values in the simulation, the protein production rate, β, the cell doubling rate ν, the diffusion coefficient, D, the production rate of AHL per molecule of luxI, $prod$, are all allowed to vary to fit the data, allowing us to extract values characterizing the behavior of the system. They are given initial values, as well as bounds, and the simulation is run to minimize the least squared difference between the fluorescence of each microcolony and the simulated response.

Though it takes 6 hours for the red fluorescence to express to a significant signal, the sender cells are manufacturing RFP and luxI for the entire time. It is only a limitation of the weak fluorescence of RFP(compared to GFP) which prevents this signal detection. In contrast, once the receiver cells receive sufficient amounts of AHL to activate, the fluorescence shoots up rapidly, as seen in 6-12(d). The camera has a natural noise floor and saturation point which limit the dynamic range of the measurement - but the measurable area allows us to determine the shape of the curve.

Using the fitted simulation, we are able to directly compare the fluorescent data to a simulated result, as seen in 6-13. The simulation gives the added benefit of visualizing the shape and behavior of the AHL concentration gradient in the hydrogel over time. However, the simulation does *not* currently take into account the fact that the distances between the bacteria change over time. Reproduction is taken into

account only insofar as it increases the rate of protein production - not as it affects the physical separation of bacteria.

Typical rates of the fitted values for β_0, the protein production per cell, are shown below. This variation is due in intrinsic interpopulation variance - the difference in the initial state of the individual mother bacteria which spawn the microcolonies. If one mother bacteria has more copies of the plasmid than another, or a greater metabolic capacity, its daughter cells will also enjoy this advantage and higher production. Typical values for β_{r0} are 15 molecules/s and 8 molecules/s for β_{g0}.

6.4 Conclusion

This data demonstrates that the term "quorum" sensing is something of a misnomer. Rather than depending on the number of bacteria in a certain place, the buildup of autoinducer, of AHL, is strongly dependent on the ability of the environment to clear the signal faster than it is produced. The light organ of *E. scolopes*, biofilms present in infectious disease, and other quorum sensing systems all have high bacterial density, but they also have transport governed solely by diffusion. Moreover, biofilms have typical diffusion coefficients similar to that found in our hydrogel.[156]

By adjusting the flow, we find that we are able to adjust the intensity/gene expression behavior of the cells in the hydrogel - this allows the cells, even safely ensconced within the hydrogel/biofilm, to detect the behavior of their outside environment. It also allows us to investigate the time-response of the quorum sensing signal, emphasizing that *transport* of the autoinducer is the dominating factor, rather than the *number* of bacteria present.[139]
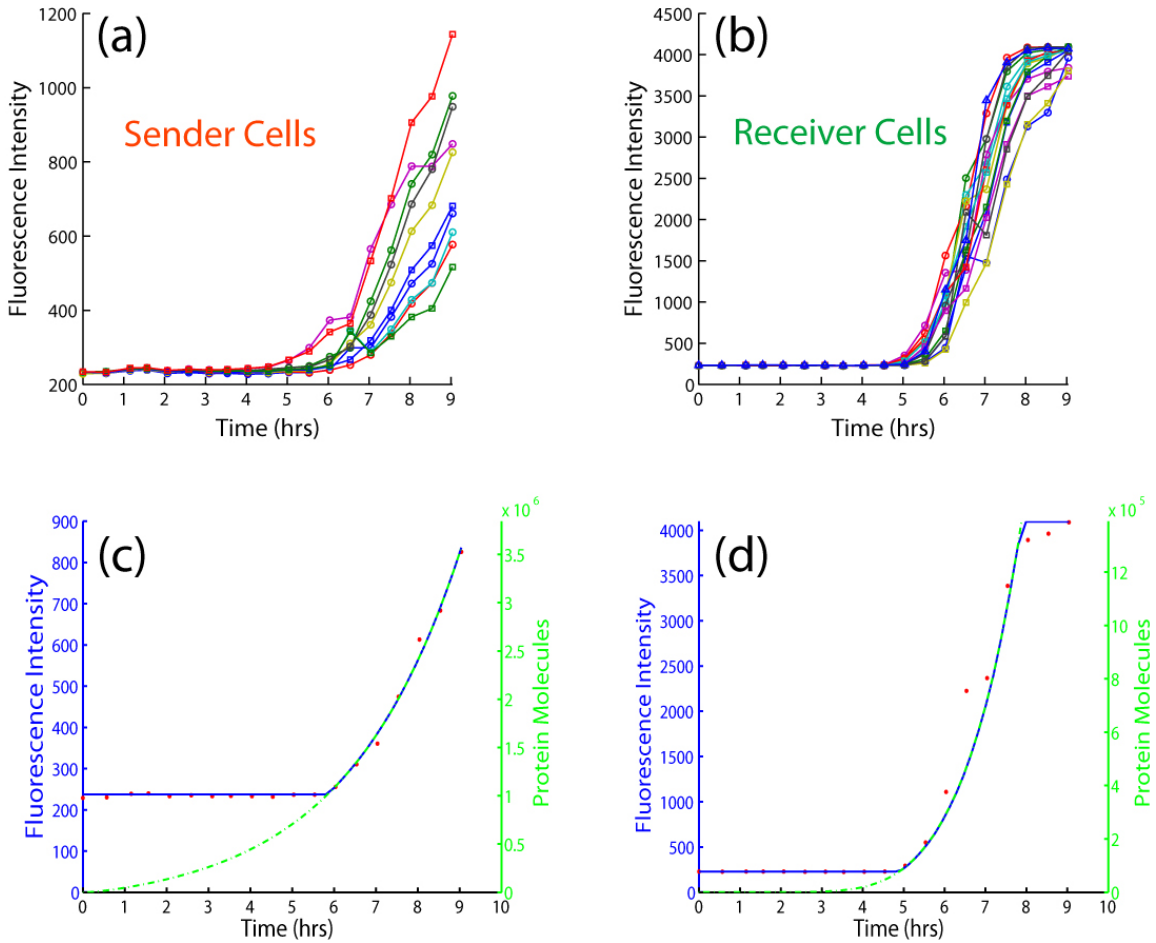
Figure 6-12: Line plot of fluorescence of individual microcolonies and corresponding fits. Fluorescent data was analyzed to determine the fluorescent intensity of each microcolony as a function of time (a) Plot of the RFP intensity of the sender cells over time (b) Plot of the GFP intensity of the receiver cells over time (c) Plot of a typical sender cell intensity (red dots) versus the fitted protein concentration(dotted green) and corresponding fitted fluorescent intensity(blue) (d) Plot of a typical receiver cell intensity (red dots) versus the fitted protein concentration(dotted green) and corresponding fitted fluorescent intensity(blue)
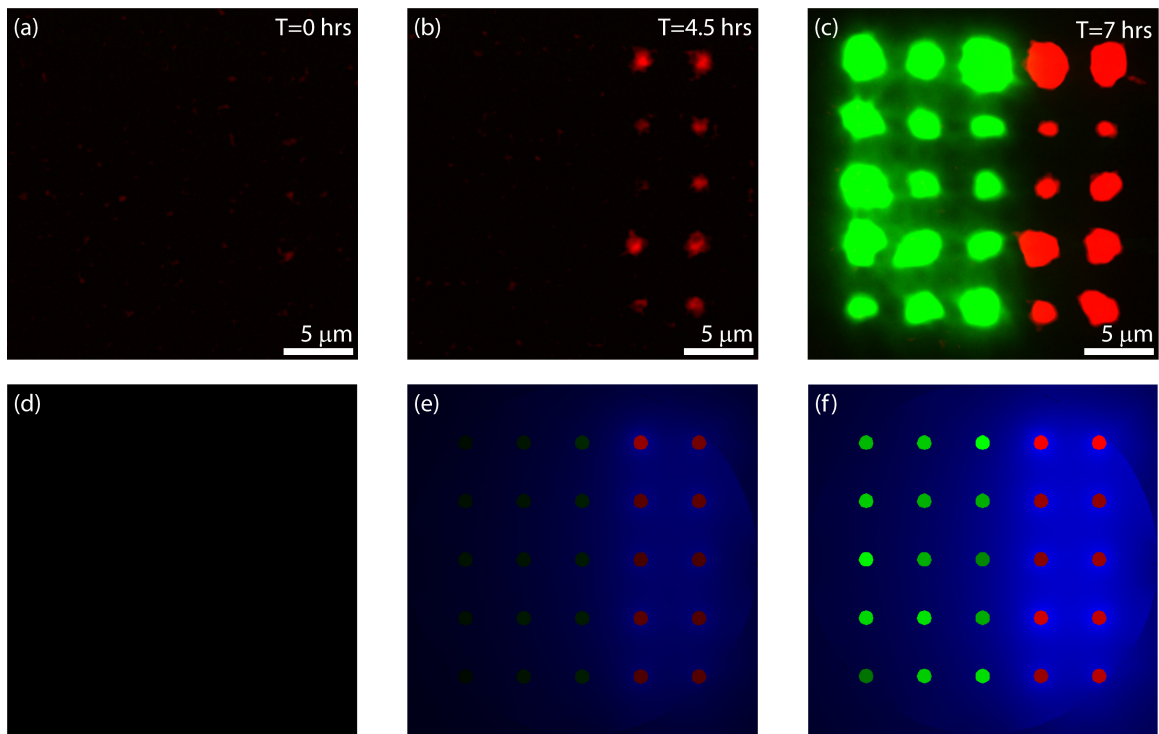
Figure 6-13: Comparison between snapshots of the space-time development of the fluorescence in a 2D microarray of (red) senders and (green) receivers (top) with simulations of protein production in an idealized array (bottom). The concentration of the gene products, RFP and GFP-LVA, are described by the ODEs given in 6.2.7. The production and degradation rates are determined from fits to the fluorescence data. The stochastic nature of the protein production is evident from the intensity variations The β values used to fit the fluorescence from the microcolonies show a large difference that can be attributed to a difference in the initial plasmid copy number and metabolic level of the individual cells.
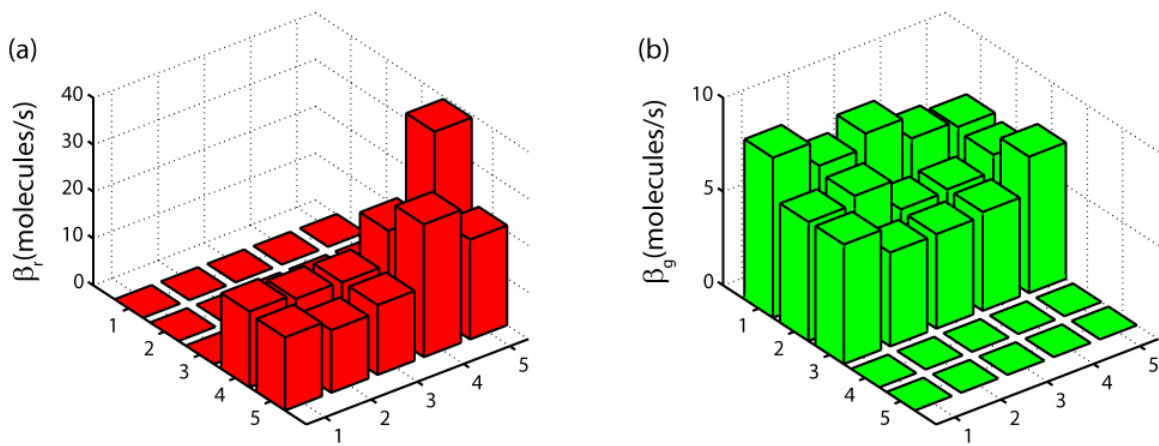
Figure 6-14: β_0 values for the individual microcolonies, plotted versus position in the array.(a) β_{r0} values with a mean of 20.08 ± 8.20 molecules/s (b) β_{g0} values with a mean of 6.36 ± 1.09 molecules/s.

Chapter 7

Conclusion

7.1 Summary

In this work, we have outlined the creation and characterization of a new method for the assembly of 3D living cell heterotypic microarrays. We then demonstrated the ability of these microarrays to study cell-cell signaling of a simple system, the quorum sensing system of *Vibrio Fischeri*. This was especially important as the *Vibrio Fischeri* system was controlled by diffusion dominated soluble signaling, which would have been difficult to effectively study with other methods.

Though each of these elements: optical trapping, photopolymerizable hydrogel, and microfluidics, have been used before, they have never been used together in such a way.

7.2 Future Work

There are several fruitful areas which this research could be extended into. First is the development this platform for the study of eukaryotic cell signaling. This will require development of viability tests which optimize the platform for eukaryotic cells, altering the hydrogel porosity, the trap beam waist, the microfluidic dimensions, in order to keep the cells alive and metabolically active.

Once this has been accomplished, there are many potential assays which hereto-

fore have been impossible. A synthetic tissue element could be assembled, containing endothelial, fibroblast, macrophage and epithelial cells. The behavior of cancer cells can then be monitored in this element, determining the action of metastasis or angiogenesis, both common targets for anti-cancer drugs.

Another possible application is in the realm of biosensors. Cells have extremely high sensitivities and selectivities coward's different chemicals and biological ligands. Cell biosensors are directly relevant to many applications, providing a possible response to even an unknown, but harmful agent.[122] Whole cell biosensors do not suffer from enzyme stability issues, even allowing for massive amplification of small signals. What's more, they could produce chemicals in response, such as a biosensor which produces insulin in response to low glucose levels.

Tissue engineering also has need of a platform form assembling cells into a 3D matrix with an ECM analog. Tissue is composed of repetitive 3D blocks of structure on the scale of 100-1000μm, such as the acinar.[26] If each block could be assembled by optical trapping, tissue of high complexity may be constructed. Using multiple spots of hydrogel, each with their own pattern of cells, the interaction of different types of tissue can be determined, or parts of tissue grown for later implantation. For example, a blood vessel could be assembled through proper positioning of endothelial cells. The cells could be cultured for a time, and trained with flow using a microfluidic device. Then the synthetic tissue, using a degradable hydrogel as a temporary support, could be implanted into an animal.

Appendix A

Cell Culture

A.1 Escherichia Coli

E. Coli, the workhorse of the world of molecular biology, is an extremely easy organism to culture. However, as it is so widely studied, there is a vast variety of different media and methods used to grow it. Below the exact recipes used in experiments in this thesis are provided.

A.1.1 M9 Minimal Media Formulations

M9 requires serveral stock solutions to make, the recipes are included below.

Sterile Water

Autoclave 18 MΩ water.

5X M9 Salts

1. Add the following to a 1L autoclavable bottle.

    - 30 g Na$_2$HPO$_4$ (0.211 M)

    - 15 g KH$_2$PO$_4$ (0.110 M)

    - 5 g NH$_4$Cl (93.5 mM)

- 2.5 g NaCl (42.8 mM)

2. Bring to 1L with 18 MΩ deinoized water

3. Autoclave

4. Bring to final volume of 1 L with sterile water, if necessary.

20% Glyecrol

1. Add 10 mL Glycerol to 40 mL 18 MΩ water.

2. Filter sterilize with 0.22 μm filter.

20% Casamino Acids

1. Add 5 g Casamino Acids to 25 mL 18 MΩ water.

2. Filter sterilize with 0.22 μm filter.

1 M $MgSO_4$

1. Add 12.32 g $MgSO_4$ to 18 MΩ water.

2. Filter sterilize with 0.22 μm filter.

200 mM Thiamine Stock

1. Add 3.37 g Thiamine Hydrochloride to 50 mL 18 MΩ water.

2. Filter sterilize with 0.22 μm filter.

100 mM $CaCl_2$

1. Add 735 mg $CaCl_2$ to 50 mL 18 MΩ water.

2. Filter sterilize with 0.22 μm filter.

To make M9-Glycerol using these solutions, add together:

- 10 mL 5X M9 Salts

- 50 μL 1 M MgSO$_4$

- 50 μL 200 mM Thiamine Stock

- 500 μL 20% Glycerol

- 500 μL 20% Casamino Acids

- 50 μL 100 mM CaCl$_2$

then bring to 50 mL with sterlie water.

A.1.2 LB Media

1. Add the following to a 1L autoclavable bottle.

   - 5 g Bacto Tryptone (BD# 211705)

   - 2.5 g Yeast Extract (BD# 212750)

   - 5 g NaCl

2. Check pH - should be around 7.5, if not, adjust with NaOH.

3. Bring to 500 mL with 18 MΩ deionized water

4. Autoclave

5. Bring to final volume of 500 mL with sterile water, if necessary.

Appendix B

Bacteria Design
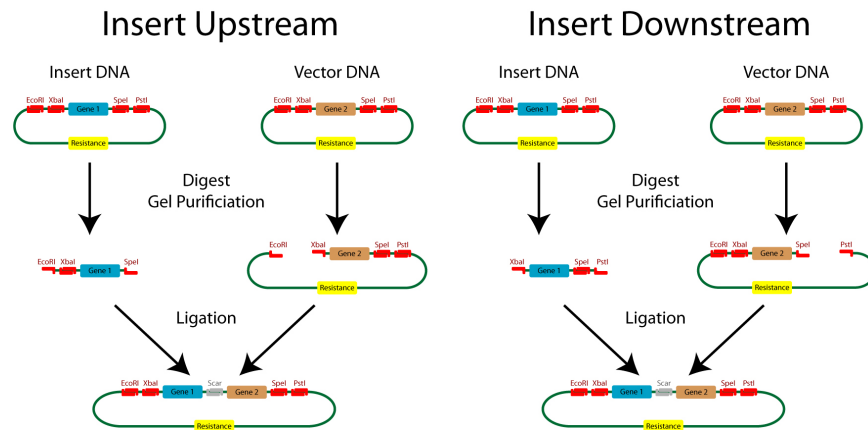
Figure B-1: Standard part assembly

B.1 Restriction Digest

1. Choose restriction enzymes.

   - —E–X—Part—S–P—–

   - Insert part upstream from Vector part

     – Digest Vector DNA with EcoRI and XbaI

     – Digest Insert DNA with EcoRI and SpeI

- XbaI and SpeI will match and make an uncuttable small scar between parts.

- Insert part downstream from Vector part

    - Digest Vector DNA with SpeI and PstI

    - Digest Insert DNA with XbaI and PstI

    - XbaI and SpeI will match and make an uncuttable small scar between parts.

- It may occasionally be the case that the Vector will be the same length as the insert - this is clearly a problem for purification. The solution is to cut the vector or insert with an enzyme - I have been using PvuI or SphI

- Keep in mind that small (<100bp parts) will be *VERY* difficult to purify – these should be vector parts.

- Miniprep is 100 ng/μL DNA usually

- Find best buffer for digest using www.neb.com

- 1 U of restriction enzyme digest 1 ug λ DNA at 37C in 1 hr.

2. Digest mix recipe:

- 32.5 μL H_2O

- 0.5 μL BSA (Bovine Serum Albumin: 10 mg/mL NEB)

- 5 μL 10X Restriction Buffer

    - If using EcoRI - use EcoRI Unique Buffer (NEB)

    - If *not* using EcoRI - use NEB Buffer #2

- 1 μL Enzyme 1

- 1 μL Enzyme 2

- 10 μL DNA from previous miniprep

3. Mix well by flicking - then spin down. Do *NOT* vortex - that will break up DNA. NEVER vortex with DNA in your tubes. NEVER vortex with enzyme in your tubes. However - it must be well mixed.

4. Put this mix in thin-walled PCR tube, and using thermacycler:

   - At least 3 hrs at 37°C (Cutting)

   - 20 min at 80°C (Heat Inactivation)

   - I have done this with a 5 hr cutting incubation, then after inactivation, storage at 4C overnight, until I get in.

B.2   Phosphatase Treatment

This entire treatment is somewhat optional. It basically prevents the vector from religating to itself, without the insert. This will remove background from screening later on - and generally makes life easier.

1. Add 5.5μL 10X Antarctic Phosphatase Buffer to Vector Digest Tube(s)

2. Add 1μL Antarctic Phosphatase Enzyme to Vector Digest Tube(s)

3. Run *ALL* tubes on thermacylcler:

   - 20 min at 37°C (Phosphatase Activity)

   - 5 min at 65°C (Heat Inactivation)

Phosphatase will not be completely heat inactivated - so be aware that purification is needed before mixing.

I suspect that this part of the protocol is not optimized - I think that PstI overhang takes longer to phosphatase than a mere 20 min . . . this might explain the amount of DNA left in the well of the gels.

B.3 Gel Electrophoresis

1. First, mix and pour gel

   - Mix:
     - 300 mg Low Melting Point Agarose
     - 30 mL 1X TBE Buffer
     - 10 μL SYBR Safe Stain
   - Microwave for 45 s, or until boiling
   - Pour into casting mold, using largest possible well comb
   - Allow gel to set and cool in 4°C cold room
   - Remove comb; fill gel box with 1X TBE Buffer

2. Load 10 μL 2-Log Ladder working mix (NEB) in lane 1

   - 50 uL 2-Log Ladder
   - 400 uL EB Buffer (Qiagen)
   - 50 uL 10X Loading Buffer (OJ)

3. Add 5.5 μL 10X Loading Buffer to Insert Digest(s); Add 6 muL 10X Loading Buffer to Vector Digest(s); Mix gently but throughly

4. Load as much of the Digest mixes as possible - typically about 50μL

5. Run for 1 hr at 100V (for 8-cm gel)

   - Longer runs will cause stain to run out of bottom of gel - be aware of this.
   - Perfect separations are not needed - just enough to see the insert versus the vector - usually a big difference.
   - Blue light and amber goggles will allow tracking of the DNA through the gel.

6. Remove gel from gel box - photograph using blue illumination(λ 488 nm) and orange filter - EtBr filter will do.

7. Using a razor blade and a sharp long straight edge, cut the lanes out of the gel first, then the desired fragments.

8. Place the fragments into a microcentrifuge tube.

9. Weigh the gel fragments by using a empty microcentrifuge tube as a tare weight.

10. Follow the Qiagen Gel Extraction Kit recipe - using the second QG wash, and eluting in 30 μL of EB Buffer

B.4   Ligation

1. First, the ratio of insert to vector DNA must be calculated.

   - The formula is: μL insert $= 6 \frac{\text{Num bp of Insert}}{\text{Num bp of Vector}} \times \mu$L vector $\times \frac{\text{Intensity of Vector}}{\text{Intensity of Insert}}$
   - So for a vector 2200 base pares long and insert 720 bp long, the ratio is approximately 2.

2. The desired amount of vector DNA is around 20 ng for a 20 μL reaction size. This is about 2 μL of minipreped DNA - at least that's the current assumption.

3. So recipe is as follows

   - 2 μL 10X T4 Ligase Buffer (NEB)
     - Do *NOT* subject this buffer to freeze-thaw cycles if avoidable - rather aliquot smaller portions. Should smell like wet dog if fresh.
   - 1 μL T4 Ligase
   - 2 μL Vector DNA
   - 2Xratio μL Insert DNA
   - Add H_2O to 20 μL total volume

4. Place in thermacycler:

  - 45 min at 16° (Ligation)

  - 10 min at 65° (Heat Inactivation)

B.5 Cell Transformation

1. Remove cell tubes from -80C freezer; place in wet ice, allow cells to thaw

2. Use single aliquot 50μL tubes if possible

3. Add 5μL Ligation Mix to Cells

4. Leave on wet ice for 30 min

5. Heat Shock at 42°C for 45 seconds.

6. Place back on wet ice for 2 min.

7. Add 950 μL SOC Medium

8. Take 1 mL cells/SOC Medium and place in culture tube - put on shaker at 37°C for 1 hrs.

9. Pipette 200 μL onto plate; Spread droplet with innoculation wand, streaking entire plate.

10. Incubate plate overnight at 37°C

B.6 Screening

The next day there should be 20-100 colonies or so on the plate. Select around 4 of these and grow them in LB for 12-16 hrs. Then miniprep(according to Qiagen standard protocol). Digest and check the DNA for insert - or better yet, sequence the DNA to check for success failure.

B.7 Supplies

- General Equipment:

  - Thermacycler(PCR Machine) - Temp range from 4C-80C - I used Strategene RoboCycler Graident 96

  - Heat Block(1.5 mL Centrifuge tubes) - 42-50C

    * Thermoylne Dri-Bath # DB16520

    * Thermoylne Modular Block # 2069Q

  - Ice Bucket

  - 4C Storage

  - -20C Storage

  - -80C Storage

- Enzymes:

  - EcoRI NEB# R0101S 10000U

  - SpeI NEB# R0133L 2500U

  - XbaI NEB# R0145S 3000U

  - PstI NEB# R0140S 10000U

  - SphI NEB# R0182S 500U

  - PvuI NEB# R0150S 300U

  - T4 DNA Ligase NEB# M0202L

  - Antarctic Phosphatase NEB# M0289S

  - 2-Log Ladder NEB# N3200S

  - 0.2 mL PCR Tubes Fisher# E0030124260

- Gel Electrophoresis Supplies:

  - SYBR Safe DNA stain Invitrogen# S33102

- – UVP Gel-Cutter Fisher# UVP85000201

- – Agarose

  - ∗ SeaKem LE OR GTG Agarose, Cambrex # 50001 OR # 50071

  - ∗ OR

  - ∗ Agarose - LE, USB # 32802

  - ∗ I should point out that I primarily used LE - though other types of agarose are indicated for DNA purification - this has proved sufficient for my stuff.

- – Blue Imaging of DNA Bands (less damage to DNA)

  - ∗ Visi-Blue Plate(converts UV to blue light) Fisher# UVP38020001

  - ∗ UV Transilluminator(UVP # 95-0180-01)

  - ∗ OR

  - ∗ Blue Transilluminator Clare Chemical # DR45M or UVP # 95-0326-01

  - ∗ OR

  - ∗ Light Box Alpha Innotech(www.alphainnotech.com) # 92-13823-00

- – Scale - <1g Mettler Toledo AB104

- Sequencing Primers(Bought from Sigma-Genosys):

  - – VF2: tgccacctgacgtctaagaa

  - – VR: attaccgcctttgagtgagc

- Cells:

  - – NEB 5-alpha F'Iq Competent (NEB# C2992H) - Extra lacI cells

  - – NEB 5-alpha High Efficiency E. Coli (NEB# C2987H) - Best cells *EVER* - strong amounts of DNA, pre-aliquotted to 50 μL

- Bacteria Culture:

- LB-Agar QBioGene # 3002-221

  - LB Media

  - Rotator/Shaker

    * Orbital Shaker IKA # 2980100

    * Roller Drum Fisher # 14-277-2

  - Incubator

    * I used Model 1915 VWR #35962-062

    * But Innova 4200 looks better, actually - has shelves for plates, and a shaker for tubes/flasks - solves 2 problems at once

- Gene Purification:

  - Qiagen Gel Purificaiton Kit Qiagen # 28704

  - Qiagen Spin Miniprep Kit Qiagen # 27106

- Storage Boxes:

  - -20C Nalgene Boxes (Fisher # 15-350-59)

  - Corning Brand Cryo-storage (-80C) (Fisher # 07-200-615)

Appendix C

Optical Trapping Background

Optical trapping, pioneered by Ashkin in the 1970s[7] is a technique which uses light pressure, force derived from photonic interactions, to manipulate objects. Essentially, though the difference in index of refraction between an object and its surrounding medium, an object will be coerced towards the focal point of the laser beam.

Working in the macroscopic world, these forces must appear insignifcant. Surely, when turning on a lamp, one is not blasted across a room from the force ementating from the light bulb. But consider what happens on a micro scale.

Quantum mechanics tells us that even massless photons have momemntum, given by $h\nu/c$. If the laser beam has a power P, there are $P/h\nu$ photons passing through a cross-section of the beam in one second. If these photons are all reflected by an object, the photons net change in momentum is twice their original momentum, $2h\nu/c$ times the number of photons per second, giving a change in momentum per second, or force, of $2P/c$. Since momentum must be conserved, the object reflecting the photons must be given an equal and opposite force. For a beam one watt in intesity, with a perfectly reflecting object, this force is 10 nanonewtons, giving an upper limit to the possible force from radiation pressure.

Bibliography

[1] GM Akselrod, W. Timp, U. Mirsaidov, Q. Zhao, C. Li, R. Timp, K. Timp, P. Matsudaira, and G. Timp. Laser-Guided Assembly of Heterotypic Three-Dimensional Living Cell Microarrays. *Biophysical Journal*, 91(9):3465, 2006.

[2] Dirk R. Albrecht, Valerie Liu Tsang, Robert L. Sah, and Sangeeta N. Bhatia. Photo- and electropatterning of hydrogel-encapsulated living cell arrays. *Lab on a Chip*, 5:111–118, 2005.

[3] D.R. Albrecht, G.H. Underhill, T.B. Wassermann, R.L. Sah, and S.N. Bhatia. Probing the role of multicellular organization in three-dimensional microenvironments. *Nature Methods*, 3:369–375, 2006.

[4] L. Almany and D. Seliktar. Biosynthetic hydrogel scaffolds made from fibrinogen and polyethylene glycol for 3D cell cultures. *Biomaterials*, 26(15):2467–77, 2005.

[5] Uri Alon. *An Introduction to Systems Biology: Design Principles of Biological Circuits*, chapter 2, pages 5–22. Chapman & HallCRC, Boca Raton, FL, 2007.

[6] J.B. Andersen, C. Sternberg, L.K. Poulsen, S.P. Bjørn, M. Givskov, and S. Molin. New Unstable Variants of Green Fluorescent Protein for Studies of Transient Gene Expression in Bacteria. *Applied and Environmental Microbiology*, 64(6):2240–2246, 1998.

[7] A. Ashkin. Acceleration and trapping of particles by radiation pressure. *Physical Review Letters*, 24(4):156–159, 1970.

[8] A. Ashkin. Forces of a single-beam gradient laser trap on a dielectric sphere in the ray optics regime. *Biophysical Journal*, 61(2):569, 1992.

[9] A. Ashkin and JM Dziedzic. Optical trapping and manipulation of viruses and bacteria. *Science*, 235(4795):1517, 1987.

[10] A. Ashkin and JM Dziedzic. Optical Levitation by Radiation Pressure. *Applied Physics Letters*, 19:283, 2003.

[11] A. Ashkin, JM Dziedzic, and T. Yamane. Optical trapping and manipulation of single cells using infrared laser beams. *Nature*, 330(6150):769–771, 1987.

[12] A. Ashkin, K. Schuetze, JM Dziedzic, U. Euteneuer, and M. Schliwa. Force generation of organelle transport measured in vivo by an infrared laser trap. *Nature*, 348(6299):346–348, 1990.

[13] Mary Helen Barcellos-Hoff and Shraddha A. Ravani. Irradiated mammary gland stroma promotes the expression of tumorigenic potential by unirradiated epithelial cells. *Cancer Research*, 60:1254–1260, 2000.

[14] MR Barer, LT Gribbon, CR Harwood, and CE Nwoguh. The viable but non-culturable hypothesis and medical bacteriology. *Reviews in Medical Microbiology*, 4(4):183–191, 1993.

[15] B.L. Bassler and R. Losick. Bacterially Speaking. *Cell*, 125(2):237–246, 2006.

[16] Subhayu Basu, Yoram Gerchman, Cynthia H. Collins, Frances H. Arnold, and Ron Weiss. A synthetic multicellular system for programmed pattern formation. *Nature*, 434(7037):1130–1134, 2005.

[17] BD Biosciences. *BD Matrigel^{TM} Basement Membrane Matrix–Product Specification Sheet*.

[18] A.V. Belikov, G.B. Altshuler, B.T. Moroz, and I.V. Pavlovskaya. Investigation of IR absorption spectra of oral cavity bacteria. *Proceedings of SPIE*, 2922:113, 1996.

[19] S. Belkin. Microbial whole-cell sensing systems of environmental pollutants. *Current Opinion in Microbiology*, 6(3):206–212, 2003.

[20] P.D. Benya and J.D. Shaffer. Dedifferentiated chondrocytes reexpress the differentiated collagen phenotype when cultured in agarose gels. *Cell*, 30(1):215–224, 1982.

[21] M.C. Berg, J. Choi, P.T. Hammond, and M.F. Rubner. Tailored Micropatterns through Weak Polyelectrolyte Stamping. *Langmuir*, 19(6):2231–2237, 2003.

[22] MW Berns. A possible two-photon effect in vitro using a focused laser beam. *Biophysical Journal*, 16(8):973–977, 1976.

[23] Sangeeta N. Bhatia, Martin L. Yarmush, and Mehmet Toner. Controlling cell interaction by micropatterning in co-cultures: Hepatocytes and 3t3 fibroblasts. *Journal of Biomedical Materials Research*, 34:189–199, 1997.

[24] SN Bhatia, UJ Balis, ML Yarmush, and M. Toner. Microfabrication of hepatocyte/fibroblast co-cultures: role of homotypic cell interactions. *Biotechnol. Prog*, 14(3):378–87, 1998.

[25] S.N. Bhatia, U.J. Balis, M.L. Yarmush, and M. Toner. Effect of cell-cell interactions in preservation of cellular phenotype: cocultivation of hepatocytes and nonparenchymal cells. *FASEB Journal*, 13(14):1883–1900, 1999.

[26] S.N. Bhatia and C.S. Chen. Tissue Engineering at the Micro-Scale. *Biomedical Microdevices*, 2(2):131–144, 1999.

[27] N.A. Bhowmick and E.G. Neilson. Stromal fibroblasts in cancer initiation and progression. *Nature*, 432:332–337, 2004.

[28] J. Bjerketorp, S. Håkansson, S. Belkin, and JK Jansson. Advances in preservation methods: keeping biosensor microorganisms alive and active. *Current Opinion in Biotechnolgy*, 2005.

[29] D. Bray. Protein molecules as computational elements in living cells. *Nature*, 376(6538):307–312, 1995.

[30] S.J. Bryant and K.S. Anseth. Hydrogel properties influence ECM production by chondrocytes photoencapsulated in poly (ethylene glycol) hydrogels. *Journal of Biomedical Materials Research*, 59(1):63–72, 2002.

[31] Stephanie J. Bryant, Charles R. Nuttelman, and Kristi S. Anseth. Cytocompatibility of UV and visible light photoinitiating systems on culture NIH/3T3 fibroblasts *in vitro*. *Journal of Biomaterial Science: Polymer Edition*, 11(5):439–457, 2000.

[32] L. Cai, N. Friedman, and X.S. Xie. Stochastic protein expression in individual cells at the single molecule level. *Nature*, 440(7082):358–362, 2006.

[33] P.P. Calmettes and M.W. Berns. Laser-Induced Multiphoton Processes in Living Cells. *Proceedings of the National Academy of Sciences*, 80(23):7197–7199, 1983.

[34] Carl Zeiss, Inc. *Zeiss Objective Trasmittance Spectra.*

[35] M. Chambard, J. Gabrion, and J. Mauchamp. Influence of Collagen Gel on the Orientation of Epithelial Cell Polarity: Follicle Formation from Isolated Thyroid Cells and from Preformed Monolayers. *The Journal of Cell Biology*, 91:157–166, 1981.

[36] C.S. Chen, M. Mrksich, S. Huang, G.M. Whitesides, and D.E. Ingber. Micropatterned surfaces for control of cell shape, position, and function. *Biotechnol Prog*, 14(3):356–63, 1998.

[37] K.P. Chen. Interfacial Energy Balance Equation for Surface-Tension-Driven Bénard Convection. *Physical Review Letters*, 78(23):4395–4397, 1997.

[38] A.M. Christensen, D.A. Chang-Yen, and B.K. Gale. Characterization of interconnects used in PDMS microfluidic systems. *Journal of Micromechanics and Microengineering*, 15(5):928–934, 2005.

[39] T. Čižmár, M. Šiler, M. Šerỳ, P. Zemánek, V. Garcés-Chávez, and K. Dholakia. Optical sorting and detection of submicrometer objects in a motional standing wave. *Physical Review B*, 74(3):35105, 2006.

[40] H.A. Clark, S.L.R. Barker, M. Brasuel, M.T. Miller, E. Monson, S. Parus, Z.Y. Shi, A. Song, B. Thorsrud, R. Kopelman, et al. Subcellular optochemical nanobiosensors: probes encapsulated by biologically localised embedding (PEBBLEs). *Sensors and Actuators B*, 51:12–16, 1998.

[41] Jenifer Coburn and Dara W. Frank. Macrophages and Epithelial Cells Respond Differently to the *Pseudomonas aeruginosa Type III Secretion System. Infection and Immunity*, 67(6):3151–3154, 1999.

[42] Corning Life Sciences. *Thermal Properties of Corning Glasses.*

[43] ME Cox and B. Dunn. Oxygen diffusion in poly (dimethyl siloxane) using fluorescence quenching. I. Measurement technique and analysis. *Journal of Polymer Science Part A Polymer Chemistry*, 24(4):621–636, 1986.

[44] GM Cruise, OD Hegre, FV Lamberti, SR Hager, R. Hill, DS Scharp, and JA Hubbell. In vitro and in vivo performance of porcine islets encapsulated in interfacially photopolymerized poly (ethylene glycol) diacrylate membranes. *Cell Transplant*, 8(3):293–306, 1999.

[45] GM Cruise, DS Scharp, and JA Hubbell. Characterization of permeability and network structure of interfacially photopolymerized poly (ethylene glycol) diacrylate hydrogels. *Biomaterials*, 19(14):1287–94, 1998.

[46] G. Csucs, R. Michel, J.W. Lussi, M. Textor, and G. Danuser. Microcontact printing of novel co-polymers in combination with proteins for cell-biological applications. *Biomaterials*, 24(10):1713–20, 2003.

[47] E. Cukierman, R. Pankov, and K.M. Yamada. Cell interactions with three-dimensional matrices. *Curr. Opin. Cell Biol*, 14(5):633–699, 2002.

[48] Edna Cukierman, Roumen Pankov, and Kenneth M. Yamada. Cell interactions with three-dimensional matrices. *Current Opinion in Cell Biology*, 14:633–639, 2002.

[49] J.E. Curtis, B.A. Koss, and D.G. Grier. Dynamic holographic optical tweezers. *Optics Communications*, 207(1):169–175, 2002.

[50] E. L. Cussler. *Diffusion: Mass Transfer in Fluid Systems*, chapter 5, pages 114–115. Cambridge University Press, second edition, 1997.

[51] C. Decker. Kinetic Study and New Applications of UV Radiation Curing. *Macromolecular Rapid Communications*, 23(18):1067–1093, 2002.

[52] William M. Deen. *Analysis of Transport Phenomena*, chapter 12, pages 488–493. Oxford University Press, 1998.

[53] D. Dendukuri, D.C. Pregibon, J. Collins, T.A. Hatton, and P.S. Doyle. Continuous-flow lithography for high-throughput microparticle synthesis. *Nature Materials*, 5(5):365–369, 2006.

[54] T. Deng, H. Wu, S. Brittain, and G. Whitesides. Prototyping of masks, masters and stamps/molds for soft lithography using an office printer and photographic reduction. *Analytical Chemistry*, 72(14):3176–3180, 2000.

[55] D. Di Carlo and LP Lee. Dynamic single-cell analysis for quantitative biology. *Anal Chem*, 78(23):7918–25, 2006.

[56] C.L. Diaz, L.S. Melchers, P.J.J. Hooykaas, B.J.J. Lugtenberg, and J.W. Kijne. Root lectin as a determinant of host–plant specificity in the Rhizobium–legume symbiosis. *Nature*, 338(6216):579–581, 1989.

[57] John Donne. *Devotions Upon Emergent Occasions, Meditation XVII*. 1623.

[58] Dow Corning. *Sylgard 184 Technical Notes*.

[59] J.L. Drury. Hydrogels for tissue engineering: scaffold design variables and applications. *Biomaterials*, 24(24):4337–4351, 2003.

[60] JC Dunn, ML Yarmush, HG Koebe, and RG Tompkins. Hepatocyte function and extracellular matrix geometry: long-term culture in a sandwich configuration [published erratum appears in FASEB J 1989 May; 3 (7): 1873]. *The FASEB Journal*, 3(2):174–177, 1989.

[61] G.M. Dunny and B.A.B. Leonard. Cell-cell communication in gram-positive bacteria. *Annual Review of Microbiology*, 51(1):527–564, 1997.

[62] M. Ericsson, D. Hanstorp, P. Hagberg, J. Enger, and T. Nystrom. Sorting Out Bacterial Viability with Optical Tweezers. *Journal of Bacteriology*, 182(19):5551–5555, 2000.

[63] E. Fällman and O. Axner. Design for fully steerable dual-trap optical tweezers. *Applied Optics*, 36:2107–2113, 1997.

[64] Dan Ferber. Synthetic biology: Microbes made to order. *Science*, 303(5655):158–161, 2004.

[65] C.J. Flaim, S. Chien, and S.N. Bhatia. An extracellular matrix microarray for probing cellular differentiation. *Nature Methods*, 2(2):119–125, 2005.

[66] A. Folch and M. Toner. Cellular micropatterns on biocompatible materials. *Biotechnology Progress*, 14(3):388–92, 1998.

[67] A.Y. Fu, H.P. Chou, C. Spence, F.H. Arnold, and S.R. Quake. An integrated microfabricated cell sorter. *Anal. Chem*, 74(11):2451–2457, 2002.

[68] C. Fuqua and E.P. Greenberg. Listening in on bacteria: Acyl-homoserine lactone signalling. *Nature Reviews: Molecular Cell Biology*, 3(9):685–695, 2002.

[69] C. Fuqua, M.R. Parsek, and E.P. Greenberg. Regulation of gene expression by cell-to-cell communication: Acyl-homoserine lactone quorum sensing. *Annual Review of Genetics*, 35(1):439–468, 2001.

[70] Rafael C. Gonzalez and Richard E. Woods. *Digital Image Processing*. Prentice-Hall, Upper Saddle River, New Jersey, second edition, 2002.

[71] Reingard Grabherr, Erik Nilsson, Gerald Striedner, and Karl Bayer. Stabilizing plasmid copy number to improve recombinant protein production. *Biotechnology and Bioengineering*, 77(2):142–147, 2002.

[72] E.P. Greenberg. Bacterial communication: Tiny teamwork. *Nature*, 424(6945):134–134, 2003.

[73] Gregory H. Underill and Alice A. Chen and Dirk R. Albrecht and Sangeeta N. Bhatia. Assessment of Hepatocellular Function within PEG Hydrogels. *Biomaterials*, 28:256–270, 2007.

[74] K.O. Greulich. *Micromanipulation by light in biology and medicine: the laser microbeam and optical tweezers*. Birkhäuser, 1999.

[75] David G. Grier. A revolution in optical manipulation. *Nature*, 424:810–816, 2003.

[76] E. Guiot, P. Georges, A. Brun, MP Fontaine-Aupart, MN Bellon-Fontaine, and R. Briandet. Heterogeneity of Diffusion Inside Microbial Biofilms Determined by Fluorescence Correlation Spectroscopy Under Two-photon Excitation. *Photochemistry and Photobiology*, 75(6):570–578.

[77] H.G. Hall, D.A. Farson, and M.J. Bissell. Lumen Formation by Epithelial Cell Lines in Response to Collagen Overlay: A Morphogenetic Model in Culture. *Proceedings of the National Academy of Sciences*, 79(15):4672–4676, 1982.

[78] D. Hanahan and R.A. Weinberg. The Hallmarks of Cancer. *Cell*, 100(1):57–70, 2000.

[79] R.L. Hansen, X.R. Zhu, and J.M. Harris. Fluorescence Correlation Spectroscopy with Patterned Photoexcitation for Measuring Solution Diffusion Coefficients of Robust Fluorophores. *Anal. Chem*, 70(7):1281–1287, 1998.

[80] R. Heim, DC Prasher, and RY Tsien. Wavelength Mutations and Posttranslational Autoxidation of Green Fluorescent Protein. *Proceedings of the National Academy of Sciences*, 91(26):12501–12504, 1994.

[81] J. Heo, K.J. Thomas, G.H. Seong, and R.M. Crooks. A Microfluidic Bioreactor Based on Hydrogel-Entrapped E. coli: Cell Viability, Lysis, and Intracellular Enzyme Reactions. *Anal Chem*, 75(1):22–6, 2003.

[82] A.R. Horswill, P. Stoodley, P.S. Stewart, and M.R. Parsek. The effect of the chemical, biological, and physical environment on quorum sensing in structured microbial communities. *Analytical and Bioanalytical Chemistry*, 387(2):371–380, 2007.

[83] DE Ingber, JA Madri, and JD Jamieson. Basement membrane as a spatial organizer of polarized epithelia. Exogenous basement membrane reorients pancreatic epithelial tumor cells in vitro. *American Journal of Pathology*, 122(1):129–139, 1986.

[84] G. Jach, M. Pesch, K. Richter, S. Frings, and J.F. Uhrig. An improved mRFP1 adds red to bimolecular fluorescence complementation. *Nature Methods*, 3:597–600, 2006.

[85] T. Jacks and R.A. Weinberg. Taking the Study of Cancer Cell Survival to a New Dimension. *Cell*, 111(7):923–925, 2002.

[86] P. Jordan, H. Clare, L. Flendrig, J. Leach, J. Cooper, and M. Padgett. Permanent 3D microstructures in a polymeric host created using holographic optical tweezers. *Journal of Modern Optics*, 51(5):627–632, 2004.

[87] P. Jordan, J. Leach, M. Padgett, P. Blackburn, N. Isaacs, M. Goksör, D. Hanstorp, A. Wright, J. Girkin, and J. Cooper. Creating permanent 3D arrangements of isolated cells using holographic optical tweezers. *Lab on a Chip*, 5:1224–1228, 2005.

[88] R.S. Kane, S. Takayama, E. Ostuni, D.E. Ingber, and G.M. Whitesides. Patterning proteins and cells using soft lithography. *Biomaterials*, 20(23):2363–76, 1999.

[89] JM Karp, Y. Yeo, W. Geng, C. Cannizarro, K. Yan, DS Kohane, G. Vunjak-Novakovic, RS Langer, and M. Radisic. A photolithographic method to create cellular micropatterns. *Biomaterials*, 27:4755–4764, 2006.

[90] S. KAWATA and T. SUGIURA. Movement of micrometer-sized particles in the evanescent field of a laser beam. *Optics Letters*, 17(11):772–774, 1992.

[91] B.C. Kim and M.B. Gu. A bioluminescent sensor for high throughput toxicity classification. *Biosens. Bioelectron*, 18:1015–1021, 2003.

[92] H.K. Kleinman, R.J. Klebe, and G.R. Martin. Role of Collagenous Matrices in the Adhesion and Growth of Cells. *The Journal of Cell Biology*, 88(3):473–485, 1981.

[93] W.G. Koh, L.J. Itle, and M.V. Pishko. Molding of Hydrogel Microstructures to Create Multiphenotype Cell Microarrays. *Analytical Chemistry*, 75:5783–5789, 2003.

[94] Won-Gun Koh, Alexander Revzin, and Michael V. Pishko. Poly(ethylene glycol) Hydrogel Microstructures Encapsulating Living Cells. *Langmuir*, 18:2459–2462, 2002.

[95] K. König, H. Liang, MW Berns, and BJ Tromberg. Cell Damage by Near-IR Microbeams. *Nature*, 377(6544):20–21, 1995.

[96] K. König, H. Liang, MW Berns, and BJ Tromberg. Cell damage in near-infrared multimode optical traps as a result of multiphoton absorption. *Opt. Lett*, 21:1090–1092, 1996.

[97] K. Konig, U. Simon, and KJ Halbhuber. 3D resolved two-photon fluorescence microscopy of living cells using a modified confocal laser scanning microscope. *Cell Mol Biol (Noisy-le-grand)*, 42(8):1181–94, 1996.

[98] K. Konig, Y. Tadir, P. Patrizio, M.W. Berns, and B.J. Tromberg. Andrology: Effects of ultraviolet exposure and near infrared laser tweezers on human spermatozoa. *Human Reproduction*, 11(10):2162, 1996.

[99] Y. Kuang, I. Biran, and D.R. Walt. Living Bacterial Cell Array for Genotoxin Monitoring. *Environ. Mutagen*, 466:97–107, 2000.

[100] HL Leffert and D. Paul. Studies On Primary Cultures Of Differentiated Fetal Liver Cells. *The Journal of Cell Biology*, 52(3):559–568, 1972.

[101] M.L. Li, J. Aggeler, D.A. Farson, C. Hatier, J. Hassell, and M.J. Bissell. Influence of a Reconstituted Basement Membrane and Its Components on Casein Gene Expression and Secretion in Mouse Mammary Epithelial Cells. *Proceedings of the National Academy of Sciences*, 84(1):136–140, 1987.

[102] H. Liang, KT Vu, P. Krishnan, T.C. Trang, D. Shin, S. Kimel, and MW Berns. Wavelength dependence of cell cloning efficiency after optical trapping. *Biophysical Journal*, 70(3):1529–1533, 1996.

[103] K.H. Lim and C.M. Counter. Reduction in the requirement of oncogenic Ras signaling to activation of PI3K/AKT pathway during tumor maintenance. *Cancer Cell*, 8(5):381–92, 2005.

[104] V.A. Liu and S.N. Bhatia. Three-Dimensional Photopatterning of Hydrogels Containing Living Cells. *Biomedical Microdevices*, 4(4):257–266, 2002.

[105] Y. Liu, DK Cheng, GJ Sonek, MW Berns, CF Chapman, and BJ Tromberg. Evidence for localized cell heating induced by infrared optical tweezers. *Biophysical Journal*, 68(5):2137–2144, 1995.

[106] Y. Liu, GJ Sonek, MW Berns, and BJ Tromberg. Physiological monitoring of optically trapped cells: assessing the effects of confinement by 1064-nm laser tweezers using microfluorometry. *Biophysical Journal*, 71(4):2158–2167, 1996.

[107] MP Lutolf and JA Hubbell. Synthetic biomaterials as instructive extracellular microenvironments for morphogenesis in tissue engineering. *Nature Biotechnology*, 23(1):47–55, 2005.

[108] MP MacDonald, GC Spalding, and K. Dholakia. Microfluidic sorting in an optical lattice. *Nature*, 426(6965):421–424, 2003.

[109] M.A. McClain, C.T. Culbertson, S.C. Jacobson, and J.M. Ramsey. Flow Cytometry of Escherichia coli on Microfluidic Devices. *Anal. Chem*, 73(21):5334–5338, 2001.

[110] M.B. Mellott, K. Searcy, and M.V. Pishko. Release of protein fromhighly cross-linked hydrogels of poly (ethylene glycol) diacrylate fabricated by UV polymerization. *Biomaterials*, 22:929–941, 2001.

[111] M.B. Miller and B.L. Bassler. Quorum sensing in bacteria. *Annual Review of Microbiology*, 55(1):165–199, 2001.

[112] Graeme Moad and David H. Solomon. *The Chemistry of Radical Polymerization*, chapter 1, page 16. In [115], second edition, 2006.

[113] Graeme Moad and David H. Solomon. *The Chemistry of Radical Polymerization*, chapter 5, pages 233–234. In [115], second edition, 2006.

[114] Graeme Moad and David H. Solomon. *The Chemistry of Radical Polymerization*, chapter 5, pages 268–269. In [115], second edition, 2006.

[115] Graeme Moad and David H. Solomon. *The Chemistry of Radical Polymerization*. Elsevier, second edition, 2006.

[116] JE Molloy. Optical chopsticks: digital synthesis of multiple optical traps. *Methods in Cell Biology*, 55:205–16, 1998.

[117] R. Montesano, P. Mouron, M. Amherdt, and L. Orci. Collagen Matrix Promotes Reorganization of Pancreatic Endocrine Cell Monolayers into Islet-Like Organoids. *The Journal of Cell Biology*, 97(3):935–939, 1983.

[118] K.C. Neuman, E.H. Chadd, G.F. Liou, K. Bergman, and S.M. Block. Characterization of Photodamage to Escherichia coli in Optical Traps. *Biophysical Journal*, 77(5):2856–2863, 1999.

[119] K.T. Nguyen and J.L. West. Photopolymerizable hydrogels for tissue engineering applications. *Biomaterials*, 23(22):4307–4314, 2002.

[120] Frank Noll, Manfred Sumper, and Norbert Hampp. Nanostructure of diatom silica surfaces and of biomimetic analogues. *Nano Letters*, 2:91–95, 2002.

[121] L. Nugent-Glandorf and T.T. Perkins. Measuring 0.1-nm motion in 1 ms in an optical microscope with differential back-focal-plane detection. *Optics Letters*, 29(22):2611–2613, 2004.

[122] SM O'Connor, JD Andreadis, KM Shaffer, W. Ma, JJ Pancrazio, and DA Stenger. Immobilization of neural cells in three-dimensional matrices for biosensor applications. *Biosens Bioelectron*, 14(10-11):871–81, 2000.

[123] A. Orimo, P.B. Gupta, D.C. Sgroi, F. Arenzana-Seisdedos, T. Delaunay, R. Naeem, V.J. Carey, A.L. Richardson, and R.A. Weinberg. Stromal Fibroblasts Present in Invasive Human Breast Carcinomas Promote Tumor Growth and Angiogenesis through Elevated SDF-1/CXCL12 Secretion. *Cell*, 121(3):335–348, 2005.

[124] E. Ostuni, R. Kane, C.S. Chen, D.E. Ingber, and G.M. Whitesides. Patterning Mammalian Cells Using Elastomeric Membranes. *Langmuir*, 16:7811–7819, 2000.

[125] K.F. Palmer and D. Williams. Optical properties of water in the near infrared. *J. Opt. Soc. Am*, 64(8):1107–1110, 1974.

[126] JJ Pancrazio, JP Whelan, DA Borkholder, W. Ma, and DA Stenger. Development and Application of Cell-Based Biosensors. *Annals of Biomedical Engineering*, 27(6):697–711, 1999.

[127] K.M. Pappas, C.L. Weingart, and S.C. Winans. Chemical communication in proteobacteria: biochemical and structural studies of signal synthases and receptors required for intercellular signalling. *Molecular Microbiology*, 53(3):755–769, 2004.

[128] M.J. Paszek, N. Zahir, K.R. Johnson, J.N. Lakins, G.I. Rozenberg, A. Gefen, C.A. Reinhart-King, S.S. Margulies, M. Dembo, D. Boettiger, et al. Tensional homeostasis and the malignant phenotype. *Cancer Cell*, 8(3):241–54, 2005.

[129] James B. Pawley. *Handbook of Biological Confocal Microscopy*. Plenum Press, New York, second edition.

[130] N. Periasamy and AS Verkman. Analysis of Fluorophore Diffusion by Continuous Distributions of Diffusion Coefficients: Application to Photobleaching Measurements of Multicomponent and Anomalous Diffusion. *Biophysical Journal*, 75(1):557–567, 1998.

[131] E.J.G. Peterman, F. Gittes, and C.F. Schmidt. Laser-Induced Heating in Optical Traps. *Biophysical Journal*, 84(2):1308–1316, 2003.

[132] Gerald B. Pier, Martha Grout, and Tanweer S. Zaidi. Cystic fibrosis transmembrane conductance regulator is an epithelial cell receptor for clearance of Pseudomonas aeruginosa from theălung. *Proceedings of the National Academy of Science*, 94(22):12088–12093, 1997.

[133] M. Polin, K. Ladavac, S.H. Lee, Y. Roichman, and D. Grier. Optimized holographic optical traps. *Optics Express*, 13(15):5831–5845, 2005.

[134] J.W. Pollard. Tumour-educated macrophages promote tumour progression and metastasis. *Nat Rev Cancer*, 4(1):71–78, 2004.

[135] A.B. Pratt, F.E. Weber, H.G. Schmoekel, R. Mueller, and J.A. Hubbell. Synthetic extracellular matrices for in situ tissue engineering. *Biotechnology and Bioengineering*, 86(1):27–36, 2004.

[136] SJ Projan. New (and not so new) antibacterial targets-from where and when will the novel drugs come? *Curr Opin Pharmacol*, 2(5):513–22, 2002.

[137] Qiagen. *QIAprep Miniprep Handbook.*

[138] GP Raeber, MP Lutolf, and JA Hubbell. Molecularly Engineered PEG Hydrogels: A Novel Model System for Proteolytically Mediated Cell Migration. *Biophysical Journal*, 89(2):1374–1388, 2005.

[139] R.J. Redfield. Is quorum sensing a side effect of diffusion sensing? *Trends in Microbiology*, 10(8):365–370, 2002.

[140] P.J. Reece, V. Garcés-Chávez, and K. Dholakia. Near-field optical micromanipulation with cavity enhanced evanescent waves. *Applied Physics Letters*, 88:221116, 2006.

[141] B. Rieger, LR van den Doel, and LJ van Vliet. Ring formation in nanoliter cups: Quantitative measurements of flow in micromachined wells. *Physical Review E*, 68(3):36312, 2003.

[142] C.L. Rocha, E.A. Rucks, D.M. Vincent, and J.C. Olson. Examination of the Coordinate Effects of *Pseudomonas aeruginosa ExoS on Rac1*. *Infection and Immunity*, 73(9):5458–5467, 2004.

[143] Y. Roichman and D. Grier. Holographic assembly of quasicrystalline photonic heterostructures. *Optics Express*, 13(14):5434–5439, 2005.

[144] EA Roth, T. Xu, M. Das, C. Gregory, JJ Hickman, and T. Boland. Inkjet printing for high-throughput cell patterning. *Biomaterials*, 25(17):3707–15, 2004.

[145] E.G. Ruby et al. Lessons from a cooperative, bacterial-animal association: The Vibrio fischeri-Euprymna scolopes light organ symbiosis. *Annual Review of Microbiology*, 50(1):591–624, 1996.

[146] RJ Russell, AC Axel, KL Shields, and MV Pishko. Mass transfer in rapidly photopolymerized poly (ethylene glycol) hydrogels used for chemical sensing. *Polymer*, 42(11):4893–4901, 2001.

[147] UK Saarialho-Kere, SO Kovacs, AP Pentland, JE Olerud, HG Welgus, and WC Parks. Cell-matrix interactions modulate interstitial collagenase expression

by human keratinocytes actively involved in wound healing. *J Clin Invest*, 92(6):2858–2866, 1993.

[148] K. Sauer. The genomics and proteomics of biofilm formation. *Genome Biol*, 4(6):219, 2003.

[149] D.C. Savage. Microbial Ecology of the Gastrointestinal Tract. *Annual Review of Microbiology*, 31(1):107–133, 1977.

[150] AL Schaefer, DL Val, BL Hanzelka, JE Cronan, and EP Greenberg. Generation Of Cell-To-Cell Signals In Quorum Sensing: Acyl Homoserine Lactone Synthase Activity Of A Purified Vibrio Fischeri Luxi Protein. *Proceedings of the National Academy of Sciences of the United States of America*, 93(18):9505–9509, 1996.

[151] A. Schönle and S.W. Hell. Heating by absorption in the focus of an objective lens. *Opt. Lett*, 23:325–327, 1998.

[152] Sigma-Aldrich. *Kanamycin monosulfate (K4000) Technical Note.*

[153] V.A. Soifer, V.V. Kotlyar, and L.L. Doskolovich. *Iterative Methods for Diffractive Optical Elements Computation.* Taylor & Francis, 1997.

[154] E. Spiess, F. Bestvater, A. Heckel-Pompey, K. Toth, M. Hacker, G. Stobrawa, T. Feurer, C. Wotzlaw, U. Berchner-Pfannschmidt, T. Porwol, et al. Two-photon excitation and emission spectra of the green fluorescent protein variants ECFP, EGFP and EYFP. *Journal of Microscopy*, 217(3):200–204, 2005.

[155] W.G. Stetler-Stevenson, S. Aznavoorian, L.A. Liotta, et al. Tumor Cell Interactions with the Extracellular Matrix During Invasion and Metastasis. *Annual Review of Cell Biology*, 9(1):541–573, 1993.

[156] P.S. Stewart. Diffusion in Biofilms The views expressed in this Commentary do not necessarily reflect the views of the journal or of ASM. *Journal of Bacteriology*, 185(5):1485–1491, 2003.

[157] Lubert Stryer. *Biochemistry*, chapter 36, pages 951–955. In [158], fourth edition, 1995.

[158] Lubert Stryer. *Biochemistry*. W.H. Freeman and Company, New York, fourth edition, 1995.

[159] V. Studer, R. Jameson, E. Pellereau, A. Pépin, and Y. Chen. A microfluidic mammalian cell sorter based on fluorescence detection. *Microelectronic Engineering*, 73:852–857, 2004.

[160] K. Svoboda and SM Block. BIological Applications of Optical Forces. *Annu Rev Biophys Biomol Struct*, 23:247–85, 1994.

[161] K. Svoboda and S.M. Block. Force and velocity measured for single kinesin molecules. *Cell*, 77(5):773–84, 1994.

[162] VL Tsang and SN Bhatia. Fabrication of three-dimensional tissues. *Adv Biochem Eng Biotechnol*, 103:189–205, 2007.

[163] K. Visscher, SP Gross, and SM Block. Construction of multiple-beam optical traps withnanometer-resolution position sensing. *Selected Topics in Quantum Electronics, IEEE Journal of*, 2(4):1066–1076, 1996.

[164] Robert A. Weinberg. *The Biology of Cancer*, chapter 13, pages 527–529. In [166], 2007.

[165] Robert A. Weinberg. *The Biology of Cancer*, chapter 13, pages 556–581. In [166], 2007.

[166] Robert A. Weinberg. *The Biology of Cancer*. Garland Science, New York, 2007.

[167] Ron Weiss and Jr. Thomas F. Knight. Engineered communications for microbial robotics. In A. Condon, editor, *DNA Computing: 6th International Workshop on DNA-Based Computers*, pages 1–16, 2000.

[168] NA Whitehead, AM Barnard, H. Slater, NJ Simpson, and GP Salmond. Quorum-sensing in Gram-negative bacteria. *FEMS Microbiol Rev*, 25(4):365–404, 2001.

[169] G. Whitesides, E. Ostuni, S. Takayama, X. Jiang, and D. Ingber. Soft lithography in biology and biochemistry. *Annual Review of Biomedical Engineering*, 3:335–373, 2001.

[170] A. Wolff, I. R. Perch-Nielsen, U. D. Larsen, P. Friis, G. Goranovic, C. R. Poulsen, J. P. Kutter, and P. Telleman. Integrating advanced functionality in a microfabricated high-throughput fluorescent-activated cell sorter. *Lab on a Chip*, 3:22–27, 2003.

[171] Jeffrey Wyckoff, Weigang Wang, Elaine Y. Lin, Yarong Wang, Fiona Pixley, E. Richard Stanley, Thomas Graf, Jeffrey W. Pollard, Jeffrey Segall, and John Condeelis. A paracrine loop between tumor cells and macrophages is required for tumor cell migration in mammary tumors. *Cancer Research*, 64:7022–7029, 2004.

[172] C. Xu, M.S. Inokuma, J. Denham, K. Golds, P. Kundu, J.D. Gold, and M.K. Carpenter. Feeder-free growth of undifferentiated human embryonic stem cells. *Nat Biotechnol*, 19(10):971–974, 2001.

[173] Hongmei Yu, Caroline M. Alexander, and David J. Beebe. Understanding microchannel culture: parameters involved in soluble factor signaling. *Lab on a Chip*, 7:726–730, 2007.

[174] M.H. Zaman, R.D. Kamm, P. Matsudaira, and D.A. Lauffenburger. Computational Model for Cell Migration in Three-Dimensional Matrices. *Biophysical Journal*, 89(2):1389–1397, 2005.

[175] S. Zhang, L. Yan, M. Altman, M. Lassle, H. Nugent, F. Frankel, D.A. Lauffenburger, G.M. Whitesides, and A. Rich. Biological surface engineering: a simple system for cell pattern formation. *Biomaterials*, 20(13):1213–1220, 1999.